

**DEVELOPMENT OF A WIND-SOLAR PV HYBRID
SYSTEM FOR SMALL-SCALE POWER GENERATION
IN LOW WIND SPEED REGIMES IN KENYA**

KENNEDY MUCHIRI

DOCTOR OF PHILOSOPHY

(Physics)

**JOMO KENYATTA UNIVERSITY
OF
AGRICULTURE AND TECHNOLOGY**

2024

**Development of a Wind-Solar PV Hybrid System for Small-Scale
Power Generation in Low Wind Speed Regimes in Kenya**

Kennedy Muchiri

**A Thesis Submitted in Partial Fulfillment of the Requirements for
the Degree of Doctor of Philosophy in Physics of the Jomo
Kenyatta University of Agriculture and Technology**

2024

DECLARATION

This thesis is my original work and has not been presented for a degree in any other university.

Signature..... Date.....

Kennedy Muchiri

This thesis has been submitted for examination with our approval as University Supervisors

Signature..... Date.....

Prof. Joseph Ngugi Kamau, PhD

JKUAT, Kenya

Signature..... Date.....

Dr. David Wafula Wekesa, PhD

Multimedia University, Kenya

Signature..... Date.....

Dr. Churchill Otieno Saoke, PhD

JKUAT, Kenya

Signature..... Date.....

Prof. Joseph Ndisya Mutuku, PhD

JKUAT, Kenya

Signature..... Date.....

Dr. Joseph Kimiri Gathua, PhD

Kenyatta University, Kenya

DEDICATION

This study is dedicated to my spouse Stella Kanini, daughter Alyssa Mwende, son Adrien Baraka and family members Joseph Muchiri, Rose Muchiri, Stanely Muchiri, Mwangi Muchiri, Karanja Muchiri, and Martin Muchiri.

ACKNOWLEDGEMENT

First and foremost, praise be to God for his blessings and guidance throughout my research work. Many thanks to my supervisors, Prof. Joseph Ngugi Kamau, Dr. David Wafula Wekesa, Dr. Churchill Otieno Saoko, Prof. Joseph Ndisya Mutuku, and Dr. Joseph Kimiri Gathua, for their unwavering intellectual direction throughout my research, publications, and thesis writing. My appreciation also goes to the government of Kenya, through NRF and JKUAT, for their financial assistance (Grant No: NRF/1/MMC/450), which enabled me to complete my research successfully.

I also thank the Institute of Energy and Environmental Technology (IEET) through Prof. Joseph Ngugi Kamau for creating an inspiring atmosphere and support during my study, Engineering Department of JKUAT through Dr. Daniel Omondi, Mr. Fred Amira and Mr. David Chitayi for provision of equipment and opportunity to do my research work in their workshops, the Electrical Department through Mr. Benson Muoki for his guidance in design and testing of my system.

Much gratitude is also extended to the Chairman of the Department of Physics and the staff for academic and technical support. Finally, I express my sincere appreciation to my dear wife Stella, daughter Alyssa, son Baraka and family members for their patience and understanding in the course of this study. My friends who have been there for me over these years and have always encouraged me to keep going even when things were difficult. Many thanks to everyone's efforts whose these fruits are now a reality.

TABLE OF CONTENTS

DECLARATION	ii
DEDICATION	iii
ACKNOWLEDGEMENT	iv
LIST OF TABLES	ix
LIST OF FIGURES	x
LIST OF PLATES	xiii
LIST OF APPENDICES	xiv
ABBREVIATIONS AND ACRONYMS	xvi
LIST OF SYMBOLS	xix
ABSTRACT	xxi
CHAPTER ONE	1
INTRODUCTION	1
1.1 Background Information	1
1.2 Statement of the Problem	7
1.3 Justification of the Study.....	8
1.4 Objectives	9
1.4.1 Main Objective	9
1.4.2 Specific Objectives	9
1.5 Research Questions	9
1.6 Conceptual Framework	10

CHAPTER TWO.....	12
LITERATURE REVIEW.....	12
2.1 Introduction	12
2.2 Theoretical Principles.....	12
2.2.1 Wind Resource Characteristics.....	12
2.2.2 Solar Resource Characteristics	17
2.2.3 Site Assessment.....	21
2.2.4 Energy Load Assessment	22
2.2.5 Solar PV System Assessment.....	22
2.2.6 Solar PV System Component Sizing	23
2.2.7 Maximum PowerPoint Tracking (MPPT)	26
2.2.8 Wind Turbine System Characteristics	29
2.2.9 Hybrid Energy System	40
2.3 Previous Works Relevant to Study.....	42
2.3.1 Wind Resource Assessment	42
2.3.2 Aerodynamic Performance Assessment	43
2.3.3 Solar PV Resource Assessment.....	47
2.3.4 Wind and Solar Resource Complementarity	49
2.3.5 Hybrid Energy Systems Assessment.....	51
2.3.6 Energy Demand Assessment	55
2.4 Summary of Research Gaps	57

CHAPTER THREE	59
MATERIALS AND METHODS.....	59
3.1 Introduction	59
3.2 Research Design.....	59
3.3 Study Area.....	60
3.4 Study Procedures	61
3.4.1 Experimental Procedures	61
3.4.2 Sampling Procedure.....	63
3.4.3 Simulation Procedure	65
3.4.4 System Component Sizing	67
3.4.5 Design and Fabrication.....	68
3.4.6 Wind-Solar PV Hybridization	73
3.4.7 Energy Optimization	75
3.4.8 Economic Viability Assessment.....	76
3.5 Study Setup	78
3.5.1 Wind Turbine Tunnel Test	78
3.5.2 Field Test Setup	79
3.6 Data Collection.....	82
3.7 Data Analysis	82

CHAPTER FOUR	84
RESULTS AND DISCUSSION	84
4.1 Introduction	84
4.2 Resource Distribution.....	84
4.2.1 Distribution of Wind Resource	84
4.2.2 Distribution of Solar Radiation	89
4.3 Wind and Solar Complementarity.....	96
4.4 Energy Demand Analysis	99
4.5 Wind Tunnel Test Results	103
4.6 Hybrid System Power Performance	108
4.6.1 Wind Shear Analysis	108
4.6.2 Power Performance Analysis	109
4.6.3 Wind Solar PV Hybrid System Specifications	112
4.7 Economic Viability Analysis	113
CHAPTER FIVE.....	115
CONCLUSIONS AND RECOMMENDATIONS	115
5.1 Conclusion.....	115
5.2 Recommendations	117
REFERENCES	118
APPENDICES	147

LIST OF TABLES

Table 2.1: Power Law Exponents and Different Terrains	15
Table 4.1: Monthly Average Wind Speeds and Temperatures in Year 2019	85
Table 4.2: GHI, DHI, DNI, and CSI Monthly Peak Values at Fixed Plane	90
Table 4.3: GHI, DHI, DNI, and CSI Monthly Peaks for Sun Track Option	91
Table 4.4: Monthly and Daily Average Solar Insolation in the Year 2019	93
Table 4.5: Average Energy Loads per Cluster, Expressed in kWh	99
Table 4.6: Cluster Average Energy Loads for Homes using less than 1 kWh daily .	100
Table 4.7: Frequency Distribution of Household Loads	100
Table 4.8: A Typical Rural Household's Load Demand in Machakos	102
Table 4.9: Annual Wind Turbine Energy Production at Increasing Hub Heights	112
Table 4.10: Specifications of the Developed Wind-Solar Hybrid System	113
Table 4.11: Hybrid Energy System's Economic Viability	114

LIST OF FIGURES

Figure 1.1: Block Diagram of the Conceptual Framework	11
Figure 2.1: Relationship between Solar Insolation and Solar Irradiance	18
Figure 2.2: (a) Pyrheliometer used to Measure DNI and (b) Pyranometer for Measuring GHI.....	19
Figure 2.3: Solar PV energy system architecture	23
Figure 2.4: Wind Turbine MPP at Optimum TSR.....	27
Figure 2.5: Solar Panel I-V Characteristics showing the MPP	28
Figure 2.6: Components of a HAWT System.....	29
Figure 2.7: Model of a WT Performance Curve.....	33
Figure 2.8: Airfoil Nomenclature	34
Figure 2.9: Relationship of Lift Coefficient Verse Angles of Attack	36
Figure 2.10: Wind Turbine Rotor Encircled by an Axial Stream Tube	38
Figure 2.11: Schematic of a Wind/PV Hybrid System.....	40
Figure 2.12: (a) Layouts of Serial and (b) Parallel HES	41
Figure 2.13: (a) DC and (b) AC Configurations of HES	42
Figure 2.14: Schematic of a Combined AC and DC Hybrid Energy System Configuration	42
Figure 3.1: Area map of Machakos County, Kenya	60
Figure 3.2: Data Logging System Flowchart.....	63
Figure 3.3: Flow Chart Showing Sampling Method.....	64

Figure 3.4: PVGIS Interface	66
Figure 3.5: Lift to Drag Ratio vs AOA for Various Airfoils	70
Figure 3.6: Layout of a Hybrid Power System	74
Figure 3.7: Process Flow Diagram for a Hybrid Energy System	74
Figure 3.8: Process Flow Diagram for Optimization	75
Figure 4.1: Daily Average and Peak Wind Speeds in 2019	85
Figure 4.2: Average Monthly Wind Speed and Temperature in Year 2019	86
Figure 4.3: Weibull's Distribution for Wind Speeds Between 0-10.0 m/s.....	87
Figure 4.4: Distribution of Wind Flow Directions	89
Figure 4.5: Daily Average Irradiance in March 2019 (a) at Fixed Plane and (b) at Vertical Tracking	92
Figure 4.6: Daily Average Irradiance in July 2019, (a) at Fixed Plane and (b) at Vertical Tracking	92
Figure 4.7: Daily Average Irradiance in March, June and July 2019	93
Figure 4.8: Simulated Solar Insolation	95
Figure 4.9: Simulated PV Energy Output.....	96
Figure 4.10: Hourly Time Series of Solar Irradiance and Wind Speed.....	97
Figure 4.11: Solar and Wind Resource Monthly Complementarity	98
Figure 4.12: Levels of Energy Use in the Three Zones	101
Figure 4.13: Patterns of Energy Consumption in Machakos	101
Figure 4.14: Load Demand Profile for a Typical Rural Household	103

Figure 4.15: (a) RPM vs Wind Speeds for Styrofoam and (b) Aluminum Blades, respectively	104
Figure 4.16: (a) TSR vs Wind Speeds for Styrofoam and (b) Aluminum Rotors, respectively	105
Figure 4.17: (a) C_P vs TSR for Aluminum Rotor and (b) Styrofoam Rotor, respectively	106
Figure 4.18: (a) Extractable Power vs Wind Speeds for Blades made of Aluminum and (b) Styrofoam, respectively	107
Figure 4.19: Expected WT Power Output	107
Figure 4.20: Vertical Wind Shear and Corresponding Power Densities	108
Figure 4.21: Voltage Outputs of the Hybrid Energy System	110
Figure 4.22: Output Currents of the Hybrid Energy System	110
Figure 4.23: Wind Shear Analysis to a Hub Height of 50 m.....	111

LIST OF PLATES

Plate 3.1: GHI Measurement using the MS-602 Pyranometer	62
Plate 3.2: Wind Vane, Temperature, and Cup-Type Anemometer Sensors	62
Plate 3.3: Data Logging System	63
Plate 3.4: Aluminum Blade Design	71
Plate 3.5: Styrofoam Blade Element Cross-Sections	72
Plate 3.6: Styrofoam Blades Strengthened with Fiber Material	72
Plate 3.7: Wind Turbine Rotor Hub	73
Plate 3.8: Wind Tunnel Test Experimental Set-Up	79
Plate 3.9: Wind Turbine and Acurite Iris 5 in 1 Sensor Installed at IEET, JKUAT in 2023.....	80
Plate 3.10: Solar PV System Installed at the JICA Workshop Rooftop, IEET in JKUAT	80
Plate 3.11: Setup of a Hybrid Charge Controller, Battery, Inverter and Loads Connected to a Data Logger.....	81
Plate 3.12: Acurite Iris 5 In 1 Data Logger with PC Connect	82

LIST OF APPENDICES

Appendix I: Contributions of the Thesis	147
Appendix II: Questionnaire used to Collect Energy Demand Data	150
Appendix III: Installation of Experimental Set-Ups in Machakos	151
Appendix IV: Data Logging System used in Capturing Wind and Solar Resource Assessment Data	151
Appendix V: Styrofoam Material used in Rotor Blade Fabrication	152
Appendix VI: Styrofoam Blade Fabrication at the IEET Workshop, JKUAT	152
Appendix VII: Co-ordinates of NACA 4418 Airfoil	153
Appendix VIII: Lift to Drag Ratios of NACA 4418 and the other Similar Airfoils .	154
Appendix IX: WT Testing in a Wind Tunnel Facility in the Fluids Laboratory, JKUAT	155
Appendix X: Rotational Speeds of Styrofoam and Aluminum Blades at different Wind Speeds	156
Appendix XI: Power Coefficient and different TSRs for the Styrofoam Blade	157
Appendix XII: Rotor Power at different TSRs of the Styrofoam Blade	157
Appendix XIII: Power Coefficient at different TSRs for the Aluminum Blade	158
Appendix XIV: Rotor Power at different TSRs of the Aluminum Blade	158
Appendix XV: Fabricated and Assembled Wind Turbine at the Engineering Workshop, JKUAT	159
Appendix XVI: Wind-Solar Hybrid Interface Testing at Electrical Laboratory, JKUAT	159

Appendix XVII: Wind-Solar Hybrid Charge Controller used to Hybridize Wind and Solar Energies	160
Appendix XVIII: Hybrid Charge Controller Connections to the Sub-Systems.....	160
Appendix XIX: Wind Tunnel Facility in the Fluids Laboratory, JKUAT	161

ABBREVIATIONS AND ACRONYMS

AC	Alternating Current
AEO	Annual Energy Output
ArcGis	Aeronautical Reconnaissance Coverage Geographical Information System
BEM	Blade Elementary Momentum Theory
BET	Blade Element Theory
CDMA	Code Division Multiple Access
CFD	Computational Fluid Dynamics
CMSAF	Satellite Application Facility on Climate Monitoring
COP28	Conferences of Parties on Climate Change
CSI	Clear Sky Irradiance
DAC	Direct Air Capture
DC	Direct Current
DOD	Depth of Discharge
DHI	Diffuse Horizontal Irradiance
DNI	Direct Normal Irradiance
EPF	Expanded Polystyrene Foam
GHG	Green House Gases
GHI	Global Horizontal Irradiance
GIS	Geographical Information System
GRASS	Geographical Resource Analysis Support System

GSM	Global System for Mobile Communication
HAWT	Horizontal Axis Wind Turbine
HES	Hybrid Energy Systems
HOMER	Hybrid Optimization of Multiple Energy Resources
HRES	Hybrid Renewable Energy Systems
IISD	International Institute of Sustainable Development
IRR	Internal Rate of Return
LIDAR	Light Detection and Ranging
MPP	Maximum Power Point
MPPT	Maximum Power Point Tracking
NACA	National Advisory Committee for Aeronautics
NPV	Net Present Value
PI	Profitability Index
PIC	Peripheral Interface Controller
PP	Payback Period
PSH	Peak Sun Hours
PV	Photovoltaics
PVGIS	Photovoltaic Geographical Information System
RE	Renewable Energy
RES	Renewable Energy Sources
RPM	Revolutions Per Minute
SDG	Sustainable Development Goals

SOC	State of Charge
STC	Standard Test Conditions
SWT	Small Wind Turbine
TSR	Tip Speed Ratio
UN	United Nations
UNESA	UN Department of Economic and Social Affairs
VAWT	Vertical Axis Wind Turbine
WPD	Wind Power Density
WT	Wind Turbine

LIST OF SYMBOLS

k	Weibull's dimensionless parameter
c	Weibull's scale parameter
a	Induction factor
C_P	Power coefficient
λ	Tip speed ratio
F_R	Rayleigh distribution function
$F(v)$	Weibull's distribution cumulative probability function
E_{pf}	Energy pattern factor
Re	Reynolds number
Z_o	Surface roughness
e	Charge of an electron
b	Wien's constant
σ	Solidity
α	Shear Exponent
Γ	Gamma function
δ	Declination angle
ε	Emissivity
μ	Fluid viscosity
ν	Kinematic viscosity
K	Boltzmann constant
C_T	Thrust coefficient

C_d	Drag coefficient
C_l	Lift coefficient
C_m	Pitch moment coefficient
ω	Angular velocity

ABSTRACT

Energy is a critical factor to society's economic growth. Increased energy demand has led to the usage of conventional energy sources such as coal, oil and natural gas, which pose ecological and health risks. Wind and solar resources are intermittent in nature, a condition that leads to fluctuations in their energies. Lack of continuous availability of these resources in nature has always brought stability challenges in power grids affecting the quality of electricity and lowering their reliability. Integration and optimization of wind and solar energy systems offer a solution. By integrating two or more energy resources through a hybrid technology, it is possible to minimize the effects caused by the intermittence of renewable energy resources. Much has been reported on solar and wind resources with little said on the viability of their complementary nature in low wind speed regime areas. This study aims at developing and optimizing a wind-solar hybrid energy system for electrification in low wind speed regimes where wind resource is rarely exploited to its full potential. Resource ground assessments were conducted using simulation and experimental methods. Wind distribution revealed Weibull's shape (k) and scale (c) parameter values of 1.9 and 3.22 m/s, respectively. A WPD of 17 W/m² at 20 m hub height and mean wind speed of 3.01 m/s has been reported. An average insolation of 5.84 kWh/m² at 1 kWp capacity is reported. Wind and solar were found to have good complementarity increasing their viability in hybrid energy systems. Energy demand has been conducted using field surveys to establish the average load demand necessary to inform on appropriate system size. The energy demand analysis revealed a daily range of 0.052 to 4.23 kWh, where a daily average energy load of 0.582 kWh is reported. Based on these findings, a wind-solar hybrid system was developed. Turbine rotor blades were made from Styrofoam and aluminum, with a pitching allowed for energy optimization. Wind tunnel tests were done to a maximum wind speed of 20 m/s to determine TSR and C_P at pitch angles between 0° and 40°. Analysis of the TSRs revealed a positively skewed pattern, implying good prospects for wind energy at low wind speeds. The foam blade performed best with a C_P of 0.465 at a pitch angle of 20° and a TSR of 2.1. The C_P translated to 238 W at a rated wind speed of 5 m/s. At a TSR of 1.9 and a pitch angle 15°, aluminum fared best with a C_P of 0.431 which translated to 220 W at 5 m/s. Foam blades are more suitable for use in rotor blade fabrications. Field tests was conducted which revealed good wind-solar power integration in spite of time and weather changes. Vertical shear analysis revealed greater wind energy productivity at higher altitudes, where hub heights between 8 m and 50 m revealed WPD between 20 W/m² and 79 W/m², respectively. The hybrid system produced 143 W of solar power and 36 W of wind power at 8 m, which translate to 0.835 kWh for 5.84 peak sun hours and 0.864 kWh daily, respectively. Shear analysis provided the rated turbine wind speed of 5.0 m/s at hub height of 50 m, with a daily energy potential of 5.4 kWh. The findings revealed that the hybrid energy systems are viable for installation in rural households and small-scale utilities. Small-scale micro-grids, mini-grids, utilities, as well as the research communities exploring hybrid energy systems, could benefit from the findings and knowledge gained from this study.

CHAPTER ONE

INTRODUCTION

1.1 Background Information

Any state's economic growth requires energy as a basic necessity. The amount of energy consumed worldwide is rising quickly; in 2022, it was 13393 TWh, up from 13004 TWh in 2021 (Wiatros, Motyka & Jones, 2022). Renewable resources (solar, wind, and hydro) provide about 28% of this demand, and their growth is rapidly accelerating (Wiatros *et al.*, 2022). The national energy demand in Kenya peaked in 2022 at 2056 MW, an increase of 3.2% from 1994 MW in 2021 (Energy and Petroleum Regulatory Authority [EPRA], 2022). This demand increase is always partly triggered by rising living standards, urbanization, industrialization, and population growth as was suggested elsewhere in a study by Saoke, Nishizawa, Ushiyama & Kamau (2015). Sustainable Development Goals (SDG) require increased energy from renewable sources and access to modern, cheap, and dependable energy amenities by 2030. As such, new energy generation techniques are necessary because conventional sources such as coal, oil and natural gas are limited and harmful to life. Climate change and global warming are two main impacts of these energy sources, which are partly caused by greenhouse gases (GHG) (Aslam-Bhutta, Hayat, Farooj, Ali, Jamil & Hussain, 2012). Continuous reliance on fossil energies is unprofitable and has recently raised concerns across the globe as GHG emissions rise (Kassem, Camur & Aateg, 2020). In terms of pollution, energy systems are major contributors of GHG emissions, responsible for raising the impact to new states of concern and uncertainty.

Zaekhan and Nachrowi (2015) reported on increased global warming, whose leading contributor is CO₂ from fossil fuels. The emission rates were 981 g, 755 g and 461 g per kWh for coal, mineral oil and natural gas, respectively (Zaekhan & Nachrowi, 2015). In Kenya, development of coal-based power plants has put pressure on various industries to make investments in carbon-reduction strategies. Geothermal productions rates of 122 gCO₂/kWh and 670–870 gCO₂/kWh for coal have been reported (Kahlen, Kirdziel, Day & Schiefer, 2019).

Sharma, Bojja and Yemula (2016) reported on CO₂ weighted average emission factor as prepared by Central Electricity Authority (CEA) in India where an emission factor of 0.82 tCO₂/MWh was reported based on the database (Sharma *et al.*, 2016; Bhawan & Puram, 2011). In Kenya, CO₂ emission rate of 0.5 tCO₂/MWh has been reported (EPRA, 2022). According to the EPRA (2022) report, CO₂ emissions have been fluctuating with electricity generation, the lowest and highest CO₂ levels being 480.51 and 547.76 thousand tons in February and May 2022, respectively. Solar panels and WT carbon footprints are significant but only during manufacturing process where solar panels produces 50 gCO₂/kWh while WT produces about 11 gCO₂/kWh (Wigness, 2023; Helman, 2021). Comparatively, fossil fuels release high CO₂ continuously during combustion while solar and WT generate close to zero level since they become carbon-neutral within the first three years of installation (Wigness, 2023). This insignificant CO₂ generation and neutrality after installation makes wind and solar systems promising in green energy generation. The high levels of carbon emission and the current environmental state raises red flags not only locally but also globally for a reversal trend in the modes of energy production.

To decarbonize the energy sector and meet the access to energy target, new energy production methods are vital (International Renewable Energy Agency [IRENA], 2022; Delbeke, Runge-Metzger, Slingenberg & Werksman, 2019; The World Bank, 2017). Conventional energy producing techniques can be replaced by renewable energy sources (RES), which are not only plentiful and limitless but also secure (Skretas & Papadopoulos, 2009). In view of these facts, accelerating energy transition into renewable based approaches of energy generation is imperative and urgent. This research offers practical solutions to guarantee access to inexpensive, dependable, and modern energy to everyone, as required in the SDGs (The World Bank, 2017; UN Department of Economic and Social Affairs (UNESA), 2016; International Institute of Sustainable Development (IISD), 2016). Thus, along with energy security and safety, a more comprehensive, equitable, and climate-resilient economy is promised (International Renewable Energy Agency [IRENA], 2022). Green energy innovations would produce a better Africa, as envisioned in African Agenda 2063, the Africa we desire, attracting improved living standards, good health, and well-being (African Union Commission, 2015). Kenya reiterated the Paris Agreement's goal of limiting the

average global temperature rise to 2°C. As such, the nation aims to cut GHG emissions by 32% nationally by 2030 through programs like boosting percentage of RES in the grid (EPRA, 2022).

By 2050, the world population is projected to reach 9 billion, which will result in increased demand for energy, food, water, and ecological destruction (Saoke *et al.*, 2015; Nishizawa, Shengning, Elson & Ushiyama, 2013). Kenya has a population of over 50 million, out of which over 15 million people live in the rural remote areas. Low population density and undeveloped economics have partly resulted to poor rate of electrification in the rural areas. Still with the grid connection in rural homes, electricity needs are unsatisfactorily met due to the high cost of electricity. Independent energy systems that rely solely on wind or solar power can hardly satisfy the nation's enormous energy needs. To provide amenities relying on electricity that are economical and sustainable, it is necessary to apply smart energy planning and technologies. This planning would speed up the creation of dependable energy systems that take into consideration local needs, priorities, and available resources. To modify the current systems, a hybrid smart technology which integrates multiple energy sources to support grids and standalone systems has been considered (Mukulo, Ngaruiya & Kamau, 2014).

These developments and decentralization of energy could ease access to energy in remote areas, reduce electricity crisis and lure related enterprises that provide employment opportunities to promote development and lifestyle improvement among local communities. Scientific advancements in energy harnessing technologies promote the African Union's 2063 agenda through proper utilization of the available and free natural resources and human capital for sustainable growth and development that is centered on human needs. The drive to meet the sustainable development goals has greatly increased public interest in renewable energy technologies (Adebayo, Layeni, Nwaokocha, Oyedepo & Folarin, 2019). With the immediate need for modern energy, exploitation of renewable energy sources using new extraction methodologies is necessary. This development will aid not only in power supply but also in reducing the negative effects of conventional sources, a matter of global concern in recent years as GHG emissions rise (Kassem, Camur & Aateg, 2020).

Wind and solar are two renewable energy sources among the most abundant, accessible, and clean. The two resources offer better ways to lessen energy shortages and environmental degradation. To this extent, the two sources are key ingredients to increasing the need for clean energy (Wekesa, Saoke & Kamau, 2020; Apunda & Nyangoye, 2017). According to Jayapriya, wind energy, which accounts for nearly 40% of all primary energy consumption, has recently become one of the RES mostly being explored (Jayapriya, Muruganandam, Raguraman, Senthilkumar & Dhinakaran, 2019). In addition, wind energy, which emits no direct emissions, is thought to be the most promising and quickly developing source of renewable energy (de Falani, Gonzalez, Barreto, de Toledo & Torkomian, 2020). As a result, wind systems would significantly lower carbon footprints and minimize pollution in the end (Evans, Strezov & Evans, 2009). According to Asim and his team, a substantial portion of the job sector has been greatly impacted by global scientific developments in wind (Asim, Islam, Hemmati & Khalid, 2022). Thus, wind energy remains preferable in the energy sector as the best complement to other renewable energy sources, particularly solar. According to the EPRA 2022 report, Kenya has a promising wind potential, with 73% of the country experiencing winds of 6 m/s or more at altitudes of 100 meters or higher (EPRA, 2022). Studies by Kamau, Kinyua and Gathua (2010), Saoke (2015), and Wekesa, Wang, Wei, Kamau and Danao (2015) reported that Kenya has a good potential of wind energy with class of over 7 in most parts of urban and rural environments thus viable for energy generation (Wekesa, Wang & Wei, 2016; Wekesa, Wang, Wei & Danao, 2014). In Kenya, hydroelectric power generation is quite unreliable due to the challenges facing most of the Sub-Saharan countries like drought attributed to global warming, deforestation and increased population among others. Power at times is rationed due to its insufficiency despite the countries efforts to provide energy access through plants like geothermal and diesel generators making the crisis persist (Wekesa, Wang & Wei, 2016). The unpredictability of weather conditions and the fluctuating cost of petrol and diesel fossil energies have greatly stimulated interest in renewable energies like wind and solar.

In low wind speed regimes, inadequate meteorological data on wind distribution in comparison to other renewable energy resources might have partly resulted to its low level of exploitation for energy production. In Kenya, information gathered by the

meteorological centers is majorly meant for other consumption like civil aviation and agriculture as opposed to wind energy generation. Recently, wind energy plants set-up in Kenya have proven to be reliable sources. Turkana power plant is one such example, which is the largest in the region, generating over 300 MW. Improper mapping of wind flow, low system design efficiencies, inaccurate location of plants in certain areas and long distances from the lines of transmission are among the major challenges that have hampered growth and development of these farms in Kenya (Wekesa, Wang, Wei & Danao, 2014; Wekesa, Mutuku & Kamau, 2012). Proper address of these key issues can be a turning point.

Solar is another suitable energy resource in the modern world which among possible options of generating renewable energy has proven to be sustainable, abundant and safe (Wiginton, Nguyen & Pearce, 2010). Solar is readily available with higher yields of around 2500 kWh/m² in East Africa (Tovey, 1992). In Kenya, the average daily solar insolation is 5 kWh/m², with ranges between 3.9 and 6.5 kWh/m² (Iakovleva, Guerra, Tsvetkov & Shklyarskiy 2022; Aboagye et al., 2021). These are indicators of good prospects for solar systems in the country. According to Reinhard, PV systems have the capacity to meet energy demands in populated areas while decongesting on urban power grid infrastructure (Reinhard, 2006). Solar thermal and solar photovoltaic energy are the two types of solar energy. Solar photovoltaic (PV) entails the conversion of sunlight into electrical energy, while solar thermal entails conversion of solar energy into heat energy. In this study, solar PV was of much interest (Kumar, Priyadharshini & Natarajan, 2015).

Complementarity is the alternate nature of energy resources in terms of their availability and energy potential. This concept is critical at the design phase of HES, since it minimizes unpredictability between any two renewable resources in their applications. According to Yang, the complementarity effect has promoted hybrid system development lately, making the technology more feasible in the 21st century (Yang, Wei & Chengzhi, 2009). Resources like wind and solar are very site-specific and intermittent in terms of their output. The development of hybrid renewable energy systems can make use of the two resources because of their complementarity as a workable solution to the challenge of their intermittence (Solomon, Child, Caldera &

Breyer 2020). Loads and distributed energy sources can work in tandem with the main grid power system to create a hybrid power system. The system may integrate a conventional source and RES, or purely RES (Lazarov, Zarkov & Bochev, 2005). Hybrid systems ensure reliability, affordability and security in local energy for both rural and urban sites, as well as narrowing the gap between power generation and power use on small scales. The hybrid technology enables integration of energy resources like wind, solar, hydro, biomass and other local resources. This integration can be realized using smart energy technology that allows dynamic control over a number of utilities, enabling autonomous and automatic operations in power systems. Such systems help in meeting the energy demands of a community in a way that fits the local geography and weather variations.

Wind and solar power generation is seasonally intermittent, on daily and hourly basis. Therefore, thorough resource assessment and analysis would be needed to determine the distribution and energy potentials of the two resource regimes before implementing a dual system supported by both. The hybrid energy system, which requires stable, dependable, and high-quality power generation, faces significant challenges as a result of resource variations. Utilizing the right technology to integrate wind and solar renewable resources would greatly minimize the impact of variability between the two resources and provide energy consumers with a sustainable supply of energy. These facts necessitate the application of hybrid technology to minimize the effect of renewable resource variations in power supply. With the climatic changes and the high level of energy demand, hybrid technology in energy production needs to be embraced. As a way to provide access to energy in remote locations where the establishment of a national grid is impracticable, hybrid renewable energy systems have gained popularity across the globe (Jha, Prashar, Rashid, Khanam, Nagpal, AlGhamdi & Alshamrani, 2022; Sanajaoba, 2019). Due to their availability, energy potential, and complementary behavior, wind-PV energies have proved better and feasible in hybrid energy systems advances. Wind and solar energy resources are homegrown and economical means of cutting down on energy bills and carbon emissions. This development eradicates the transient nature of energy production by single resource driven systems, introducing the generation of sustainable and reliable energy with zero negative effects. This study aimed to close the energy demand gap by hybridizing wind

and solar energies. In-depth assessments of wind-solar potentials for electricity generation were conducted for, examination of energy demand level, evaluation of wind-solar complementarity, and its viability in hybrid energy system (HES). These evaluations provided information on wind turbine integration with solar PV system for rural electrification.

1.2 Statement of the Problem

Today's globe suffers greatly from a lack of clean energy, which is also a resource that is essential for the economic growth of any society. Kenya still faces the challenges of insufficient, unsustainable and unreliable energy, particularly in rural and remote areas. Communities living in remote areas are partly isolated from the national grid due to topological factors, and so they lack access to the national electricity. High population in some areas triggers an increase in energy demand which is insufficiently met by the national grid. Other than topology, high installation cost, monthly bills and maintenance cost have partly caused the lack of grid connectivity in rural households, resulting in economic instability. The national grid is unable to fully meet and sustain the energy demand due to the rising population. As a result, most energy consumers rely on traditional energy sources like fossil fuels, which have negative impact on the environment and health. These conventional energy sources have attracted the attention of the world through the United Nations climate change conferences around the world (currently COP28) (Burnett, 2023; Erbach & Roniger, 2023). Such energy sources are leading contributors of GHG emissions, which are poisonous and hazardous to life. Global warming, pollution and climate change are among the leading effects of GHG, making the earth quite inhabitable.

Power outage as a result of unreliable energy generation systems has raised many complaints attracting the need for alternative sources of power. Single resource driven energy systems like solar are effective only during the day when solar is available, sudden change in weather conditions or cloud cover switches off power generation by solar systems. Low wind speeds in some areas make the wind resource unattractive in large-scale energy generation. This makes wind resource less exploited to its full potential.

Wind and solar resources have been reported to have good characteristics that make them good candidates for the production of energy. However, the two resources are highly intermittent and site-specific, a challenge that affects power generation and stability in grids. Intermittence makes power supply periodic, reducing the feasibility of wind and solar systems in the energy market. This current study sought to address the challenge of intermittence through resource integration and system optimization to create access to reliable energy in low wind speed regimes.

1.3 Justification of the Study

Research and acceleration of development in new and emerging low emission technologies which target alternative renewable resources which are reliable, less costly and safe to the ecosystem is a priority. About 800 million people in the world have zero access to energy. Out of this number sub-Saharan African has the highest number where people living in the rural making up the majority (EPRA, 2022). Sparsely populated regions hardly develop due to lack of power to run the basic facilities like health, schools and also for use in households. Off-grid stand-alone systems driven by renewable sources offer viable solution in mitigating the huge energy crisis in remote areas (Misak & Prokop, 2010). Challenges in the energy sector call for a reverse trend in the mode of energy production.

Wind and Solar renewable resources have attracted widespread attention due to their advantages. These resources offer a feasible resolution through hybrid technology. Wind and solar resources can be integrated due to their good complementarity behavior to reduce mismatch due to intermittency (Jurasz, Canales, Kies, Guezgouz & Beluco, 2020; Neto, Saavedra & Oliveira, 2020; Rosa, Christo, Costa & Santos, 2020; Jurasz, Beluco & Canales, 2018). Due to the limited studies on the complementarity of wind/PV systems in Kenya, there is a need to evaluate the viability of this characteristic in hybrid systems' development (Johannsen, Ostergaard & Hanlin, 2020). To provide alternative energy source by 2030, in line with the SDGs (The World Bank, 2017), lower global warming below 2.0°C as per the Paris Agreement (EPRA, 2022;The World Bank, 2017), and meet the African Union's Agenda 2063's No. 1 Aspiration, geared towards ensuring Africans' quality of life and sustainable development (African Union Commission, 2015), research in renewable energy

technologies is indispensable. In this study, free and readily available wind and solar energy provide significant research motivation into their integration technology. Thus, wind and solar complementarity with the right harnessing technology could unlock the two resource potentials increasing their viability in energy production.

1.4 Objectives

1.4.1 Main Objective

To develop a wind-solar PV hybrid energy system for small-scale rural electrification in low wind regime areas in Kenya.

1.4.2 Specific Objectives

1. To determine wind/solar resource energy potentials and their complementarity in Machakos for establishment of the local wind/solar characteristics and their viability in hybrid power system.
2. To analyze energy utilization levels for the determination of the appropriate hybrid system size for a rural household in Machakos.
3. To design and fabricate a horizontal axis wind turbine for hybridization with solar PV for site specific optimization.
4. To carry out field tests on the designed wind-solar PV hybrid system to evaluate its performance characteristics.

1.5 Research Questions

- i. Are the wind-solar resource energy potentials and complementarity characteristics viable for wind-solar hybrid energy system installation in Machakos?
- ii. What is the average energy demand and daily load profile for a rural household in Machakos which would inform a proper energy system size?
- iii. What would be the most appropriate HAWT design to optimize energy in low and varying wind speed regimes to satisfactorily meeting the load requirement of a rural household in Machakos?
- iv. What would be the field power performance characteristics of the designed wind-solar PV hybrid system?

1.6 Conceptual Framework

This study's goal was to design and optimize flexible HES from wind and solar PV integration to power of a typical rural household in Machakos, Kenya. Prior to designing and putting into place the proposed system, the wind and solar regimes were assessed to ascertain their level of complementarity, energy potential, and viability. The average house load was determined, which informed on component sizes. Last but not least, a horizontal axis wind turbine was fabricated and hybridized with solar PV based on the assessment's findings. To characterize the power performance behavior of the developed hybrid energy system. A field test was undertaken. Figure 1.1 shows a flow chart that outlines the study activities. There are five chapters in this thesis. The introduction is covered in chapter one. This section includes the study's background, theory, research questions, objectives, problem statement, study justification, and conceptual framework. The literature review is covered in chapter two and includes prior studies that are pertinent to this study, as well as the underlying theoretical ideas. Much focus is given to wind and solar system design and hybridization, which ends in development of an optimized wind-PV hybrid energy system suitable for areas like Machakos. Chapter three provides a description of the procedures and materials employed to achieve the goal of this study. Much focus was on the evaluation of wind and solar resources potential, energy demand analysis, design, optimization, and development of the wind-solar PV hybrid system. In relation to the research questions and study objectives, chapter four presents and discusses the research findings. Chapter five summarizes the study's accomplishments and offers suggestions for areas to concentrate on in subsequent research on this topic.

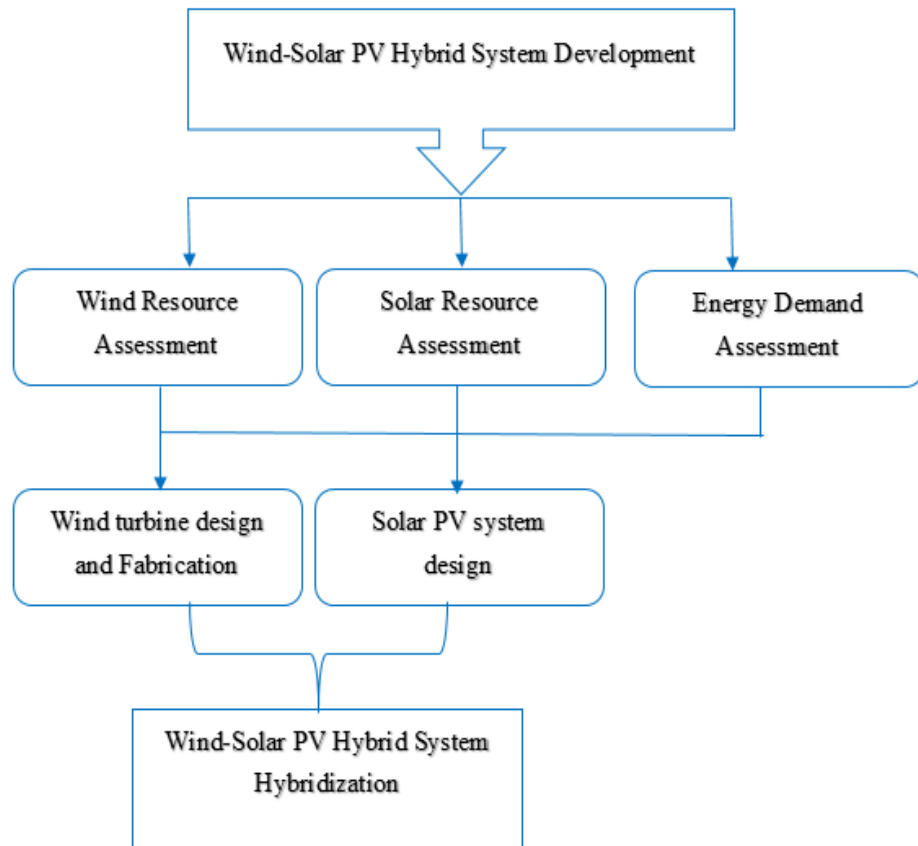


Figure 1.1: Block Diagram of the Conceptual Framework

CHAPTER TWO

LITERATURE REVIEW

2.1 Introduction

This chapter consists of three sections, theoretical principles, previous studies related to this current study and the research gaps. Fundamentals in wind/solar resource characteristics, study assessments, aerodynamic characteristics as well hybrid system configuration are presented.

2.2 Theoretical Principles

This section describes the characteristics of wind and solar resources, assessments of solar PV and wind turbine systems, energy demand evaluations as well as wind/solar hybrid system configurations.

2.2.1 Wind Resource Characteristics

The periodic nature of wind can be revealed by analyzing the wind distribution of a certain site across time. The energy density, wind speed, and Weibull's distribution parameters are only a few of the wind parameters that are discussed. The wind speed distribution can be described by Weibull's models provide in Equations. (2.1) and (2.2) (Manwell, McGowan & Rogers, 2010);

$$f(v) = \frac{k}{c} \left(\frac{v}{c}\right)^{k-1} \exp\left[-\left(\frac{v}{c}\right)^k\right] \quad (2.1)$$

$$F(v) = 1 - \exp\left[-\left(\frac{v}{c}\right)^k\right] \quad (2.2)$$

where $f(v)$ represents the wind speed likelihood, c the scale parameter in m/s and k the shape parameter. $F(v)$ represents the Weibull's distribution's cumulative probability function. Equation (2.3) displays the Weibull's model's special case for the Rayleigh distribution function $F_R(v)$ at $k = 2$. (Arikan, Arslan & Cam, 2015);

$$F_R(v) = \frac{2v}{c^2} \exp \left[-\left(\frac{v}{c}\right)^2 \right] \quad (2.3)$$

A linear fit of Equations (2.2) would be required in order to calculate the k and c parameters. Equation (2.4) is the result when the natural logarithms of Equation (2.2) are taken (Ulgen & Hepbasli, 2002) ;

$$\ln \left\langle -\ln [1 - F(v)] \right\rangle = k \ln(v) - k \ln c \quad (2.4)$$

Equation (2.4) generates a linear model with a y intercept of $-k \ln c$ and a gradient of k , from which c can be derived. It is possible to estimate c and k factors using Equations (2.5) and (2.6), which connect the energy pattern factor (E_{pf}) to the mean wind speeds obtained by Equation (2.7) (Manwell *et al.*, 2010; Indhumathy & Sukkiramathi, 2007);

$$k = 1 + \frac{3.69}{(E_{pf})^2} \quad (2.5)$$

$$c = \frac{v_m}{\Gamma \left(1 + \frac{1}{k} \right)} \quad (2.6)$$

$$E_{pf} = \frac{(v^3)_m}{(v_m)^3} = \frac{\frac{1}{n} \sum_{i=1}^n v_i^3}{\left(\frac{1}{n} \sum_{i=1}^n v_i \right)^3} \quad (2.7)$$

Where Γ is gamma, v_m is the mean wind speed, v is the wind speed, n is the number of wind speed data points. Wind speed is affected by tower height, a condition known as wind shear (Jha, 2011; Manwell *et al.*, 2010). Studies have shown that wind speed and installation height above the earth's surface affect power generation capacity of a wind turbine. Due to surface roughness, wind experiences opposition to flow across the earth's surface. This resistance is majorly caused by turbulence around obstacles like mountains, hills, trees, buildings and rocks. The effect decreases with height until non-obstructed air flow is restored. The rate of wind speed increases as turbulence decreases depending on the degree of surface roughness. A standard height of 10 meters is used to install the majority of meteorological equipment (Kamau *et al.*,

2010). However, for better wind energy yields, installation at higher heights is necessary despite the cost. Thus, wind shear offers an opportunity for higher wind speeds and permits the deployment of larger turbine blades, increasing systems power output significantly (Jha, 2011). Increase in wind speed with height is not constant, in times of temperature inversion during calm wind atmospheres, wind speeds increase to a certain height and then begin to decrease (Jha, 2011). Moreover, temperature in different layers of the atmosphere changes with height, leading to change in wind speeds. Wind power estimation at higher heights can be done using extrapolation methods. Logarithmic and power law methods are frequently employed (Manwell *et al.*, 2010; Ray, Rogers & McGowan, 2006). The logarithmic law is provided by Equation (2.8), where z and z_r represent the new and reference heights, respectively. The new and reference wind speeds are $U(z)$ and $U(z_r)$, respectively, and the roughness length is z_o (Ray, Rogers & McGowan, 2006);

$$\frac{U(z)}{U(z_r)} = \frac{\ln\left(\frac{z}{z_o}\right)}{\ln\left(\frac{z_r}{z_o}\right)} \quad (2.8)$$

Vertical shear is characterized by surface roughness (z_o), where z_o is the altitude with wind speed hypothetically at 0 m/s. Surface roughness is dependent on the geography of a place. Wind speed cannot always be extrapolated using the logarithmic rule because the law is indefinable when the speed is the same at different heights. Therefore, to overcome this limitation, the power law provided in Equation (2.9) serves as the commonly used shear model (Arikan *et al.*, 2015);

$$\frac{U(z)}{U_r(z_r)} = \left(\frac{z}{z_r}\right)^\alpha \quad (2.9)$$

where U and U_r are wind speeds at heights z and z_r , respectively, while α is the shear exponent. Shear exponent is a coefficient that varies from 0.10 to 0.4 for flat and urban locations, respectively, with tall buildings depending on factors like atmospheric stability and surface roughness. Shear exponent can be approximated using Equation (2.10) (Ray *et al.*, 2006);

$$\alpha = \frac{1}{\ln\left(\frac{z}{z_0}\right)} \quad (2.10)$$

Given the existing scenario, an exponent value of 0.1429 has frequently been chosen for neutral stability (Gerard, 1958). Table 2.1 provides power law exponent values at different terrains (Anjum, 2014; Ray *et al.*, 2006).

Table 2.1: Power Law Exponents and Different Terrains (Ray *et al.*, 2006)

Landscape Description	Exponent, α
Lake, ocean, or a smooth, hard surface	0.10
Sparse vegetation on bare terrain	0.14
Level terrain with some trees and foot-high grass.	0.16
Long rows of crops. Trees and hedges	0.20
Several trees and few buildings	0.22-0.24
Wooded countryside, suburbs and small towns	0.28-0.30
Crowded cities with tall building	0.4

Based on this literature, the power law technique was used in this study with an assumed shear exponent value of 0.25 as the system installation and test were done at IEET, JKUAT, an area characterized by many trees and buildings. Wind power is a cubic function of wind speed, thus, wind power and hub height are connected using Equation (2.11) (Jha, 2011; Masters, 2004).

$$\frac{P}{P_r} = \left(\frac{H}{H_r}\right)^{3\alpha} \quad (2.11)$$

where P denotes power at a new height H , P_r denotes power at a reference height H_r , and α denotes the shear exponent.

Wind power density (WPD) is the amount of power per unit area perpendicular to the wind direction, given by Equation (2.12) (Letcher, 2017);

$$WPD = \frac{1}{2} \rho v^3 \quad (2.12)$$

Where ρ is density of air and v is the wind speed. The maximum power available for a given rotor area P_A can thus be determined using Equation (2.13), (Letcher, 2017; Keshavan, Ramu & Sankar, 2016) ;

$$P_A = \frac{1}{2} \rho A v^3 \quad (2.13)$$

where A is the rotor's sweep area, v is the wind speed, and ρ denotes the air density. Wind power is harvested based on wind speed, with cut-in and cut-out wind speeds, between which the best power is obtained. Decrease in exit velocity v of wind results when a turbine is used in harvesting the energy at velocity u . The same mass of air leaves the plane of the turbine as it comes, and therefore it expands on leaving the turbine causing expansion of the flow tube. Equation (2.14) can be used to compute the yearly and monthly WPD (P_w) for a particular location based on the Weibull's PDF (Adeyeye, Ijumba & Colton, 2021)

$$P_w = \frac{1}{2} \rho c^3 \left(1 + \frac{3}{k} \right) \quad (2.14)$$

where ρ is air density, c is the Weibull's scale parameter and k is the shape parameter. The c and k parameters are related to the mean wind speed (\bar{v}) as illustrated in Equation (2.15) (Ulgen, & Hepbasli, 2002);

$$\bar{v} = c \Gamma \left(1 + \frac{1}{k} \right) \quad (2.15)$$

where Γ is gamma. When the value of k is 2 for the Rayleigh density function, power density (P_w) is given by Equation (2.16);

$$P_w = \frac{3}{\pi} \rho v_m^3 \quad (2.16)$$

where v_m is the mean wind speed and ρ is air density. As a result, wind power is proportional to the cube of wind speed and air density. More energy will be extracted

in a more dense air near the sea level than at higher elevations, since density is highly dependent on elevation and temperature. The Betz limit, which is 0.593 of the total wind energy as shown in Equation (2.17), restricts the amount of power (P_E) extracted from the wind resource. Notably, even for the most advanced turbine designs, real-life C_P values range between 0.35 and 0.45 (Twidell & Weir, 2015);

$$P_E = \frac{1}{2} \rho A v^3 C_P \quad (2.17)$$

Annual energy output (AEO) can be calculated using Equation (2.18) (Udoakah & Ikafia, 2017),

$$AEO = \frac{1}{2} \rho A U^3 C_P (8760 \text{ hrs} / \text{ yr}). \quad (2.18)$$

2.2.2 Solar Resource Characteristics

The sun is an unlimited source of energy that can be directly or indirectly harvested (Timilsina, Kurdgelashvili & Narbel, 2012). Two technologies are used to harvest sunlight and heat from the sun, namely: passive, which uses solar energy directly without conversion, and active, which transforms solar energy into photovoltaic or solar thermal energy (Ullah, Saidur, Ping, Akikur & Shuvo, 2013).

Solar energy from the sun, which takes the form of electromagnetic radiations, is referred to as solar radiation. Depending on the radiation wavelength, a medium can absorb, transmit, or scatter the light from the sun. Solar radiation can be measured in two different ways: solar irradiance, which is the instantaneous solar radiation in a given area expressed in W/m^2 , and solar insolation, which is the cumulative solar radiation of a given area over time expressed in kWh/m^2 . The relationship between solar irradiance and solar insolation is shown in Figure 2.1. The average daily global insolation under clear skies is $5 \text{ kWh}/\text{m}^2$, but the average solar energy reaching the earth's surface is $1 \text{ kW}/\text{m}^2$.

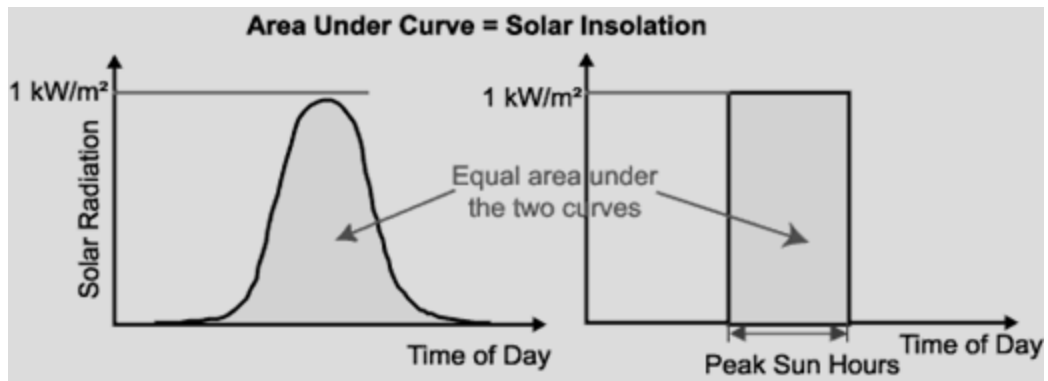


Figure 2.1: Relationship between Solar Insolation and Solar Irradiance

(Honsberg & Bowden, 2019)

Direct normal irradiance (DNI), diffuse horizontal irradiance (DHI), and global horizontal irradiance (GHI) are the three forms of sun radiation that are transmitted (Stoffel, Renne, Myers, Wilcox, Sengupta, George & Turchi, 2012). DNI is visible from a 5° field of view on a surface leaning perpendicular to the sun's direction and reaching the ground without scattering. A Pyrheliometer, as shown in Figure 2.2 (a), is used to measure DNI. Pyrheliometer DHI is the percentage of solar radiation that is reflected from a horizontal surface by airborne atoms and molecules. A shaded Pyranometer is utilized to measure this component. GHI is the combination of DNI and DHI on a horizontal surface related through the solar zenith angle. Figure 2.2 (b) shows an unshaded Pyranometer is used to measure GHI. These instruments work under the principle of Seebeck effect, an effect that occurs when voltage difference is produced between two electrical conductors at different temperature. The electrical signal is converted and recorded as watt per square meter (Keshavan *et al.*, 2016). GHI can be used together with DNI and DHI to approximate the amount of solar radiation on a solar collector.

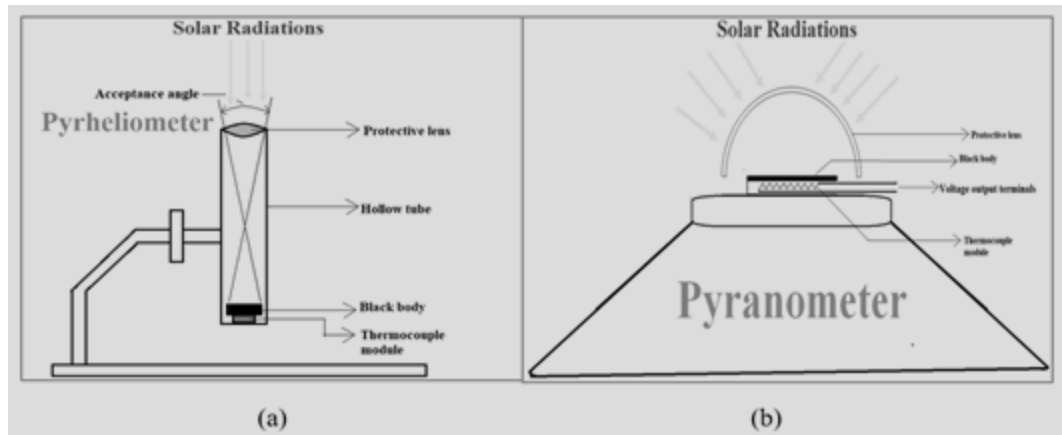


Figure 2.2: (a) Pyrheliometer used to Measure DNI and (b) Pyranometer for Measuring GHI (Raja, 2019)

The quantity of electromagnetic energy that strikes the ground surface from the sun is known as solar insolation (Beckman, Blair & Duffie, 2020). The globe experience various seasons as the earth revolves around the sun because of its elliptical nature. During summer solstice in the Southern Hemisphere, the earth is approximately 1.47×10^{11} m from the sun. The sun declination angle is -23.5° , on the tropic of Capricorn on December 22nd. All the Southern Hemisphere locations experience increased solar intensity due to sun's proximity. The winter solstice occurs in the Southern Hemisphere in June 21st when the earth is furthest from the sun, about 1.52×10^{11} m (Beckman *et al.*, 2020). The sun is high in the sky, shining at the tropic of cancer, with a declination angle of 23.5° . The Northern Hemisphere experiences high solar intensity, while the Southern Hemisphere Experiences low solar intensity (Kothari, Kaushik & Panwar, 2009).

According to Johnson, solar radiation's intensity decreases as it moves away from the sun. When the sun is farthest from the earth, the solar intensity that reaches the planet is at its lowest, and when it is closest to the planet, it is at its highest. The inverse square relation is provided by Equation (2.19) (Johnson, 2012);

$$I = \frac{P}{4\pi r^2} \quad (2.19)$$

where I is intensity, P is total power in watts radiated from the source, and r denotes the source distance in metres.

More energy is anticipated during hotter seasons of the year. Absolute temperature affects the wavelength and energy of radiations that are released. This phenomenon is described by the Wien's and Stefan-Boltzmann radiation laws, which are given in Equations (2.20) and (2.21) (Marr & Wilkin, 2012);

$$\lambda_{\max} = \frac{b}{T} \quad (2.20)$$

$$E = A\sigma\varepsilon T^4 \quad (2.21)$$

Where A denotes the surface area, b denoted the Wien's constant, T denotes the absolute temperature, λ is the wavelength σ represents the Stefan-Boltzmann constant, and ε is the emissivity constant.

According to Rathod, Mittal and Kumar (2017), the amount of solar radiation that reaches the earth's surface is dependent on the environment, time of day, local features, ecological and biological processes, human activities, and surface inclination. Additionally, from the perspective of PV technology, the quantity of solar insolation that strikes a surface also fluctuates according to the sun's location, the earth's declination angle, the latitude angle, the zenith angle, the azimuth angle, and the sun's hour angle (Beckman *et al.*, 2020; Šúri, Huld, Dunlop & Ossenbrink, 2007). The declination angle, denoted by δ , is the incline of the Earth's around the sun, which varies from -23.5° to 23.5° in a year. The declination angle can be computed using Equation (2.22) (Kaushika, Mishra & Rai, 2018; Karafil, Ozbay, Kesler & Parmaksiz, 2016; Cengiz & Mamis, 2015). Latitude is the angle made by the projection of the line on the equatorial plane with the radial line joining the site to the centre of the earth. It varies from -90° to $+90^\circ$. Azimuth is the angle on the horizontal plane between line due south and the projection of normal to the surface on the horizontal plane. Measure from south. Positive towards east. South is 0° , east $+90^\circ$, west -90° and north 180° or -180° . Zenith is the angle between the sun rays and the vertical direction, complement to the solar altitude angle. The angle between the location's longitude and the longitude of the sun is known as the hour angle (ω). It is provided by Equation (2.23). Angles before and after noon are (-) and (+), respectively. At noon, the hour angle is zero (Kaushika *et al.*, 2018; Karafil *et al.*, 2016);

$$\delta = 23.5 \sin \left[\frac{360}{365} (284 + n) \right] \quad (2.22)$$

$$\omega = 15(t_s - 12) \quad (2.23)$$

where n denotes the day in a year beginning with the 1st of January and t_s represents the hour of the day.

The solar position at any given time and season of the year influences how much solar insolation reaches the panel surface. The perspective at which solar reaches a specific location affects the solar panel's orientation for best energy harvest (White, 2018). These components and solar angles are responsible for the diurnal and seasonal fluctuation of the solar resource. These qualities compel the requirement for an appropriate supplementary resource for integration in its energy generation applications.

2.2.3 Site Assessment

Before installing a system, it is important to conduct a site assessment to assess the strength, viability, and availability of the RES. Some RES like wind and solar are highly intermittent in space and time. For a good site, several factors need to be considered. For the solar system, factors like solar angles, peak solar hours, shading caused by topographical features, clouds, structures, and trees must be put into consideration. Such features influence the absorption of solar radiation by a PV, slowing down the rate at which they generate electricity.

As earlier discussed in section 2.2.2, the magnitude of solar insolation received on the ground's surface is determined by sun angles. These angles include, the tilt angle, latitude, azimuth, and zenith, all of which must be analyzed for a site's potential and dependability for solar electricity. Peak sun hours (PSH) are the hours in a day when a location receives the maximum solar irradiation (peak sun) at standard test condition (STC) (White, 2018). PSH determines a PV system's size in relation to a given daily load demand. For sites located in the equatorial zone, a nearly average daily insolation is received. As a result, the solar module fixed option was preferred to the tracking option, which is mostly used in locations further from the equator.

2.2.4 Energy Load Assessment

A specific site's or household's load estimation must be accurate and use the proper load profiles. System sizing is carried out as the bare minimum necessary to provide the daily energy load. This assessment considers the total number of household appliances in use, their rated power, and the active appliance hours per day. The total energy consumed is calculated by adding the products of the rate in watts and the number of hours (watt-hours). When evaluating the best PV system, the total daily watt-hours (Wh) provided the daily load.

2.2.5 Solar PV System Assessment

Solar-PV systems actively convert sun radiations into electrical energy. Its design is based on a number of considerations namely; available solar radiation, daily energy load, the amount of energy backup needed and the type of power needed (DC or AC) (Goswami, 2015). There are two types of energy systems: stand-alone and grid-connected. Figure 2.3 shows the layout of a stand-alone solar system. While detached systems are beneficial for producing power in isolated places, grid-connected are commonly employed as power sources in urban areas. These two systems can power a single home or a large village. Even though battery systems are the best storage options for stand-alone systems, they are expensive to purchase and maintain.

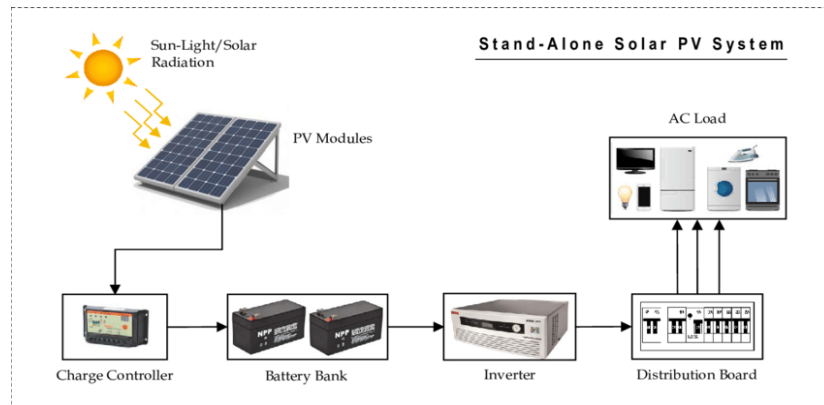


Figure 2.3: Solar PV energy system architecture (Ali, Awais, Farooq, Jamis, Rehman & Noman, 2019)

In order to protect batteries from the effects of charge-discharge, it is necessary to operate them under ideal conditions. Due to their lower cost and longer lifespan, lead acid batteries have been utilized in standalone PV systems and have performed well (Jossen, Garche & Sauer, 2004). In this study, a standalone solar PV system was taken into consideration for hybridization to provide solar energy to a rural household.

2.2.6 Solar PV System Component Sizing

Sizing is the process of determining the best current and voltage values for a power system components to satisfy the energy requirements of a specific facility or a household (Al-shamani, Yusof, Othman, Mat, Ruslan, Abed & Sopian, 2013). System performance is strongly dependent on climatological conditions at a given site (Lasnier & Gan , 2017). In sizing, the need for system reliability and economic concerns are thus two influential factors to avoid an undersized or oversized system. For any suitable wind/PV hybrid system, an optimal system sizing approach is necessary. The ratings and quantities of solar panels, batteries, inverters, and charge controllers that make up a hybrid wind-solar PV system must be determined for a specific installation based on local energy demand models, wind speeds and solar radiation data (Ariyo, Famutimi, Olowu, Akintade & Abbas, 2016).

2.2.6.1 PV Module

A PV module is a group of solar cells in a sealed unit that convert photons into electricity (White, 2018). PV modules are manufactured, and their specifications provided under standard test conditions (STC) corresponding to one atmosphere and solar irradiation value of 1000 W/m^2 at 25°C (Benghanem , Haddad, Azahrani *et al.*, 2023). Solar module specifications include: short circuit current (I_{SC}), open circuit voltage (V_{OC}), maximum output current (I_{max}), maximum output voltage (V_{max}), maximum output power (P_{max}), module efficiency (%) and the temperature coefficient ($\%/^\circ\text{C}$).

Monocrystalline, polycrystalline, and amorphous silicon are the most prevalent types of silicon used in PV technology. Monocrystalline is more efficient with an average of 16% to 23% whereas polycrystalline are slightly less efficient with an average of 13% to 16%. (Elsayed, Elsamhay, Haggag *et al.*, 2022). The difference between the two modules is not significant, since monocrystalline is more expensive and has a higher carbon footprint (White, 2018). Amorphous silicon has the lowest efficiency of between 5% and 7% (Kaushika et al., 2018). In this study, polycrystalline module was used due to its low cost and carbon footprint. PV modules are rated at STC, however, real-world variations in temperature and solar irradiance brought on by shading from clouds, buildings, trees, and other physical features may make these conditions less than ideal. Solar panels can be joined to form a larger array which produces the desired voltage or current. Equation (2.24) was used to calculate the actual PV system capacity in kW expected from the PV array. This is the ratio of daily household demand in kWh to the location's PSH. The size is scaled up by 30% to account for losses in the system (White, 2018; Masters, 2004);

$$\text{System capacity} = \frac{\text{Daily demand in kWh}}{\text{Solar peak hours (Average daily solar insolation)}} \quad (2.24)$$

PV modules are rated in watts with a tolerance of between 0 to 5% at a cell temperature of 25° . Dirt build up still reduce the PV output depending on the location. The accepted dirt derating factor is up to a maximum of 5%. Derating is also done with respect to ambient temperature. The output voltage reduces when temperature rises

above 25° and increases for temperatures below 25°(White, 2018). To account for temperature losses, tolerance losses and dust losses, the size of the panel size is always increased by 30%. Equation (2.25) can be used to calculate the number of panels necessary to meet a given load by comparing the actual system capacity to the panel rating (White, 2018; Masters, 2004);

$$\text{No of solar panels} = \frac{\text{System capacity}}{\text{Panel power rating}} \quad (2.25)$$

2.2.6.2 Storage System

This system element is necessary to store energy for use when the solar panel is unable to provide enough power to the load (Ariyo *et al.*, 2016). This occurs at night and in overcast weather. Size requirements for batteries are based on load capacity and backup power requirements (Akikur *et al.*, 2013). By preventing strain during the worst cases of sunlight, battery sizing helps to prolong the battery life. The two main types of batteries are lithium-ion (watt-hour capacity) and lead-acid (ampere-hour capacity). For small standalone PV systems, lead acid accumulators are more common and are therefore preferred. They are more affordable, readily available locally, and have a higher charging efficiency. In order to account for the days of autonomy, lead-acid batteries should be sized up by a factor of 2 to 5 depending on the load, since they can only be discharged to a maximum of 50% of their capacity. Capacity of a battery is affected by parameters such as inverter size, efficiency, total appliance load, autonomy days, depth of drain (DOD), and nominal voltage. The battery capacity can be calculated using Equation (2.26) (Masters, 2004);

$$\text{Battery capacity} = \frac{\text{Energy load Wh} \times \text{Days of autonomy}}{\text{Nominal voltage} \times \text{DOD} \times \text{Efficiency}} \quad (2.26)$$

where the DOD is the level to which the battery can be drained, while days of autonomy are the days the battery can last without recharge under poor sunlight conditions. Batteries have recommended maximum DOD from the manufacture. Draining batteries beyond this recommendation makes them lock up hence destroying them. PV system requires determination of the actual voltage depending on the system size and total energy consumption. Batteries are commonly supplying power in 12, 24

or 48 volts small, average and large loads, respectively. This study involved small-scale energy application and thus 12 V battery was applicable.

2.2.6.3 Inverter

An inverter is used to convert DC to AC in order to power the household's AC appliances. A system's inverter input should always be greater than the sum of its appliances' wattage while maintaining the same voltage as the battery. This component capacity should be sufficient for a standalone system to handle the total power used at any given time; ideally, as a safety measure, it should be 25–30% higher than the total appliance wattage (Ariyo *et al.*, 2016). The inverter size can be determined using Equation (2.27) (Ariyo *et al.*, 2016; Masters, 2004);

$$\text{Inverter size} = 1.25 \times \text{Total appliance wattage} \quad (2.27)$$

2.2.6.4 Hybrid Charge Controller

This component controls the current and voltage from WT and PV to the battery. It accommodates varying wind velocities as well as low- or no-irradiance conditions, such as cloudy, rainy, and nighttime days. By making sure the battery is not overcharged or deeply discharged, it increases battery life (Al-shamani *et al.*, 2013). It monitors the maximum power point to ensure that the subsystems receive and expend power as efficiently. A charge controller's voltage rating should be more than the panel's open circuit voltage, and its current rating should be equal to the panel's short-circuit current up-scaled by 30% safety factor. As a result of this capacity, it can withstand currents from the turbine and PV systems. The controller size can be determined using Equation (2.28) (Masters, 2004);

$$\text{Controller rating} = 1.3I_{SC} \quad (2.28)$$

Where I_{SC} is the PV short circuit current.

2.2.7 Maximum PowerPoint Tracking (MPPT)

Wind and solar energies are highly intermittent in nature. The WT generator's best speed must be maintained to extract maximum energy from the turbine (Malik *et al.*,

2020). A location's solar irradiance varies according to time, cloud and mountain shading effects, and other physical factors. Due to these fluctuations, wind and solar power systems produce non-linear power outputs (Singh, Vinary, Balyan, Gangadhara & Prabhu, 2021). In order to ensure maximum energy capture from turbines and solar panels at varying solar irradiance and wind speeds, the systems ought to operate at their maximum power points (MPP), which is shown in Figures 2.4 and 2.5, respectively. (Singh *et al.*,2021; Pande, Nasikkar, Kotecha & Varadarajan, 2021; Mousa, Youssef & Mohamed, 2019).

Since solar and wind energy systems produce power at various frequencies, a step-up system was required to match their outputs with the battery. This synchronization is accomplished with the help of a Maximum PowerPoint Tracking (MPPT) controller. A wind turbine's rotational speed can be modified with the help of a hybrid controller to provide the best TSR and maximum C_P throughout a wide range of wind speeds.

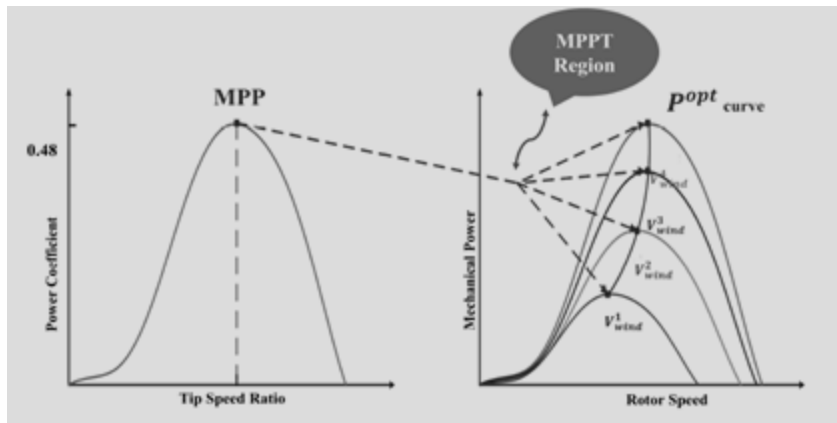


Figure 2.4: Wind Turbine MPP at Optimum TSR (Mousa et al., 2019)

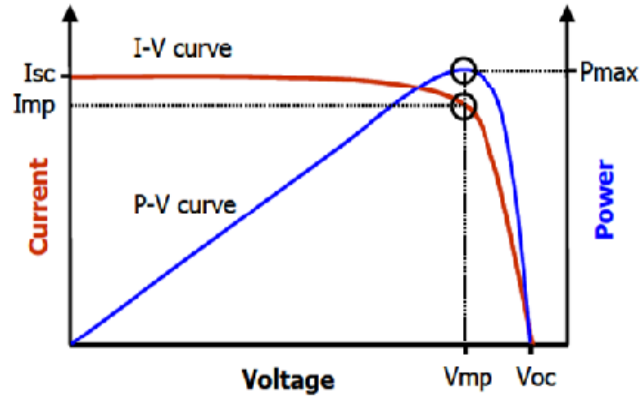


Figure 2.5: Solar Panel I-V Characteristics showing the MPP (Singh *et al.*, 2021)

Additionally, it modifies the voltage and currents from the solar panels, whose output is depended on meteorological conditions, the wind generator, and the battery bank. MPPT controller converts DC into high-frequency AC before converting it back to another DC value to precisely match the panels with the batteries. Therefore, by adjusting the initial PV voltage and the initial rotor speed for equivalent outputs, the controller aids in increasing the system's efficacy. A DC-to-DC boost converter is used to increase voltage from solar and wind systems. A diode, transistor, and a capacitor or an inductor serve as the converter's storage elements. A switching transistor's duty cycle is modulated by a buck converter, a DC to DC component, to keep a constant output DC bus for both PV and WT generators (Singh & Sharma, 2018). Matching output voltages are obtained by controlling the buck-boost duty cycles set using the Proportional Integral Controller (PIC). Equations (2.29) and (2.30) give the output voltages of the boost and buck converters, respectively (Almi, 2014);

$$V_0 = \frac{1}{1-\alpha} V_i , \quad (2.29)$$

$$V_0 = \alpha V_i , \quad (2.30)$$

where α is the varying duty ratio, V_i denotes the input voltage, and V_0 denotes the output voltage As stated by (Badwawi *et al.*, 2015), voltage converters play a vital role in improving DC or AC power. By ensuring maximum power harvest from the two

renewable resources, the MPPT controller enables the hybrid energy system to operate at MPP.

2.2.8 Wind Turbine System Characteristics

Wind energy is transformed into electrical form by use of a WT (Shankar & Kumar, 2019; Jayapriya *et al.*, 2019; Wolfram, Shelef & Gertler, 2012). A WT changes a portion of wind's mechanical energy into rotational motion which drives a generator to produce electricity through electromagnetic induction (Bianchi, De Batista & Mantz, 2006). Wind turbine rotors can be propelled by the drag or lift forces created by the interactions of the wind. The interaction between wind and rotor is therefore crucial for the system to generate power. Depending on the axis orientation, WT can be categorized as either VAWT or HAWT. A diagram showing sections of a HAWT is shown in Figure 2.6.

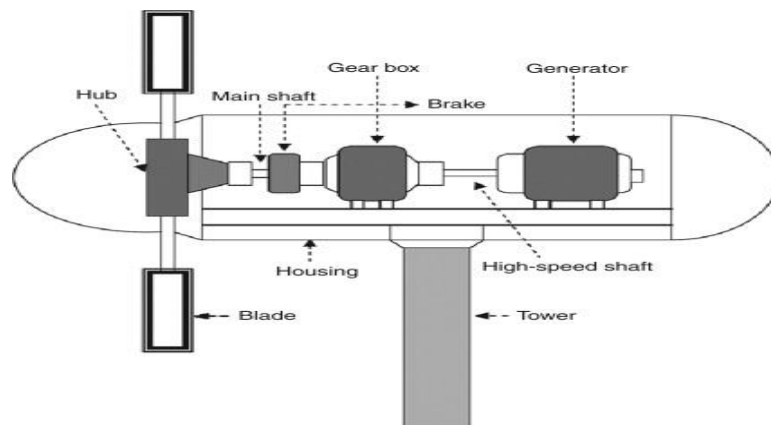


Figure 2.6: Components of a HAWT System (Elprocus, 2020)

Because VAWT's generator and transmission are at ground level, they can access energy coming from all directions without yawing. Due to their interception with the low energy wind speeds, their disadvantage is that they generate little energy. Their use has significantly decreased due to their expensive maintenance requirements. Turbines with horizontal axis have their rotors up top, where the wind has the most energy. Additionally, the turbines have a yaw machinery that turns the propeller and nacelle to face the direction with the strongest wind, capturing as much energy as possible. In this study, a HAWT was considered for the application. In practice, energy

transformation by HAWT designs make use of airfoils whose performance is depended on the blade shape and airfoil characteristics (Manwell *et al.*, 2010).

The HAWT system consists of a rotor (blade and hub), shafts, gear system, tower and a generator. The rotor which is made up of blades and hub changes wind speeds into rotatory motion. Blades are parts that generate torque from wind necessary to drive the generator. The hub connects the blades to the main shaft, which links the rest of the drives. There are three different kinds of hubs: rigid, teetering, and hinged hubs. While tethering hubs permit relative motion between the parts that connect the blade to the main shaft, rigid hubs keep their blades fixed to the main shaft. Hubs with hinges enable flapping motion in relation to the plane of rotation. Rotors can have one, two, three, four, or more blades. Since the moment of inertia is lower in a vertical position than it is in a horizontal position, single bladed rotor designs are impractical because they throw the rotor out of balance. Therefore, a counterbalance is always needed on the rotor to lessen vibration. Two-bladed rotors are robust and easy to design, but in recent years, three-bladed rotors have gained popularity due to their advantages over two-bladed rotors. When the system turns or yaws, three blades ensure uniform stress distribution. Three-bladed rotors, as opposed to two-bladed rotors, create constant centrifugal force, against which the tail smoothly glides to alter the turbine's direction (Manwell *et al.*, 2010).

The main shaft, which transmits torque from the rotor to the gearbox, is a low-speed shaft held using bearings. A gearbox is a part that quickens the generator's input shaft's rotational speed. Because of the varying wind speed, wind rotors and the main shaft occasionally rotate at low speed. As a result, gears are essential parts of wind systems because they speed up the generator's rotation, enabling it to produce significant power from the wind resource. The HAWT's yaw system allows the WT to align itself with the direction of wind. Yaw systems can be either free or active. In order to align the turbine, active yaw systems are typically used for up winds. Downwind applications use free yaw systems, which rely on the rotor's aerodynamics to align in the direction of wind.

To maximize power extraction from wind resources, key concerns affecting the aerodynamic properties of wind turbines must be addressed prior to WT system

designing stage (Asim *et al.*, 2022). According to Gomez, Lopez, J., Jimenez, Lopez, G. and Villalon (2014), a turbine's conversion efficiency is dependent on the airfoil, where the forces that contribute to the torque required to rotate the generator occur. According to Shankar and Kumar (2019), it is critical to understand the greatest amount of energy that can be recovered from wind resources. This is because WT extract the most energy from the wind current flow. This knowledge informs designers on creation of structures as perfectly as possible to reduce energy loss due to blades, wakes, and drag effect. In this study, rotor hub and blades were fabricated for wind tunnel experimental tests. The WT blades were constructed based on blade element and momentum theories (Gomez *et al.*, 2014; Burton, Jenkins, Sharpe & Bossanyi, 2011). At design stage aerodynamic parameter like Reynolds number, solidity, angle of attack and tip speed ratio are key in determining power conversion efficiency of a wind turbine. Some of these parameters can be determined using Equations (2.31) to (2.35) (Asim *et al.*, 2022; Ssenyimba, Kiggundu & Banadda, 2020; Adebayo *et al.*, 2019; Nijssen & Povl, 2013);

$$\text{Rotor radius: } R = \sqrt{\frac{2P}{\rho\pi U^3 C_p}} \quad (2.31)$$

$$\text{Tip speed ratio: } \lambda = \frac{\omega R}{U} = \frac{2\pi Rn/60}{U} \quad (2.32)$$

$$\text{Solidity: } \sigma = \frac{BS}{\pi R^2} \quad (2.33)$$

$$\text{Power coefficient: } C_p = \frac{2\pi n/60 Q}{1/2 \rho A V^3} = 4a(1-a)^2 - \frac{Bc}{2R} c_d \lambda^3 \quad (2.34)$$

$$\text{Torque and Power } P = Q\omega, C_p = C_Q \lambda \quad (2.35)$$

where U represents the free stream wind speed, P denotes the wind power, Q denotes the torque, C_p represents power coefficient and C_Q represents torque coefficient, a denotes the induction factor, n represents rotational speed, ρ denoted air density, B number of blades, S represents the area of one blade, A represents the swept area, C_d

denotes the coefficient of drag, R represents the rotor radius, c represents the chord, ω denotes rotational velocity, λ denotes the TSR and σ represents solidity.

The power coefficient C_P , which connects the power extracted by the wind turbine to the free stream wind power, is calculated using Equation (2.36). This coefficient gives the measure of turbines ability to transform wind energy into useful energy, with the TSR and blade pitching angle playing important roles (Letcher, 2017);

$$C_P = \frac{P}{P_W} \quad (2.36)$$

P_W denotes wind flow power, whereas P denotes rotor power. In practice, even the greatest turbine designs operate below the Betz limit at 0.35 to 0.45 as earlier alluded to by Bianchi *et al.* (2006) and Lund (2005). According to Oğuz and Özsoy (2015), for low wind speed turbines with more than two blades, the coefficient varies between 0.2 and 0.45, but between 0.4 and 0.5 for two-bladed high speed turbines.

WT system output power varies with wind speeds, where each has a specified power performance curve used to predict its energy (Elistratov & Kudryasheva, 2019). Figure 2.7 shows a model of a turbine power performance curve. On a wind speed scale, the cut-in, rated, and cut-off wind speed points can be used to characterize turbine operation. The cut-in speed is the point at which the system begins to produce power. The cut-off speed is the point where the system brakes, whereas the rated speed is the value where the generator produces its maximum power. The power output is regulated utilizing controls for the maximum rated value between the cut-off and rated speeds (Hemeida, El-Ahmar, El-Sayed, Hasanien, Alkhalaf, Esmail & Senjyu, 2020). Region A covers the period from start-up to the point at which the generator is turned on. The turbine is in Region B when cut-in speed is exceeded, but still inadequate to produce maximum power. The goal is to enhance aerodynamic efficiency below the turbine's rated speed in order to absorb as much energy as possible.

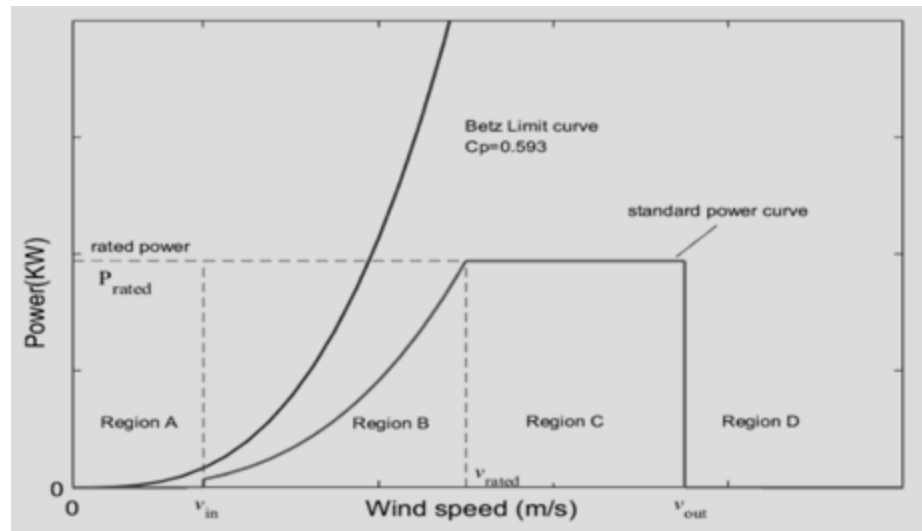


Figure 2.7: Model of a WT Performance Curve (Hemeida *et al.*, 2020)

Wind speeds in Region C are sufficient to rotate the generator at its rated power; so, the purpose at this level is to carefully regulate speed and power at regulated levels. Region D is reached when the turbine is halted to prevent damage due to high speeds (Aho, Bucksan, Laks, Fleming, Jeong, Dunne, Churchfield, Pao & Johnson, 2012).

In wind turbine design, aerodynamic efficiency is utmost to ensure maximum energy conversion from the available wind speeds (Hansen, 2015; Maalawi & Badr, 2003). The design ought to maximize lift which yields power and minimize draft for which opposes the motion of the rotors. For optimum WT performance, high lift to drag ratio, preferably above 30 is critical (Schubel & Crossley, 2012). Wind turbine rotor performance is also dependent on the type of blade material used. Some of the blade materials used are fiber glass, carbon fiber, wood compounds, aluminum alloy, steel, Polyurethane among others. Selection of these materials ought to consider strength, durability, cost, density and availability. In this study, aluminum and Styrofoam materials were used. Aluminum is readily available, non-toxic, light, cheap and easy to machine. Expanded polystyrene foam (EPF) is a composite generally called Styrofoam. Styrofoam is easy to mold and has special properties due to its structure. It is incredibly light due to the low density of its cells and the material's 90% air content. Composites are lightweight, strong, stiff, corrosion-resistant, electrical insulators, and resistant to environmental deterioration. They are also simple to cut into desired

aerodynamic shapes (Manwell *et al.*, 2010). These properties make it a good shock absorber and suitable for use in fabrication of wind turbine airfoils.

2.2.8.1 Rotor Blade Aerodynamics

When designing WT blades, structural and aerodynamic properties are among the most crucial aspects to take into account for optimum performance. Wind speed, turbine rated power, TSR, solidity, and the blades number are a few of the aerodynamic factors that affect airfoil performance. WT blades designs can be flat, curved or bent. Flat blades have been used for thousands of years before in windmills. Of late they have become less common due to their low efficiency. The blades push against oncoming wind resulting in slow rotational motion. Flat blades are easy to design and cut from plywood or metal sheet. However, their power generation rate is low. Figure 2.8 shows an airfoil nomenclature

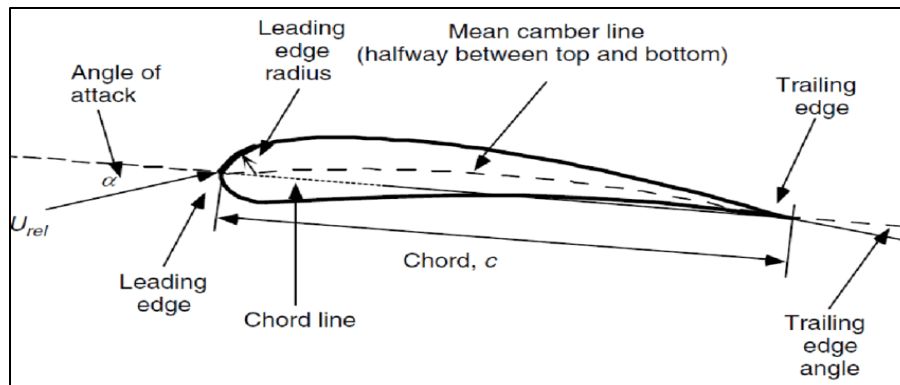


Figure 2.8: Airfoil Nomenclature (Sayed, Kandil & Shaltot, 2012)

An airfoil is a geometrical aerodynamic structure that generate mechanical forces out of its relative motion with wind (Ardany, Pandiangan & Hasan, 2021). The airfoil shape makes air flow faster at the top side of the blade than it does at the lower (concave) side. The pressure difference caused by the velocity difference between the top and bottom surfaces leads to aerodynamic lifting forces that cause blade movement. The measurements of the airfoils that make up wind turbine blades depend on their strength, assumed airfoil properties, and desired performance. Airfoils have a number of structural characteristics that describe them. The mean camber is the

centroid of all locations that are equally distanced from the upper and lower surfaces. The leading and trailing edges have the most forward and backward mean camber locations, respectively. The chord line (c) joins the leading and trailing edges. Camber is defined as the difference between the mean camber line and the chord line measured normal to the chord line. The airfoil thickness is the distance between the upper and lower faces perpendicular to the chord line. The angle of attack is the angle formed by the chord with respect to the direction of the wind (Ardany *et al.*, 2021)

WTs operate throughout a wide range of attack angles, especially deep into the stall region, where little is known about the airfoil's behavior (Nijssen & Povl, 2013). The airfoil's span, which is the length normal to its cross-section, provides the aspect ratio, a crucial parameter in the performance of an airfoil. The geometric parameters that affect an airfoil's ability to perform aerodynamically are the leading edge radius, the greatest thickness and its distribution, mean camber line, and trailing edge angle (Manwell *et al.*, 2010). According to NACA four digit airfoil description, the first digit gives the maximum camber as a percentage of the chord, second digit gives the distance of the maximum camber from the leading edge in tenths of the chord while the last two digits gives the maximum thickness of the airfoil as a percentage of the chord (Singh & Sharma, 2024).

There are two types of airfoil shapes: symmetrical and asymmetrical. The chord and mean camber lines overlap on the top and lower sides of the symmetrical airfoil. This airfoil produces no lift at zero angle of attack. The center of pressure remains constant as the angle of attack and lift coefficient change. For all angles less than the stalling angle, the tip remains at 0.25 of the chord. An asymmetrical airfoil is an airfoil whose shape on either sides of the chord is different. These are cambered airfoils with either a negative or positive camber. The center of pressure and aerodynamic center are different, making the lift generate a moment about the aerodynamic center. Under the same conditions, asymmetrical airfoils are more efficient and generate greater lift force than symmetrical airfoils (Singh & Sharma, 2024).

Lift forces in curved airfoils enable wind turbine blade tips to rotate more quickly than the wind, producing more power and achieving higher efficiencies. This contributes to the rise in popularity of lift-based wind turbines. Along their length, airfoils experience

drag, a force that works to slow them down. The drag force is orthogonal to the lift force and can be reduced to the absolute minimum by bending, twisting, tapering, or inversely tapering. These characteristics increase the blades' efficiency. A high lift to drag ratio is required for a greater power coefficient.

The AOA determines the lift force where the point of minimum pressure advances, and the pressure gradient widens as the angle widens. Up until a maximum approximate attack angle of 20° , the lift component increases. After that point, the lift component starts to decrease as the drag component sharply increases. Figure 2.9 represents the relationship between the power coefficient and angle of attack

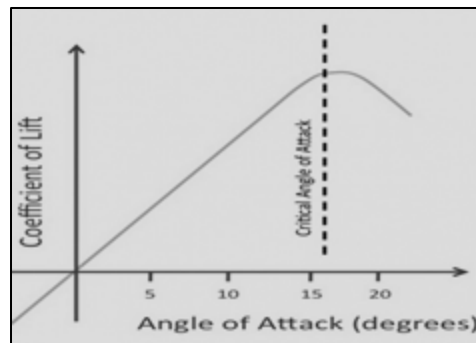


Figure 2.9: Relationship of Lift Coefficient Verse Angles of Attack

(Andrew,2017)

Turbulence increase encourages separation of the boundary layer which leads to flow reversal, reducing lift. An ideal angle of attack thus exists when the rotor creates the best rotational motion. Current blades are made with a twist of between 10° and 20° from the root to the tip. This twist reduces the AOA from the root, where air moves slowly, to the tip, where air moves more quickly. The blade receives the best rotation and lift from this. Viscous friction resists the motion caused by airfoils, resulting in two forces and a turning effect at a quarter chord length from the leading edge. Drag force develops parallel to the wind direction, whereas lift force develops perpendicular to the wind direction. Lift is formed by uneven pressure between the upper and lower surfaces, whereas drag is induced by viscous forces as well as uneven pressure on surfaces facing away from and toward the wind flow. The pitching moment circulates around the axis perpendicular to the airfoil cross-section.

The Reynolds number (Re), which is the ratio of inertial forces to viscous forces, as provided by Equation (2.37), is an important characteristic that defines fluid flow properties (Nijssen & Povl, 2013);

$$\text{Re} = \frac{UL}{\nu} = \frac{\rho UL}{\mu} \quad (2.37)$$

where $\nu = \mu/\rho$ denotes kinematics viscosity, μ denotes dynamic viscosity, ρ represents fluid density, U represents velocity, and L denotes the characteristic length. Two-dimensional coefficients established in wind tunnel testing for various angles of attack and Reynolds numbers are employed in rotor design. The coefficients of lift (c_l) and drag (c_d) are determined by Equations (2.38) and (2.39), respectively. The pitching moment coefficient (c_m) is given by Equations (2.40) (Manwell *et al.*, 2010);

$$c_l = \frac{\text{Lift}}{\frac{1}{2}\rho U^2 c} \quad (2.38)$$

$$c_d = \frac{\text{Drag}}{\frac{1}{2}\rho U^2 c} \quad (2.39)$$

$$c_m = \frac{\text{Moment}}{\frac{1}{2}\rho U^2 A c} \quad (2.40)$$

where A denotes the airfoil area, c represents the chord, U denotes the velocity of undistributed air flow, and ρ represents air density.

2.2.8.2 Blade Element Momentum Theory

Blade element momentum theory merges momentum and blade element theories to analyze the performance of a WT rotor. Description of rotor annular sections is done, which are then combined to obtain the rotor's overall performance characteristics. Momentum theory makes use of a momentum balance on a revolving annular stream tube going through the rotor, while blade element theorem examines the lift and drag coefficients produced on the blade sections (Ingram, 2011)

The thrust of a WT can be calculated by taking into account the law of conservation of linear momentum (Ingram, 2011; Manwell *et al.*, 2010). An axial stream tube encircling a WT is presented in Figure 2.10. The tube has four sections, section 1 upstream of the turbine, sections 2 and 3 just before and after the wind turbine and section 4 downstream of the WT blades. Energy is extracted from wind between section 2 and 3 leading to pressure change in the tube. Assuming the pressure at section 1 and 4, P_1 and P_4 are equal, while wind velocities in sections 2 and 3, V_2 and V_3 are equal and that the flow is frictionless, then the pressure difference between section 2 and 3 can be given by Equation (2.41) where ρ is the fluid density (Letcher, 2017);

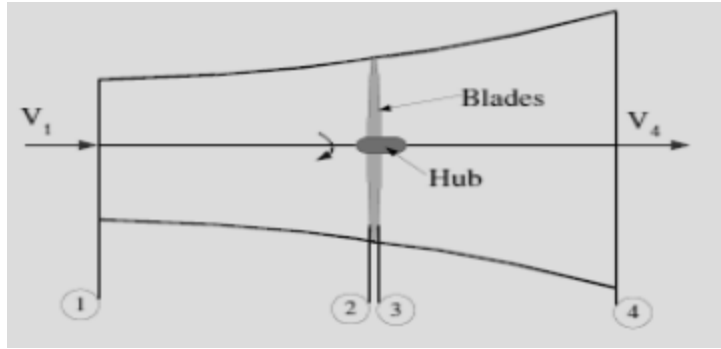


Figure 2.10: Wind Turbine Rotor Encircled by an Axial Stream Tube (Letcher, 2017)

$$p_2 - p_3 = \frac{1}{2} \rho (V_1^2 - V_4^2) \quad (2.41)$$

Force is the rate at which momentum changes and a product of pressure and area, therefore force can be given by Equation (2.42) (Ingram, 2011);

$$dF = \frac{1}{2} \rho (V_1^2 - V_4^2) dA \quad (2.42)$$

Axial induction factor, reduced velocity in section 2 and velocity in the wake section (section 4) are given in Equations (2.43) to (2.46) which after substitution gives the force generated as shown in Equation (2.51) (Ingram, 2011);

$$a = \frac{V_1 - V_2}{V_1} \quad (2.43)$$

$$V_2 = V_1(1-a) \quad (2.44)$$

$$V_4 = V_1(1-2a) \quad (2.45)$$

$$dF = \frac{1}{2} \rho V_1^2 [4a(1-a)] 2\pi r dr \quad (2.46)$$

With the reduced velocity and the velocity in the wake section, the extracted wind power (P) can be written as in Equation (2.47) (Letcher, 2017);

$$P = 2\rho a(1-a)^2 V_1^3 A \quad (2.47)$$

Power coefficient is depended on induction factor (a) and can be calculated using Equation (2.48) (Letcher, 2017);

$$C_p = \frac{P}{\frac{1}{2} \rho V_1^3 A} = 4a(1-a)^2 \quad (2.48)$$

At an induction factor value of $1/3$, C_p reaches its upper limit of 0.593. This is the Betz limit of wind turbines, as earlier discussed. The trust coefficient C_T is given by Equation (2.49), where the maximum theoretical value of thrust coefficient is $8/9$ which occurs at $a = 1/3$ (Letcher, 2017);

$$C_T = \frac{T}{\frac{1}{2} \rho V_1^2 A} = 4a(1-a) \quad (2.49)$$

2.2.8.4 Blade Element Theory (BET)

The theory of blade elements describes the forces acting on a blade as a function of the lift and drag coefficients, as well as the wind AOA. WT blades are divided into N elements, each with a unique flow caused by differences in rotational speed, chord, and twist angle. For good overall performance, the section properties along the blade span must be integrated (Ingram, 2011). It is believed that there is no aerodynamic interaction between the components and that the airfoil's lift and drag qualities are the only factors influencing the forces.

2.2.9 Hybrid Energy System

Hybrid energy systems are systems made by combine one or more conventional sources with at least one renewable resource, or a combination of two or more renewable energy with or without storage (Kartite & Cherkaoui, 2019). This system is an important step in moving away from economies dependent on fossil fuels. The most popular types of hybrid electrical power generators, excluding diesel generators, are solar thermal + biomass, solar + wind, hydraulic + wind, and solar + hydraulic. In this study, a wind-solar hybrid system was considered. A schematic of wind/ PV hybrid system configuration is presented in Figure 2.11.

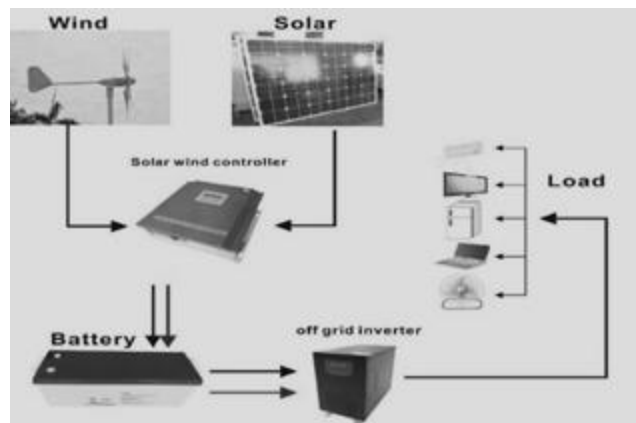


Figure 2.11: Schematic of a Wind/PV Hybrid System (*Wind And Solar Power System, Wind Solar Hybrid System, Solar Wind Turbine, n.d.*)

Based on their mode of operation and hybrid system structure, hybrid systems can be categorized. Hybrid Renewable Energy Systems (HRES) can be grouped into two depending on the operational modes, namely: grid connected which can be run parallel, and stand-alone which function independently. In remote locations without grid connection, stand-alone systems are primarily used to produce electricity. Additionally, hybrid systems can be categorized based on their structure, which details the systems according to: the presence or absence of conventional sources of energy, the quantity of combined renewable resources, and the type of energy produced, where systems can produce mechanical, electrical, thermal, light, fuel production, or mixed forms of energy.

Energy systems may also be categorized depending on their rated power, with low power systems having a 1 kW rating or less, middle power systems rating between 1 kW and 10 kW, and high power systems ratings of over 10 kW. The presence or absence of energy storage systems can also be used to classify hybrid systems; systems may have energy storage units or not.

Hybrid system configuration methodologies categorize these systems as AC, DC or both AC and DC as well as serial or parallel energy flow (Lazarov *et al.*, 2005). In serial category the energy flow in the system is unidirectional while in parallel the flow is bidirectional. Figures 2.12 (a) and 2.12 (b) show layouts of serial and parallel hybrid systems, respectively, while

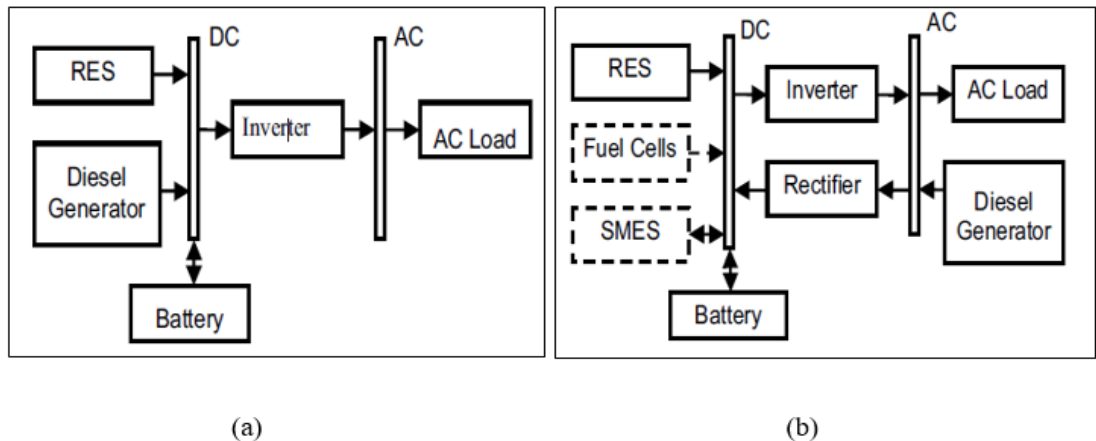


Figure 2.12: (a) Layouts of Serial and (b) Parallel HES (Lazarov *et al.*, 2005)

The hybrid energy system layout considered for installation in a given site largely depends on factors like renewable resource energy potential, system purpose, topology of the area, the energy demand and the cost of installation. In this research, a serial DC-AC combine wind-solar hybrid energy system was considered for implementation to cater for both AC and DC loads. Figures 2.13 and 2.14 show DC, AC and the combined DC and AC systems.

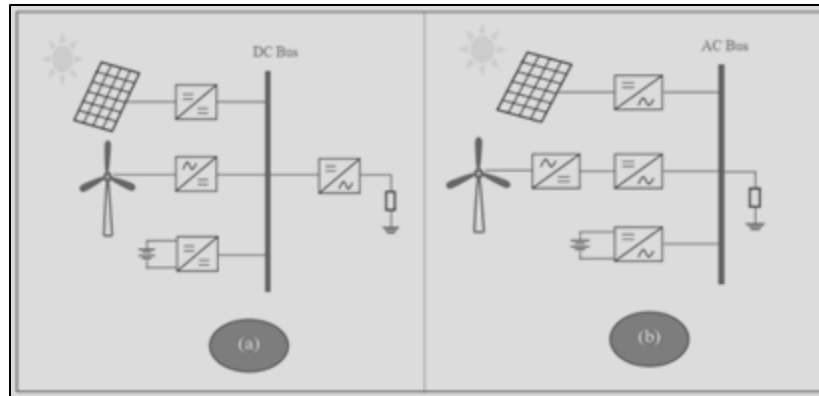


Figure 2.13: (a) DC and (b) AC Configurations of HES (Senthil, Araavind & Ghosh, 2018)

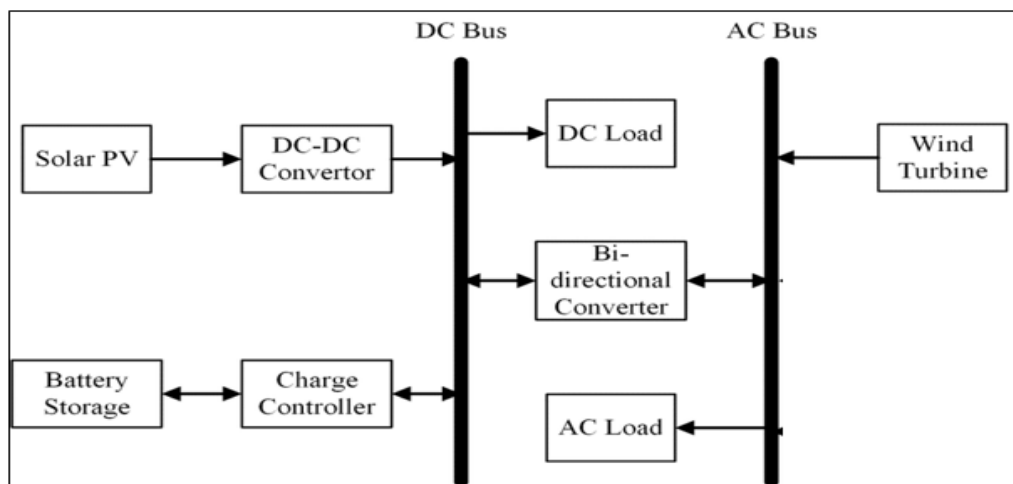


Figure 2.14: Schematic of a Combined AC and DC Hybrid Energy System Configuration (Rawat, 2013)

2.3 Previous Works Relevant to Study

This section presents the previous wind-solar assessments, turbine aerodynamic, wind-solar complementary characteristic, hybrid energy systems and energy demand.

2.3.1 Wind Resource Assessment

According to Kumar C., Kumar J. and Majid (2019), one of the electricity sources with the quickest growth rate globally has been identified as wind. However, in Kenya the

energy input from wind resource is still fairly low, despite its fast growth. In light of these facts, for wind resource to significantly contribute towards meeting the energy demand, it is necessary to make separate investments in wind energy (Cozzi & Gould, 2021; US EIA, 2013; Bekele & Tadesse, 2012). Choge, Rotoch, Tonui and Maritim (2013) studied the Uasin-Gishu County's wind energy probability distribution in Kenya, where the range of 1.3 m/s to 4.0 m/s of meteorological wind speed was characterized using the Weibull and Rayleigh distribution models. The distribution revealed k and c ranges of 3.0 – 5.21 and 3.0 – 4.0, respectively. The predicted wind power density at 20 m was found to range between 40.67 W/m² and 80.38 W/m² revealing its suitability for small-scale wind energy exploitation. Using weather information from 2001 to 2006, Kamau *et al.* (2010) examined the potential for wind energy in Marsabit County, Kenya. According to the report, wind classes 7 to 8 revealed a WPD range of 1776 W/m² to 2202 W/m² whereas the k and c parameters ranged from 2.5 to 3.05 and 11.86 to 12.97 m/s, respectively. In Kisii region, Kenya, Ongaki, Maghanga and Kerongo (2021) evaluated energy potential in wind using Weibull and Rayleigh models. The distribution revealed a k and c values of 1.91 and 3.25, respectively. At hub heights of 10 m and 13 m, Ikobe and Kisii University stations recorded typical wind speeds of 1.7-2.0 m/s and 2.4-2.8 m/s, respectively. The sites revealed low wind speeds which were unviable for large scale electricity generation. However, with increase in hub height the potential was adequate to run small-scale wind turbines. Empirical and numerical methods were used by Wekesa, Wang, Wei and Zhu (2016) to examine the performance of a small-scale VAWT at Mwingi-Kitui in Kenya. The wind resource was represented using empirical statistics, and the aerodynamic performance was addressed using computational fluid dynamics (CFD) technique. WPD range of 44.50 W/m² to 85.48 W/m² was recorded at a hub height range of 20 m to 60 m. This hub height range was found to be viable in power generation using small wind turbines (SWTs). These studies showed that Kenya's wind resource potential could be useful, especially in small-scale energy applications.

2.3.2 Aerodynamic Performance Assessment

Wind energy is one of the most recent areas of interest in the field of renewable energy research, as previously highlighted by Singh *et al.* (2012). Pressure difference makes

air travels from areas of high pressure to areas of low pressure, resulting in wind (Blaabjerg & Ma, 2017). Wind resource is characterized by aspects like wind speed, density of air and wind distribution which quantify its energy. Therefore, prior to planning and designing any wind based energy system, wind resource assessment and evaluation is important to determine its viability in energy production at a given site. Wind distribution, flow velocities, turbulence, wind orientation, and vertical shear are a few of the wind resource characteristics to evaluate (Zhang, Chowdhury, Messac & Hodge, 2013). These factors are crucial in the estimation of wind resource energy potential as well as in future projection of its power output.

There are two types of wind energy converters, lift and drag. In the drag type, wind direction is symmetrical to the rotor's spin, a condition that reduces its relative speed. Despite it being widely used, drag type converter has been reported to be ineffective, according to a study by Saoko *et al.* (2015). Due to their greater ability to harness energy, lift machines were considered in this study (Asim *et al.*, 2022; Smulders, 2004). The efficiency of a wind energy converter can be increased by making the blades rotate more quickly than the wind (Nelson, 2013). The relative velocity at which the wind hits the blade at a certain radius determines the lift magnitude. At equal surface area, lift machines can produce greater force than a drag machines. According to Konstantinidis and Botsaris (2016), a much higher lift and power coefficient is provided by the wind force. These facts partly support the choice of lift-driven WT developed in this study. In view of these facts, good understanding of the aerodynamic factors influencing a wind system's performance is crucial to ensure system designs which are dependable and efficient (Asim *et al.*, 2022).

To maximize wind turbine performance, designers need to consider employing aerodynamic characteristics like rotor area, blade area, blade material, and blade shape at fabrication stage (Cozzi & Gould, 2021; US EIA, 2013). As also supported by Nandurkar *et al.* (2017), design parameters increase the system's efficiency by allowing for variations in lift and drag coefficients across the blade span. Cambered airfoils offer much lift in wind turbine and as such, they are often utilized by designers than symmetrical ones due to their ability to operate in any direction with reduced drag coefficient (Schubel & Crossley, 2012). Furthermore, to maximize rotor lift, it is crucial to consider the blade's angle of attack, which is the angle between the wind

incidence angle and the blade. In comparison to symmetrical airfoils, cambered blades can create lift at a pitch angle of zero and a greater lift at higher angles of attack (Schubel & Crossley, 2012). In this study, cambered blade shape was preferred to symmetrical shaped ones.

According to Manwell, McGowan and Rogers (2010), a rotor's aerodynamic performance is influenced by its design rated power, rated wind speed, tip speed ratio, solidity, airfoil, number of blades, rotor power control, and orientation. The rotor swept area and wind speed are directly related to the rotor power. High TSR causes low solidity, which, when all other factors are held constant, leads to a smaller blade area resulting in lighter and more affordable turbine blades. Three blades are found on the majority of wind turbines used to generate electricity. In this work, a three-bladed rotor was developed with the intention of minimizing stress on the blade roots and keeping a constant polar moment of inertia with respect to yawing. In fluid dynamics, turbulence is a factor characterized by chaotic changes in pressure and flow velocities. This factor greatly impacts power yields from wind energy systems, more so the small wind turbines which are set-up near obstacles like buildings and trees (Scheurich & Brown, 2013). Turbulence also has a range of implications on wind energy, such as effects on power performance, turbine loads, fatigue and wake effects, and noise propagation (Bardal & Sætran, 2017).

Researchers have examined the influence of turbulence intensity on the efficiency of WT aerodynamics (Emejeara, Tomlin & Millward 2015; Pagnini, Burlando & Repetto, 2015). Two small turbines with HAWT and VAWT axes were used in the study by Pagnini *et al.* (2015) for power curve analysis in turbulent sites. According to the reports, in more turbulent conditions, VAWT was found to be more effective in generating power than HAWT. In this study, a HAWT which performs well in areas of low turbulence was considered.

Numerical models, fine scale and large eddy simulations can give statistical data on turbulence whose characterization can help in turbine power predictions. As measured by turbulence intensity measurements, which is the ratio of the horizontal wind speed's standard deviation to its average for a specific period of time, turbulence is quantified (Bardal & Sætran, 2017). In turbine performance characterization, numerical and

experimental methods have been applied with the experimental being limited to several factors like cost, technical skills, constraints of time, physical and environmental factors that affect the measurements (Eboibi, 2013). Blade Element Momentum (BEM) theory and Computational Fluid Dynamics (CFD) are the two types of numerical approaches. CFD is a technique that visualizes how fluid flow and their effects on the objects they interact with. Using mathematical models, numerical methods and software tools, CFD gives qualitative expectation of the fluid flow pattern. A system's performance is assessed using a BEM model based on mechanical, geometrical, and flow characteristics. Castelli and Benini (2010) reported the difficulty associated with BEM theory in comparison to CFD in studying the aerodynamic operation in the unsteady fluid flow. By use of CFD which incorporates the Navier Stokes equations in the turbine profile, these limitations could be overcome.

Solidity-ratio of chord length to pitch was investigated by Consul, Willden, Ferrer and McCulloch (2009) where a two and four blade VAWTs of the NACA profile were modelled using the 2D CFD approach. The solidities were, $\sigma = 0.019$ and $\sigma = 0.038$, correspondingly. The effect of varying solidity was investigated for a range of TSRs of $\lambda = 3$ to $\lambda = 8$. From the higher solidity examination, VAWT maximum power coefficient was realized at $\lambda = 4$ and $\lambda = 6$ for smaller solidity evaluations. In areas with turbulent flow like urban sites, the VAWT is the most appropriate since they have the ability to contain winds from any side without yawing, they have lower tip speed ratios hence low noise emissions, ease maintenance and low cost of manufacturing (Wekesa, Wang, Wei, Kamau & Danao, 2015; Wekesa, Wang, Wei & Kamau, 2014). Saoke, Kamau, Kinyua, Nishizawa and Ushiyama (2015) investigated the performance of folded straight, tapered and inversely tapered blades. The blades varied in power coefficient at various bend angles, with the inversely tapered blade having two parallel fold lines of 5° and 10° giving the maximum C_P of 0.372 at a pitch angle of 20° .

In accordance to a study by Komor (2009), design and installation of wind turbines are heavily influenced by the site's topological features, energy needs, and wind conditions. For wind turbines, wind speeds as high as 15 m/s, 25 m/s, or even 34 m/s can provide a sizable amount of power. Nevertheless, as stated by Apunda and Nyangoye (2017), low energy yields are the result of resource intermittence and low

wind speeds, less than 4 m/s in some areas. To increase the quantity of energy yields from the available wind, energy optimization is necessary.

In this study, energy optimization was achieved through modifications of blade material, blade geometry (size and shape), pitch and yaw controls. Wind turbine rotors get affected by torque and thrust forces where torque is the force responsible for turning the rotor and energy generation, whereas thrust force pushes against it. Highly cambered airfoil design with a large area and variable pitching was used to maximize energy production. Moreover, system yawing was deployed to capture wind energy from the directions with high wind speeds. These adjustments were made to help the rotor efficiency get closer to Betz limit of 59.3%, the uppermost limit in wind power conversion.

2.3.3 Solar PV Resource Assessment

Solar photovoltaic is among the best-known methods used in harnessing energy from the sun. Deployment of solar energy systems in an area requires prior assessment to establish the solar resource local characteristics. The assessment is dependent on the exposure of the local area to sunlight that might change depending on the site's geographical location. The amount of solar radiation striking an area varies depending on local, spatial, meteorological and global factors. It therefore calls for an ideal assessment model that would account for each of these aspects. Solar radiation models that can do well considering spatially changing attributes like inclination, orientation and latitude have been suggested and used in open source software like the ArcGis Solar Analyst (Fu & Rich, 1999) and GRASS r. sun (Hofierka & Suri, 2002). The simulations have been used to determine solar PV potentials in areas based on digital terrain model at the municipal level and in a city centered on roof geometry (Kausika & Sark, 2021; Nguyen & Pearce, 2012)

Studies done by Paidipati, Frantzis, Sawyer and Kurrasch (2009) reported on developments of models of estimating solar potentials considering factors like population, shading and climate as required in this current study. Roof surfaces were evaluated in a study by Lukač, Zlaus, Seme, Zalik, and Stumberger (2013) for solar potential and LiDAR installation compatibility. Using a Pyranometer, the diffuse and

global sun irradiations were measured and the normal vectors of the surfaces computed at each point. Considering non-ideal climatic conditions, Gooding, Crook and Tomlin (2015), and Jacques, Gooding, Gieseckam, Tomlin and Crook (2014) developed a method for assessing the capacity of PV using a low-resolution LIDAR data. Jochem, Hofle, Rutzinger, and Pfeifer (2009) used LIDAR to determine solar energy potential considering the influence of the nearby objects and cloud effects. Santos, Gomes, Brito, Freise, Fonseca and Tenedorio (2011) created elevation and digital surface models using LIDAR, GIS and PVGIS that helped in determining energy production. Among the developments of estimating solar radiation, PVGIS model was applied whose results were validated using ground measurements which were measured using a Pyranometer.

According to reports on resource assessments of solar energy, solar is one of the most promising and practicable alternatives for dependable power generation in Kenya. According to earlier assessments, Kenya has a sizable amount of solar PV potential with an average daily insolation range of 4-6 kWh/m² (Tigabu, 2016). This possibility affirms the country's readiness to utilize solar photovoltaic electricity. Solar resource quantity and ubiquity in the tropics make solar energy a better and more dependable source in comparison to other renewable energy sources. Therefore, PV systems are promising with a significant ability to meet the continuously increasing need for energy (Mulaudzi, 2018).

To assess Kenya's potential for PV electricity, Oloo, Olang and Strobl (2015) carried out a feasibility study. Focusing on variables that affect solar radiation, such as atmospheric transmissivity, diffuse ratio, altitude, and topological effects, the study used a hemispherical perspective and shed analysis based on terrain orientation. The study discovered a 5 kWh/m² daily average solar PV potential, with the Rift Valley, Mount Kenya, and Western regions having the highest potential and Eastern regions having the least. These studies prompted further research on the complementarity of renewable energy sources and their integration impacts positively on the system flexibility and reliability. Kariuki and Sato (2018) analyzed the temporal and spatial variability of global horizontal irradiance (GHI) and direct normal irradiance (DNI) using a 19-year meteosat satellite dataset. Low GHI and high DNI inter-annual variability were observed primarily in Kenya's eastern and northern deserts. GHI was

taken into account in this work because of its low level of variability. These prior studies triggered the curiosity to further investigate solar-wind resource complementarity and its feasibility in hybrid energy systems development.

2.3.4 Wind and Solar Resource Complementarity

The ability of renewable energy sources to vary in terms of their availability and energy potential is referred to as complementarity. As was previously mentioned, Kenya's equatorial location provides ample solar and wind resources, making it a suitable location for the harnessing of these renewable energies. Wind and solar have long been viewed as clean, limitless, and secure forms of energy despite their intermittent nature (Dihrab & Sopian, 2010; Mousa, AlZu'bi & Diabat, 2010). A few previous studies on renewable resources have reported on high intermittence and site specificity of wind and solar resource. In this view, therefore, a successful implementation of wind-solar driven energy systems necessitates thorough resource assessment and analysis to determine the extent of complementarity on daily and monthly time scales. Development of hybrid energy systems which integrate more than one renewable energy sources would require a careful consideration of their complementarity behavior. This allows for systems flexibility in energy generation. In the light of this characteristic, variability in power generation could be overcome by taking its advantage. Recently, resource complementarity has made it possible to explore on wind-solar PV hybrid technology, increasing its market popularity (Malik, Zehra, Ali, Ubedullah, Ismail, Hussain, Kumar, Abid & Baloch, 2020; Yang *et al.*, 2009). Renewable energy hybrid systems have advanced in delivering cost-effective and dependable clean energy, as reported by Ahmed, Miyatake and Al-Othman (2008). Other studies have shown a remarkable pattern of switching between wind and solar energy, outstanding practicality, and higher energy outputs. Performance of the two resources reveals that they could be used in the creation of hybrid energy systems by 2030 in order to meet the rising demand for energy (Fesli, Bayir & Ozer, 2009).

Wind-powered systems are significantly impacted by weather, seasonal, and geographic variations, whereas solar-powered systems are impacted by shading effects. These factors result in a sharp decline in wind and solar energy potentials. Consequently, a methodology is needed to determine their degree of complementarity

(Neto *et al.*, 2020). Previous studies have created approaches for determining the level of complementarity between wind and solar resources, with interesting findings. Energy, time, and amplitude complementarities have been used as three different components in a quantitative method to evaluate the complementarity between renewable resources by Risso, Beloco and Alves (2019). Using time series and energy, the energy potentials and likelihood of either a wind or solar resource supporting hybrid systems at different times were illustrated. Using energy and time complements, the complementarity of wind and solar resources and its impact on energy generation by hybrid systems was examined in this study. In Poland, Jurasz *et al.* (2018) investigated how complementarity affected power supply was in small-scale hybrid systems. The effects of the resources were examined on time frames of fifteen minutes, an hour, and a month. Sizing of a solar-wind hybrid systems using this nonlinear relationship between complementarity, storage capacity, and hybrid system capacity was discussed. Jurasz *et al.*, 2020 reviewed on complementarity of renewable resources for future solutions in energy. A good match between energy demand and supply from renewables has been reported. Thus, complementary metrics are key in optimizing energy system designs for maximum energy harnessing. Neto *et al.* (2020) examined how the complementary nature of solar, wind, and tidal energy played a role in isolated hybrid micro-grids where it was reported that using a variety of sources increased energy production.

Xu, Ruan, Mao, Zhang and Luo (2013) employed the relative fluctuation rate to examine how well-suited wind and solar power sources are for both on-grid and isolated micro grids. The study found that the mismatch between energy generation and demand decreased as a result of the combination of renewable energy sources. The impact of the complementary nature of wind and solar resources on energy storage capacity was investigated by Solomon, Kammen and Callaway (2016). It was reported that wind-solar complementarities provide large benefits to future grids, unlike stand-alone wind-solar based grids. It was shown that the best complementarities led to a high penetration of renewable energy, with a 20% overall energy loss and reduced requirement for storage and backup. According to a study on wind-solar complementarity by Thomaidis, Santos-Alamillos, Pozo-Vazquez and Usaola-Garcia (2016), using both resources boosted the dependability of power supply systems.

Sun and Harrison (2019) investigated the effectiveness of the wind-solar complementarity in increasing the capability of distribution networks. The study showed that by using the complementarity between renewable energy sources, a hybrid design can enable the network to handle additional generation capacity with higher energy levels. Due to the above-mentioned disadvantages of a single resource driven energy system, this study explores further on wind and solar resource complementarity particular in a low wind speed regime to establish its viability in generating energy through hybrid energy systems optimized based on the local characteristics.

The complementarity of renewable energy resources is a topic with little literature in Kenya. In particular, the complementary nature of solar and wind and the benefits of integrating them in hybrid mini-grids are allegedly largely unrecognized in Kenya (Johanssen *et al.*, 2020). From a technological and theoretical perspective, this is partially caused by the absence of small-scale wind turbines in Kenyan mini-grids. Further, systemic, technological, and financial obstacles are reportedly impeding the growth of hybrid mini-grids in Kenya. This study seeks to fill this gap by analyzing and characterizing wind and solar regimes in terms of their complementarity and energy potential.

Given the state of the art, much focus is placed on the complementarity of renewable resources for large-scale deployment, the evaluation of individual resources, and the independent development of wind and solar PV systems. Systems powered by a single renewable resource have proven unreliable due to low wind speeds and resource intermittence. To counteract this trend, it is necessary to assess the viability of wind-solar complementarity in hybrid energy systems. This study focuses on the complementarity and energy potential of wind and solar resources as key factors to inform on the development of a suitable standalone HES for low wind speed regime areas.

2.3.5 Hybrid Energy Systems Assessment

As concerns on environmental pollution and climate change increase, renewable energy sources such as solar, wind, biomass, tidal, geothermal, among others, are growing in popularity as alternatives to conventional energy sources. Nowadays,

hybridizing two or more of these renewable sources is a topic of intense research interest. Assessments have been carried out previously to establish the viability of combining two or more resources for energy production. Such an integrated system is referred to as hybrid. Most of these systems consists of more than one energy sources, among which at least one is renewable (Lazarov *et al.*, 2005). Al Badwawi, Abusara and Mallick (2015) reviewed on hybrid solar PV and wind energy systems reporting integration as a solution to their intermittent and unpredictable behavior. Further, major issues in grid and stand-alone systems as power fluctuation and harmonics were reported. These issues could be resolved through proper systems designing, control facilities and system optimization.

Proper energy system optimization is necessary as it would inform on the size and number of the components needed for energy harnessing. Optimization shows the viability and reliability of energy system models in particular applications. Srikanth, Muni, VishnuVardhan and Somesh, (2018) developed and simulated a wind-PV hybrid energy system. The primary components of the simulation modeling, which was done in MATLAB, were the PV and wind subsystems, the inverter, and a backup battery. Simulation results showed usefulness of hybrid systems both in industrial and household applications. Dixit and Bhatia (2013) considering low wind speeds in northern India, designed and tested a home hybrid solar-wind energy system. An improvement in productivity and consistency of power generation from integration of the two renewables was reported. It was further reported that, though unsuitable for grid connection, such hybrid systems would be beneficial for small-scale domestic applications like lighting.

Nema, P. and Nema, R. (2010) designed an optimized PV-wind hybrid system for CDMA/GSM for telephone-based station in Bhopal, central India. A site's meteorological data on wind speed and solar insolation was used to inform the design. For the application, the WT and PV array sizing determined by simulation and optimization in HOMER was optimal. In Afyonkarahisar, Turkey, an isolated wind-photovoltaic hybrid power system with battery storage for laboratory general illumination was sized, designed, and installed (Oğuz & Özsoy, 2015). Out of the required load of 500 W, 400 W was to be supplied by the PV system while 100 W was

to be supplied by the WT in accordance to the energy potentials of the two renewable resources. The energy load in this case was similar to the typical rural household energy load in Machakos. Solar resource in Machakos has a higher potential for energy than wind resource. As a result, photovoltaics is likely to produce more energy when solar radiation is at its peak compared to wind turbines.

Aghenta and Tariq Iqbal (2019) used BEOpt software to evaluate a thermal model and determine the hourly load to develop a hybrid power system for a household in Nigeria. Using HOMER Pro, the single-phase step-up transformer, single phase full-bridge inverter, inverter voltage mode controller (P.I.C), DC-DC boost converter, MPPT controller, and PV arrays were all modelled. The outcomes of a MATLAB/Simulink simulation revealed that hybrid wind-solar PV systems have the potential to power homes. Thus, hybrid energy systems are potential solutions in reducing domestic energy crisis. This technology could similarly be deployed in Machakos for rural household electrification.

Efficiency of PV systems is dependent on solar flux density, location, type of PV technology, system configuration and component efficiency. Of all these considerations, location and available irradiance play a key role (Radha Charan, Laxmi & Sangeetha, 2017). Another study by Rezzouk, and Mellit (2015) revealed that hybrid systems driven by solar resource and other sources like diesel are viable and reliable due to resource intermittence. Recent studies on renewable energy have significantly increased the effectiveness of clean energy harvesting systems (Page, Turan & Zapantis, 2020). Such systems are becoming more common in small projects like pumping and electrifying off-grid communities (Bogno, Sawicki, Petit, Aillerie, Charles, Hamandjoda & Beda, 2018; Rahrah, Rekioua, Rekioua & Bacha, 2015; Mohammedi, Rekioua & Mezzai, 2013). To reduce the discrepancy between daily generation and load demand, energy generation capacity is calculated to fit the power load requirement. This is in accordance to studies by Takada, Ijuin, Matsui and Yamada 2024. Energy production and demand matching is based on solar radiation, hourly average wind speed, and power consumption. Bekele (2009) studied the viability of wind/PV hybrid systems to power 200 households in selected areas of Ethiopia, where HOMER was used in optimization and sensitization analysis. The

findings in these studies revealed interesting strengths of wind and solar PV, justifying their choice in this current study.

In Kenya, a hybrid wind-solar power system's modeling, simulation, and best-sizing have been done in northern Kenya (Okinda & Otero, 2016). The main conclusions supported the integration of complementary wind and solar regimes. A perfect system design for off-grid deployment was developed in light of these findings, with a standard energy cost of 17 US cents per kWh. However, there was need for site optimization of wind turbine and solar PV in hybrid power generation system. Utilizing wind and solar energy resources to develop a hybrid wind/PV energy system is thus justified by the viability of the resources' complimentary nature.

The periodic nature of the environmental conditions like wind, solar and water hinder the rapid development of these RES (Soetedjo, Lomi & Mulayanto, 2011; Adzic, Ivanovic, Adzic & Katie, 2009). HRES with energy storage devices as a backup have been developed to increase the dependability of renewable resources (Bhandari, Lee, K. Lee, G., Cho & Ahn, 2015). Among other combinations, these HRES may consist of PV-battery, PV-diesel, wind-battery, wind-diesel, PV-wind-battery, or PV-wind-diesel. Recently, most researches have concentrated on developing single systems that integrate two or more renewable energy sources, with the outcomes showing higher levels of dependability and great cost-effectiveness (Bernal-Agustín & Dufo-López, 2009).

Numerous studies have documented the effective use of standalone duo- and tri-hybrid systems to electrify rural and urban areas around the world. Off-grid system use, analysis, modeling, optimization, and social-economic research have all been done successfully in recent years., Daut, Irwanto, Suwarno, Irwan, Gomesh and Ahmad (2011) performed a feasibility analysis of solar radiation and wind speed for PV-wind hybrid generation systems in Perlis, north Malaysia. According to the study, addition of wind resources would support energy production in Perlis up to 10% of the total output.

Panahandeh, Bard, Outzourhit, and Zejli (2011), used HOMER to model the installation of a PV-wind hybrid system with hydrogen storage for rural electrification in Essaouira, Morocco. Akikur, Saidur, Ping and Ullah (2013) carried out research on stand-alone solar systems and hybrid systems, including solar-wind, solar-hydro, solar-wind-diesel, and solar-wind-diesel-hydro/biogas systems. HOMER was used to study small hydro-PV-wind hybrid systems for off-grid rural electrification in Ethiopia by Bekele and Tadesse (2012). The feasibility of wind/PV hybrid systems in lowering energy consumption in both rural and urban settings was reported in these studies. Integration of renewable energy resources through hybrid systems has proven to be reliable means of energy production in areas with varying environmental conditions. Thus, in this study, hybrid technology was deployed to provide an opportunity to explore on wind and solar resource characteristics which would open up the creation of access to clean energy for electrification in rural areas.

2.3.6 Energy Demand Assessment

To reduce poverty and promote social and economic development, it is crucial to provide energy to developing nations. The Sustainable Development Goals, which are based on the Millennium Development Goals, recognize this fact (Modi, McDade, Lallement & Saghir, 2005). Energy deficiency can be alleviated by adopting SDG No. 7, which aims to achieve inexpensive and universal access to electricity by 2030. Though it's relatively expensive to achieve this using the extended grid connection for the scattered and sparsely populated rural areas only, ensuring a balance between the energy supply and demand for users is crucial (Shabbir & Taneez, 2013; Szabo, Bodis, Huld & Moner-Girona, 2011).

Estimation of the impact of electrification on development has been discussed in literature. According to studies on rural electrification by Dinkelman (2011), Khandker, Samad, Ali and Barnes (2014), and Kitchens 2013), electrification is a factor that significantly improves the employment, education, agricultural, and health sectors. Due to the high cost of energy, low-income households in developing countries incur a hefty burden, spending more than 20% of their income on energy alone. Because of this, policymakers view the energy crisis in communities as a problem that needs to be solved as soon as possible (Njiru & Letema, 2018). The use

of renewable energy sources found in nature, such as biomass, solar, and wind, can help solve this issue by increasing their share in electricity generation as also required by COP28. To meet the rising demand for energy and ensure stability in supply of electricity, new energy generation technologies must be developed. Thus, prior to planning, sizing, and installation of renewable energy systems, it is essential to carry out a thorough load demand evaluation and analysis (Mwakitalima, King'ondeu & King, 2015).

Energy demand assessments have previously been carried out successfully in Kenya and other African nations, laying the groundwork for the installation of RES. Diemuodeke, Addo, Dabipi-Kalio, Oko and Mulugetta (2017) examined the coastline of the Niger Delta in Nigeria for local energy consumption. In the evaluation, HOMER hybrid optimization software was employed to predict the load demand required for deciding on the optimal PV energy system. The findings revealed an expected load demand of 5.64 kWh daily. In order to lessen the possibility of a power supply interruption at Potou, on the northern coast of Senegal. Ould Bilal, Sambou, Nduaye, Kebe and Ndongo (2010) presented a storage-based solar-wind system design scaling problem, where a significant financial impact on the ideal configuration and the influence of the load profile on system design was reported.

In the Tanzanian settlement of Kikwe, the total daily energy consumption was 601.33, 54.43, 70.01, and 31.25 kWh, respectively, for household, community, commercial, and small-scale industrial loads. In the entire village, the daily load demand was 757.02 kWh, with maximum and minimum loads of 56 kW and 5 kW, respectively. According to Mwakitalima *et al.* (2015), the daily average load for a small household is 1.2 kWh. Such a load is comparable to the usual Machakos household energy load, which for most residences is less than 1.5 kWh per day. As reported in a study by Ondraczek (2013), installation capacities could be insufficient to supply energy in rural and urban areas, but due to a high rate of consumption. The sparse demography of the country was observed as having impeded the establishment of the national grid in rural and semi-urban areas. As a result, it cost a lot of money to establish the national grid network as reported by (Msyani, 2013; Kassenga, 2008; Kabaka & Gwang'ombe, 2007). Due to these demographics in a country, renewable energy sources like wind

and solar outstand as promising sources of creating access to energy (Tigabu, 2016). In Nairobi, Kenya, middle-class estates, Magambo and Kiremu (2010) carried out a study on residential electricity use and demand trends. It was reported that the average yearly energy load per family varied from 285 W to 3.6 kW, and the average monthly energy usage per household was 208 kWh.

Access to energy has a direct impact on the development index, which is measured by improvements in standards of living, education levels, and life expectancy (Cvrlje & Ćorić, 2010). Innovative approaches must be looked for to expand access to clean and safer energy in order to promote this development. In this regard, easily accessible and abundant renewable resources like solar and wind can be a solution. Majority of the studies that are currently available in literature only address the demand for solar and wind energy on a large scale. This study focused on small-scale energy consumption levels with daily loads of below 1 kWh, an average household was used as sample case to size and develop a wind-PV hybrid system for site-specific optimization.

2.4 Summary of Research Gaps

Some existing gaps have been presented in the previous studies on the diffusing of wind–solar hybrid energy systems in the market (Johannsen *et al.*, 2020). This has partly been attributed to the lack of meteorological data on their energy potential and level of complementarity to ascertain their viability in power generation. Further, complementarity aspect between solar and wind resource and its impact on energy generation especially in low wind speed regime areas in Kenya has been scanty and inconclusively discussed. As a result, the two resources are less exploited to their full potential.

Despite their being free and readily available in nature, wind and solar resources have been reported to be highly intermittent a characteristic that leads to mismatch between energy production and demand (Jurasz *et al.*, 2018). Low wind speeds make the resource less attractive for energy generation. However, their viability in energy generation in low wind speed regimes could be increased by exploring on their complementarity characteristic.

Taking advantage of the aforementioned gaps, to ensure full exploitation of wind and solar resources, this study focused development and optimization a wind/solar hybrid energy system based on local wind-solar characteristics in areas with low wind speeds regimes. This development entailed in-depth assessment of the local wind and solar characteristics as well as the energy demand level. The study findings aided in a site-specific wind turbine design optimized to operate in low wind speed regimes in Kenya.

CHAPTER THREE

MATERIALS AND METHODS

3.1 Introduction

This chapter presents the methods that were used in data collection and analysis. The field experimental set-up, methods, data collections methods, wind turbine design and fabrication procedures are discussed. Similarly, wind-solar hybrid system development and its field tests are presented, whose performance analysis reveals its effectiveness in overcoming resource intermittence. Moreover, the system potentials to meet household energy demand under varying environmental conditions are also presented. Lastly, the hybrid systems economic analysis and its environmental impact assessment procedure necessary for the systems cost-benefit analysis are presented.

3.2 Research Design

Research design is the conceptual structure within which research is conducted (Kothari, 2015). This study applied both exploratory and experimental research designs to realize its research objectives. Quantitative approach was employed where energy demand, wind and solar resource data was generated. Rigorous analysis of this data was done to draw conclusions and inform on the proper design of wind-solar hybrid energy system for Machakos. Inferential, experimental, simulation approaches were used in data collection and while correlational approach was employed in data analysis. Inferential approach employed the survey method, where energy demand analysis was used to obtain the relationship between energy demand and the energy production by wind and solar resources. Energy optimization was achieved through experimental and iterative approached, which entailed linear manipulation of the wind and solar resource variables to achieved optimal solutions needed for maximum energy yields. Simulation approach provided an artificial environment to investigate the solar resource characteristics in remote areas where experimental set-up was impossible. Finally, the research findings yielded an optimized wind/solar hybrid system that would operate under varying conditions of wind and solar resources during the day and night.

3.3 Study Area

Field set-ups and experiments were conducted in Machakos, a low wind speed regime area where wind and solar data were collected, and energy demand surveys done concurrently. Wind turbine designs, fabrication and testing was done in Jomo Kenyatta University of Agriculture and Technology (JKUAT) which is also a low wind speed regime area. Figure 3.1 shows the study area which is located in Machakos County.

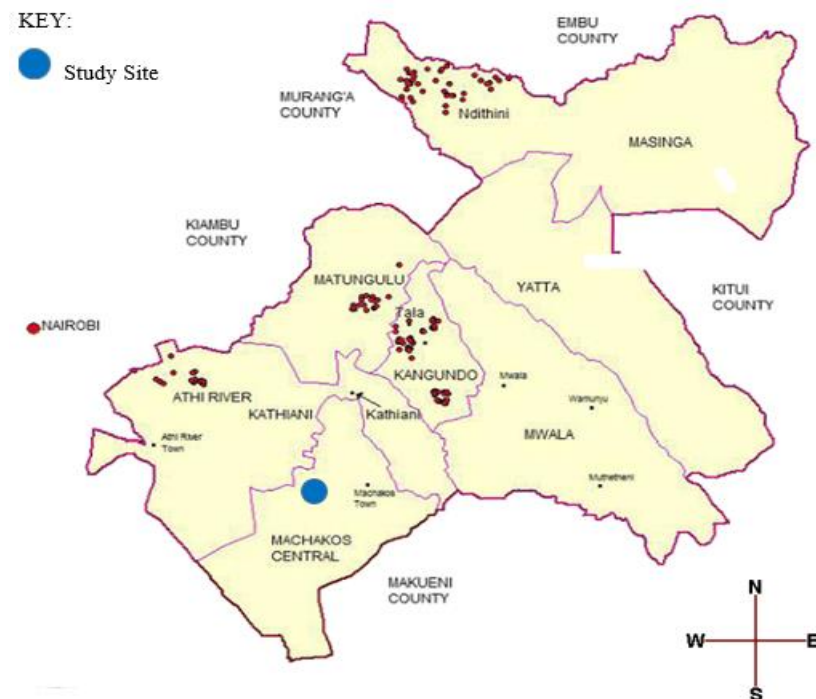


Figure 3.1: Area map of Machakos County, Kenya (Kaluwa, Oduwa, Abdirahman *et al.*, 2022)

The selected site whose geographical location is $1^{\circ}31'S$ and $37^{\circ}16'E$, is found in Machakos about 62 km from Nairobi, Kenya. Machakos County has an approximate area of 6208 sq. km with a population of about 1.5 million people. Of all the nine sub-counties in Machakos County, Machakos central is the most populated with a population of over 260000 people. Machakos has a hilly terrain covering most of the parts and lies within the equatorial, a zone which is endowed with vast solar resource. Solar and the available wind were exploited through suitable technology for energy production.

3.4 Study Procedures

This section discusses the field assessments, simulations and experimental design, system component sizing and fabrication procedures adopted in this study. Field study entailed assessments of wind and solar resource characteristics and well as investigation of the energy demand level in the rural households.

3.4.1 Experimental Procedures

The tools employed in this investigation comprised of a temperature sensor, a wind direction and speed sensor, a radiation sensor, and a data logging system. Using the radiation sensor, the solar flux density reaching on the ground was measured. The irradiance range of the radiation sensor, a thermopile pyranometer-MS-602 type, was 0 to 2000 W/m², its wavelength range was 285 to 3000 nm, and its spectral sensitivity range was 0.35 to 1.5 μ m. Its sensitivity threshold was 7.26 μ V/m²/W/m². The wind direction and speed were determined using a wind vane (scale 0-360°), and a cup-anemometer (scale 0-50 m/s, accuracy +/- 0.1 m/s), respectively. Temperature was measured using a temperature sensor that produced an analog output voltage proportional to the ambient temperature. Data logging was carried out using the Yokogawa LX100 (Datum-Y), a microprocessor-based logger with computerized serial connection and data collecting technologies. Yokogawa LW100 has a DC voltage measurable range of +/-100 mV to +/- 50 V. Waveform display is off for voltage less or equal to 0.9 V and on for voltages greater or equal to 2.1 V. The logging frequency was 30 times quicker than the rotating frequency of the cup-anemometer to minimize errors (Wekesa *et al.*, 2016).

The field set-ups used in solar and wind resources evaluation are presented in Plates 3.1 to 3.3. To ascertain the solar and wind distribution pattern of and their energy potentials, a specific set of wind variables were recorded. The solar radiation, wind speed, wind direction, and temperature were measured from January to December 2019, using the Pyranometer, the cup-anemometer, wind vane, and temperature sensors, each fixed at 20 m above the ground.

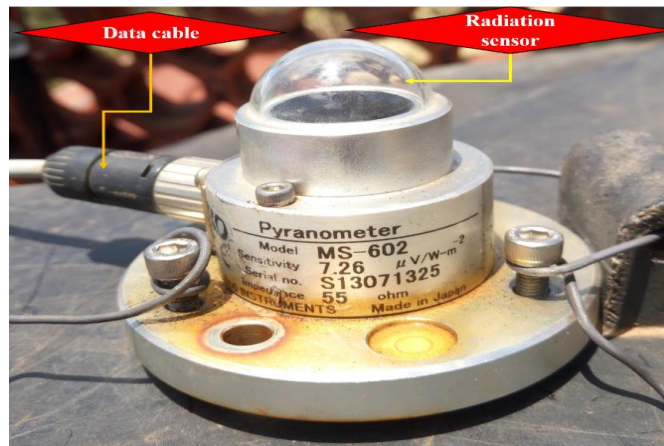


Plate 3.1: GHI Measurement using the MS-602 Pyranometer



Plate 3.2: Wind Vane, Temperature, and Cup-Type Anemometer Sensors

The data logger was used to record each instrument's output signal at a frequency of 1 Hz (Wekesa, Wang, Wei & Kamau, 2014). Eqns. (2.12) and (2.14) have been used to examine the wind speed distribution using OriginPro8 on hourly, daily, and monthly time intervals to determine its energy viability. The data logging system's operation flowchart is presented in Figure 3.2

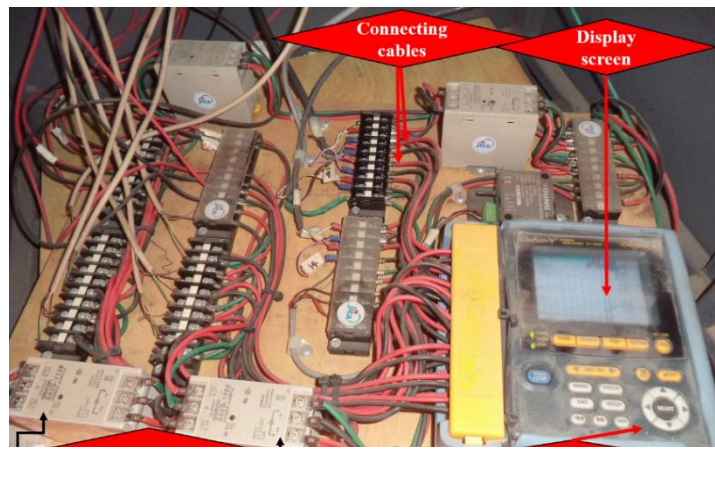


Plate 3.3: Data Logging System

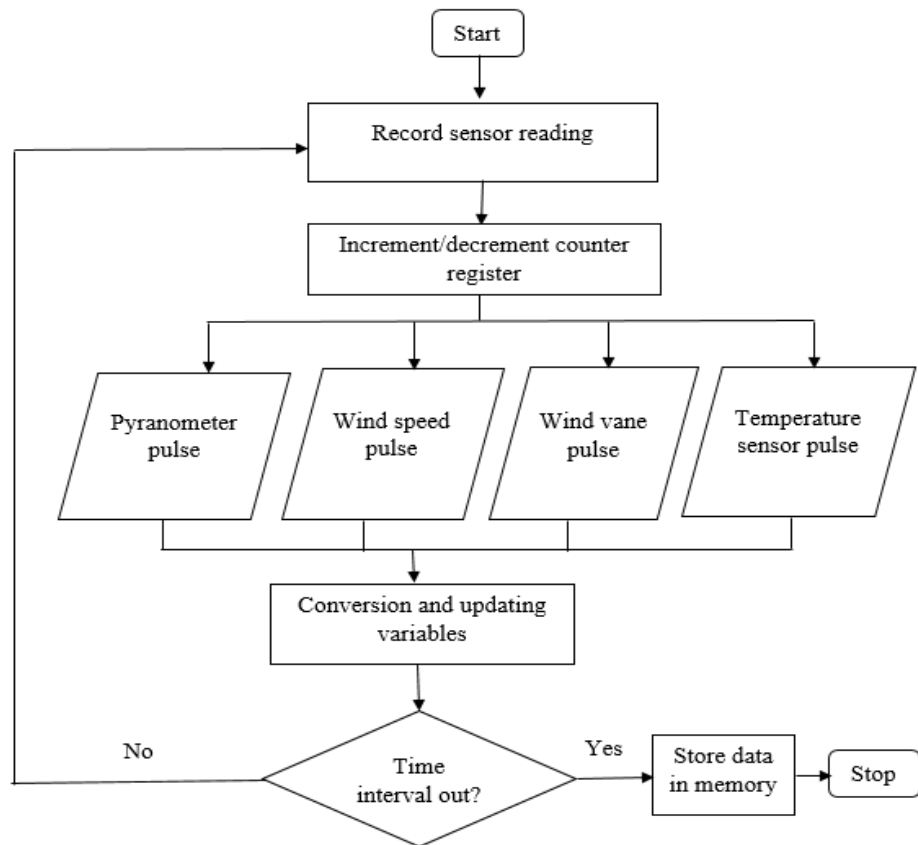


Figure 3.2: Data Logging System Flowchart

3.4.2 Sampling Procedure

Sizing a perfect renewable energy system that is appropriate for installation depends heavily on the assessment of daily energy use and the load profile of a specific household. This is because wind and solar resources are ephemeral in nature. Using households as the sample population, data on energy use was collected using the

cluster sampling method. The sampling approach used is illustrated in Figure 3.3. Yamane offers a method for estimating the sample size (n) of a given data using Equation (3.1) (Yamane, 1967);

$$n = \frac{N}{1 + N(e)^2} \quad (3.1)$$

where e is the degree of precision and N is the size of the population. Using this methodology, a sample size of 75 households was determined by assuming an average of 300 households in each village, a 90% confidence level and a 10% precision level.

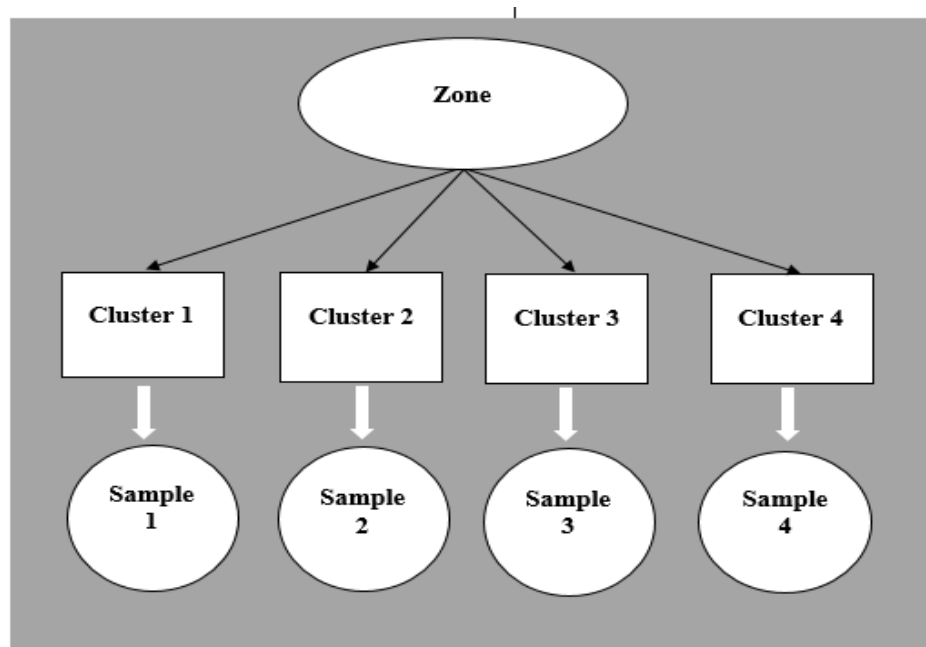


Figure 3.3: Flow Chart Showing Sampling Method

Four clusters in a given zone were considered, where information was acquired based on the houses' active appliances. The survey's components included the types of electrical appliances accessible and their power ratings, the energy sources employed, household size, monthly income, and the daily usage rates of each electrical equipment. According to the research, a household has an average of five members. In rural locations, the most common appliances were those utilized for communication, illumination, and entertainment. Utilizing the end-use approach, which makes use of customer-owned appliances, load analysis was performed. Phones, lights, TVs, radios,

heaters, fans, ironing boards, vacuum cleaners, hair dryers, and blenders were among the common active appliances. Homes with appliances like refrigerators, ovens, and stoves were quite rare. By use of a Microsoft excel the total and average loads were calculated using Equations (3.2) and (3.3), respectively (Magambo & Kiremu, 2010);

$$E_{Total} = \sum_i^N P^k t \quad (3.2)$$

$$E_A = \frac{1}{N_H} \sum_i^N P^k t \quad (3.3)$$

where E represents energy, P represents an appliance's power rating, k represents the number of similar appliances, t represents the period of usage, N denotes the number of homes in the zone, E_A represents the daily average load, and N_H represents the number of appliances in use. The daily demand curve was plotted, which revealed the energy demand pattern of a typical rural household.

3.4.3 Simulation Procedure

Solar radiation characteristics were simulated using the PVGIS (Photovoltaic Geographical Information System) tool for comparison and validation using the experimental measurements. PVGIS was picked because of its outstanding features, which include a fresh database, extensive coverage, detailed time series calculations, and downloadable profiles. The PVGIS online software interface used in this study is shown in Figure 3.4

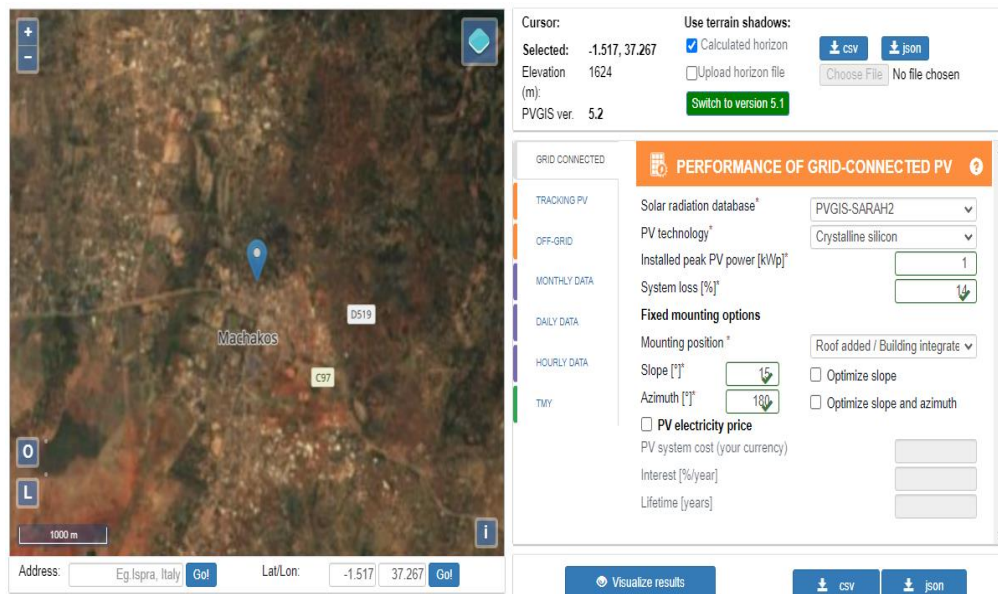


Figure 3.4: PVGIS Interface

The software simulates and displays results in a minute. PVGIS estimated the daily and monthly irradiance, annual PV energy output, and annual solar in-plane irradiance based on the provided parameters (Dondariya, Porwal, Awasthi, Shukla, Sudhakar, Murali & Bhimte, 2018). In its estimation of solar radiation, the PVGIS took into account the location's topography, geometry, and atmospheric factors (Gooding, Crook, *et al.*, 2015; Gooding, Smith, Crook & Tomlin, 2015). The simulation took into account the geometric factors affecting an area's declination, latitude, and sun hour angle. These exceptional considerations of PVGIS made its use in resource assessment justifiable. The following steps were used to complete the PVGIS simulation:

Step 1: The URL for the web-based software located as

http://re.jrc.ec.europa.eu/pvg_tools/en/tools.html#PVP. This aided in finding the terrestrial latitude and longitude of the study sites.

Step 2: Choice of the location, which was done by keying in the geographical coordinates for the sites ($1^{0}31'S$, $37^{0}16'E$).

Step 3: Solar PV parameter setting. Simulation was done based on PVGIS-CMSAF and PV technology crystalline silicon PV technology, where installation peak PV power capacity was set at 1 kWp to size the PV system components. To cater for

system performance inefficiencies partly due to resistance and heat, a system loss of 14% was set for low voltage consumers. The mounting option was set to be freestanding while azimuth and slope angles were set at 180° and 15°, respectively.

Step 4: The PVGIS is then run.

On clicking the visualization tab, a report is produced containing average annual energy production, average annual irradiance, yearly variability which is expected over the 10-year period of data capture.

3.4.4 System Component Sizing

Based on the wind and solar energy potentials, a HES components were sized to meet an average daily load of 0.588 kWh in a rural household.

3.4.4.1 Solar Panel

Even under the worst conditions of solar insolation, a solar system must be able to support the load and system losses (Voss & Reise, 2012). Using the ratio of daily household load in watt-hours to PSH in July as in Equation (2.24), the solar panel size was determined as given in Equation (3.4);

$$\frac{588 \text{ Wh}}{4.7 \text{ hrs}} = 125.1 \text{ W} \quad (3.4)$$

To account for system losses, the solar panel was up-scaled by a factor of 0.3, increasing the panel rating to 163 Watts. Thus, a 165 Watts solar panel would be suitable.

3.4.4.2 Battery

Due to its low cost, a lead acid battery would be appropriate. The storage capacity considering 588 Wh daily load was calculated using Equation (2.26), which took into account a battery efficiency of 85%, a DOD of 60%, and a nominal voltage of 12 V. The battery capacity was calculated as given in Equation (3.5);

$$\frac{588 \text{ Wh}}{0.85 \times 0.6 \times 12 \text{ V}} \times 2 = 192 \text{ AH} \quad (3.5)$$

For the household load, a 12 V, 200 AH battery with a two-day autonomy would be sufficient.

3.4.4.3 Inverter

A suitable inverter size should be 25–30% larger than the combined wattage of the appliances. This size would allow it to withstand the household wattage without getting damaged. This sizing is consistent with the study done by Ariyo *et al.* (2016). From Equation (2.27), the inverter size was determined as shown in Equation (3.6). Consequently, a 12 V, inverter giving at least 225 W was appropriate.

$$178 \text{ W} \times 1.25 = 222.5 \text{ W} \quad (3.6)$$

3.4.4.4 Hybrid Charge Control

The size of an HCC would be determined by current and voltage values to match the 12 V battery, WT and solar panel. The HCC rating was computed using Equation (2.28), yielding a value of 1.3 times the PV module's short circuit current. A 25 A controller would be ideal for a maximum current of 18 A.

3.4.4.5 Wind Turbine

A low wind speed regime with a wind speed range of 0 – 10 m/s, average cut-in wind speed of 2.0 m/s, 5.0 m/s rated wind speed and 15 m/s cut-off wind speed determined using a power curve specified the ideal wind turbine suitable for application.

3.4.5 Design and Fabrication

The characteristics of a WT shown in Table 3.1 were calculated using Equations (2.17) and Equations (2.35) to (2.41).

Table 3.1: Wind Turbine Design Parameters

Rotor diameter (m)	2.9
Blade number	3
Solidity	0.2
Type of airfoil	NACA4418
Reynolds number	100000
TSR	2.3
Power coefficient (Cp)	0.46
Efficiency	85%
RPM	75
Rotor power (W)	235
Chord length (mm)	300
Rated wind speed (m/s)	5
Generator power (W)	200

The blade element momentum theorem, which takes into account aerodynamic forces that depend on free-stream velocity as well as the distance from the axis, formed the foundation for the construction of wind turbine blades. After creating the blades out of two lightweight materials, aluminum and Styrofoam, the rotor was fabricated and put through aerodynamic tests in a wind tunnel to evaluate its performance. The optimal blade airfoil was chosen using the analysis of lift-to-drag ratio at different angles of attack, shown in Figure 3.5. Based on the wind flow variations and the characteristics of the airfoil type, the Reynolds number of Machakos' wind regime was estimated at 1×10^5 , classifying it as a turbulent flow zone.

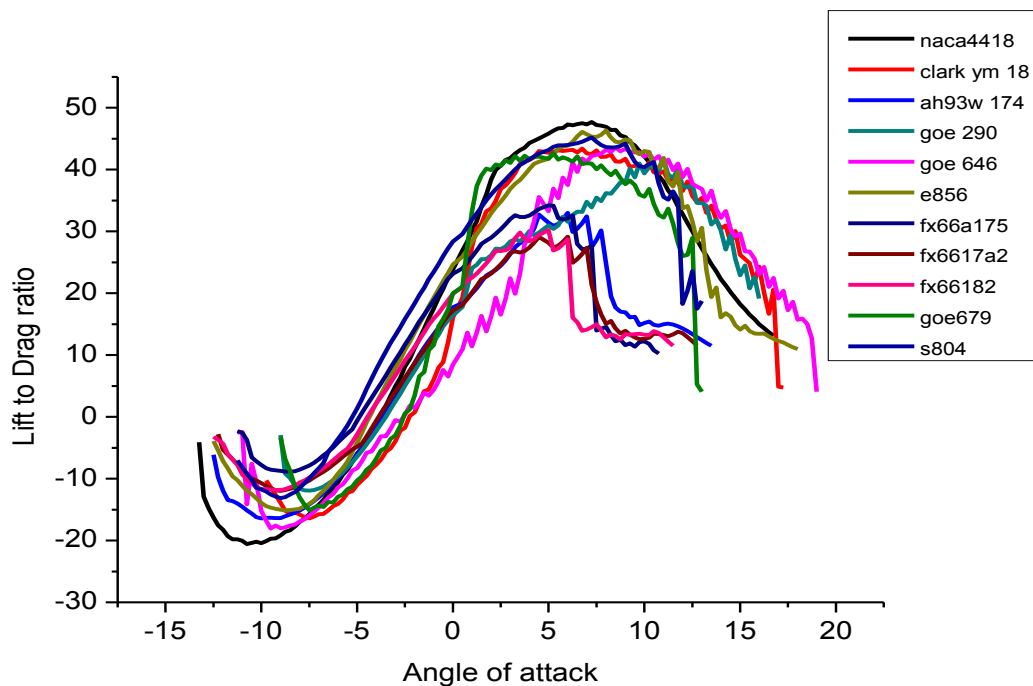


Figure 3.5: Lift to Drag Ratio vs AOA for Various Airfoils

The NACA 4418 was determined to be the appropriate airfoil based on this flow regime due to its high lift to drag ratio of 47 in comparison to other airfoils. An ideal airfoil for a lift-driven machine, according to Smulder's notion, should have a lift-to-drag ratio of at least 30, and this ratio was found to be in conformity with his recommendation (Schubel & Crossley, 2012). In this study, WT blades characteristics were customized to maximize energy in low wind speed areas.

3.4.5.1 Aluminum Blades

Using a 4 mm thick aluminum sheet, a blade with a 1300 mm span and a 10° tapered trailing edge was fabricated. Three folds of 20°, 15°, and 15° parallel to the leading edge were used to increase the blade's strength while ensuring that the blade surface was in constant fluid dynamic contact. A 4 mm thick blade is strong enough to avoid flexing when rotating, easy to form and bent without breakage. By manually adjusting the pitch angles, it was possible to attain the optimum angle at which the rotor would have the greatest lift. The aluminum blades fabricated were as shown in Plate 3.4.



Plate 3.4: Aluminum Blade Design

3.4.5.2 Styrofoam Blades

In accordance with the blade element theory, a piece of styrofoam was shaped into a tapered blade using 13 sized sections cut from a manila paper. The sections were as Plate 3.5 illustrates. The Styrofoam blades were sized and shaped using the NACA 4418 model characteristics, which produced the uniformly tapered blade shown in Plate 3.6.

A fiber-reinforced plastic was glued together to form the cover coat, which was then strengthened with resin. In order to make the blades more resilient, smooth, and watertight, a body filler was used in the molding process



Plate 3.5: Styrofoam Blade Element Cross-Sections



Plate 3.6: Styrofoam Blades Strengthened with Fiber Material

3.4.5.3 Rotor Hub

As shown in Plate 3.7, an aluminum cast was used to fabricate a three-blade rigid hub with a diameter of 300 mm. The hub had three pipes each of diameter 30 mm and length 150 mm, spaced 120° apart. Bearings were fixed to allow for smooth rotation. This hub's variable pitching capabilities were intended to maximize wind power conversion. During the wind tunnel testing phase, energy optimization via pitching allowed for lift variation at different angles of attack.



Plate 3.7: Wind Turbine Rotor Hub

3.4.6 Wind-Solar PV Hybridization

Figure 3.6 illustrates the hybrid energy system's block diagram. The experimental set-ups used included the fabricated WT rotor coupled to a 12 V, 200 W, 750 RPM induction generator, a 12 V, 200 W polycrystalline solar panel, MPPT hybrid wind-solar controller rated 25 A, 300 W wind, 40 A, 500 W solar with a 300 W damp load, Yokogawa LX100-Datum-Y data logger and AcuRite Iris 5 in 1 weather station instrument with a wireless data logger. AcuRite Iris has a wireless range of 100 m, temperature range of -40°C to 70°C , wind speed range of 0 to 159 km/h, 16 points of wind direction and an operating frequency of 433 Hz.

The hybrid charge controller measures the wind power and if sufficient meets the loads and charges the battery if the state of charge (SOC) is below maximum conducting the excess power to the damp load. If wind power is not sufficient the controller measures solar PV power which if sufficient meets the loads and charges the battery if SOC is below maximum. If the battery is full, the controller channels the excess power to the dump load. When both wind and solar power is insufficient the controller measures the battery power which if sufficient meets the load. Figure 3.7 shows the system's operational flowchart.

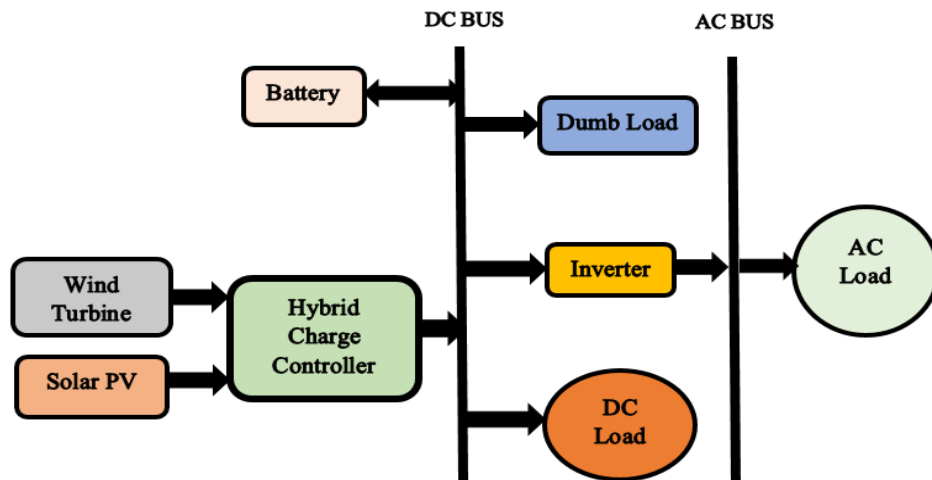


Figure 3.6: Layout of a Hybrid Power System

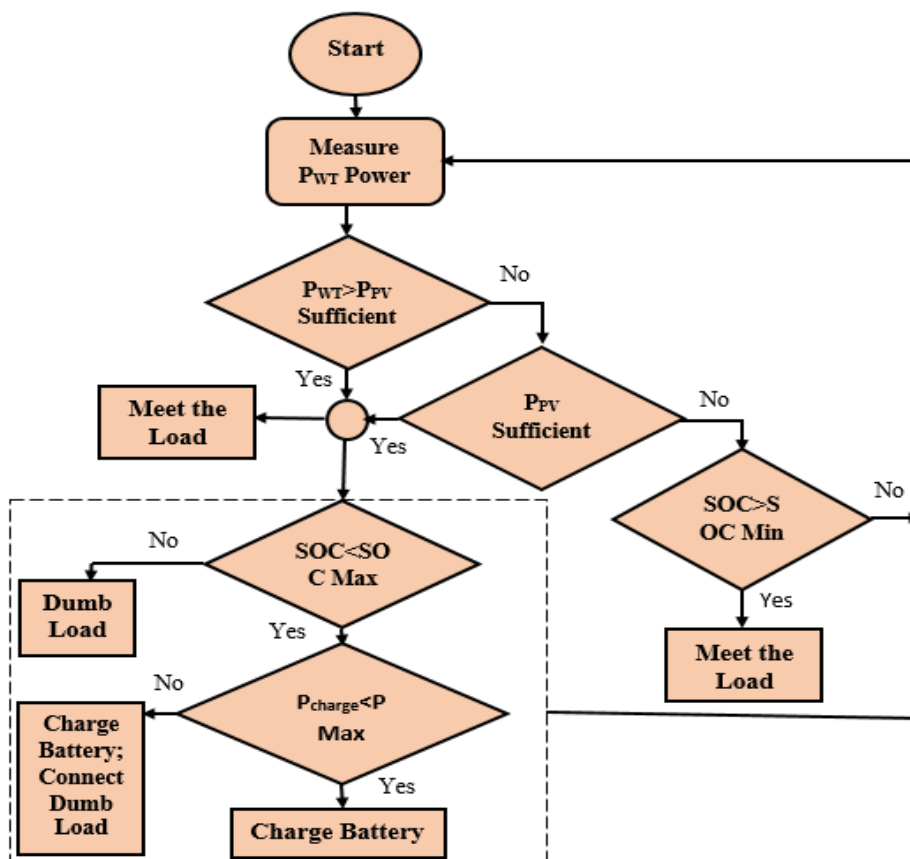


Figure 3.7: Process Flow Diagram for a Hybrid Energy System

3.4.7 Energy Optimization

The wind turbine's ability to produce electricity is greatly influenced by its design and optimization factors. In this light, it's critical to consider the site's energy potential as well as the distribution of wind when defining the specifications of a WT. As a result, using blade type, shape and area, pitching and yaw mechanisms, the WT design was optimized to ensure energy capture in low wind speed regimes. A flow chart illustrating how energy optimization using iterations was accomplished is presented in Figure 3.8.

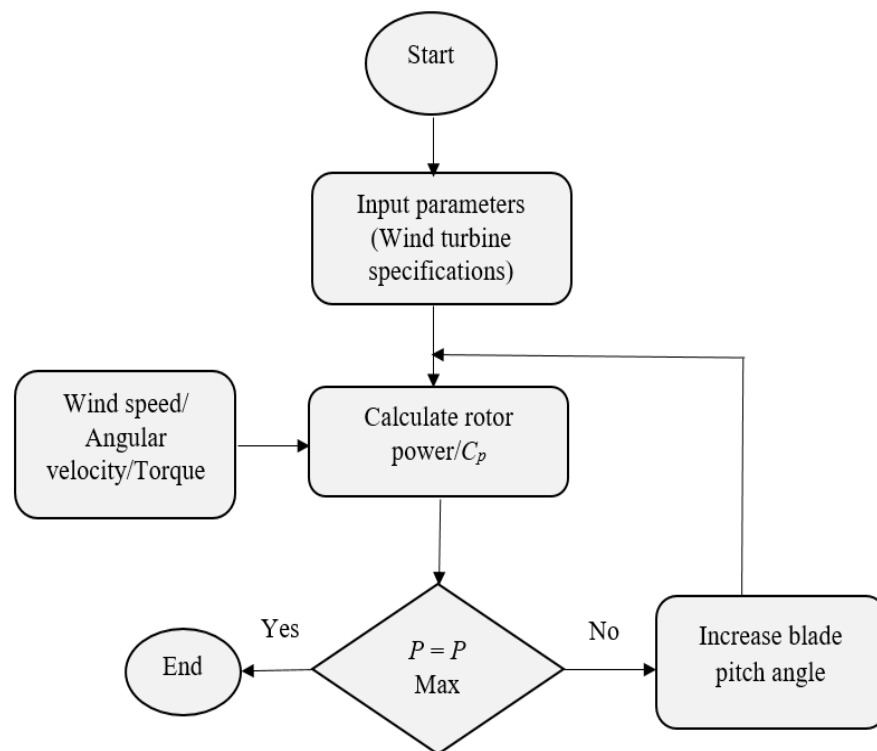


Figure 3.8: Process Flow Diagram for Optimization

To harness maximum energy at the rated wind speed of 5 m/s, rotor design specifications were determined. The two sets of fabricated blades; Styrofoam and aluminum, were used to perform iterations on the variables affecting rotor power, such as rotor area, revolving speed, torque, TSR, and pitch angles. Wind tunnel speeds up to a maximum of 20 m/s were used to vary the rotor speed. The optimal point at which the rotor produces its greatest amount of power was determined through iterations for a blade pitch angle range of 0° to 40° at intervals of 5° . Equation (2.13) was used to calculate wind power, while Equation (2.35) was used to calculate rotor output power

based on the specifications presented in Table 3.1. The rotor C_P value was determined by comparing the free wind power and the rotor power.

3.4.8 Economic Viability Assessment

Cost-benefit analysis of a project informs on its economic viability, supporting future decision-making on its implementation. According to national and private economic valuations, economically feasible projects must meet certain criteria. Systems economic viability can be determined using a number of tools, namely: payback period (PP), accounting rate of return (ARR), net present value (NPV), internal rate of return (IRR) and profitability index (PI) (Zeraatpisheh, Arababadi & Pour, 2018). Payback period gives the length of time required to recover the funds expended in a project, whereas ARR is the ratio of average net profit to average investment cost. Both PP and ARR are non-discounted methods and thus ignore the time value of money, though they show some economic value of the investment. The longer the PP, the less attractive the investment. PP and ARR can be calculated using Equations (3.7) and (3.8), respectively (Zeraatpisheh, Arababadi & Pour, 2018);

$$PP = \frac{\text{Initial investment cost}}{\text{Cash inflow per year}} = \frac{C_{\text{system}}}{E_{\text{day}} \times C_u \times 365} \quad (3.7)$$

$$ARR = \frac{\text{Average net profit}}{\text{Average investment cost}} \quad (3.8)$$

Net present value gives the project value in terms of the difference between the present value of cash inflows and the current value of cash outflows over a period. It considered time value of money where a positive NPV indicates a profitable project, a negative NPV indicates loss while a zero NPV indicates a neutral investment with neither gain nor loss. NPV can be calculated using Equation (3.9) (Zeraatpisheh, Arababadi & Pour, 2018);

$$NPV = \sum_{t=0}^T \frac{c_t}{(1+r)^t} - c_o \quad (3.9)$$

Where C_o is the total initial cost, C_t is the net cash flow during time t , r is the discount rate of 6% on average in accordance to CBK, (2024) press release and t is the number

of time periods. Internal rate of return (IRR) is the pace at which the cash returns after investment. It determines the rate at which the NPV becomes zero. Similarly, it considers the time value of money and a higher value of IRR is an indicator of a more desirable investment. IRR can be calculated using Equation (3.10) (Zeraatpisheh, Arababadi & Pour, 2018);

$$0 = \sum_{t=0}^T \frac{c_t}{(1 + IRR)^t} - c_o \quad (3.10)$$

Lastly, profitability index (PI) gives the profit investment ratio. A greater value is desired as it indicates a profit making investment. A PI of one gives the minimum acceptable profit for a project. PI can be calculated using Equation (3.11) (Zeraatpisheh, Arababadi & Pour, 2018);

$$PI = \frac{\text{PV of future cash flows}}{\text{Initial Investment cost}} \quad (3.11)$$

These mathematical models were used to determine the economic benefits of investing in wind-solar hybrid systems in relation to the national grid and conventional energy sources. Benefits of the hybrid energy system include independence from national grid whose cost fluctuates depending on inflation rates as well as shift from over reliance on fossil fuels, which are major contributors of greenhouse gases. These benefits are in terms of avoided costs of natural grid and CO₂ direct air capture (DAC) technology. The cost of grid power (C_{grid}) for the system's lifetime was calculated using Equation (3.12) (Sharma *et al.*, 2016);

$$C_{grid} = 365 \times E_{day} \times C_u \times L \quad (3.12)$$

where E_{day} is the daily energy load, C_u is the cost of a unit of energy as per KPLC utility including all levies, adjustments and taxes incurred in grid power supply. L is the project life span, which is the time taken for most of the components to depreciate to a point of replacement for economic viability (Zeraatpisheh *et al.*, 2018).

In this study, the estimated project life span was estimated as 20 years. Considering labor and the costs of the hybrid system components which include panel, turbine, battery, inverter and charge controller, the hybrid system's net present cost (C_{system})

was estimated using Equation (3.13) (Hemeida, El-Ahmar, El-Sayed, Hasanier, Alkhalaf, Esmail & Senjyu., 2020; Sharma *et al.*, 2016);

$$C_{\text{system}} = (C_{\text{panel}} + C_{\text{turbine}} + C_{\text{battery}} + C_{\text{inverter}} + C_{\text{controller}} + C_{\text{installation}}) \quad (3.13)$$

According to the EPRA 2022 report, the rate of CO₂ emission in Kenya is 0.5 kg/kWh (EPRA, 2022). Based on this rate, the amount of reduction of CO₂ emission per household was determined using Equation (3.14) (Sharma *et al.*, 2016);

$$CO_2 = E_{\text{day}} \times \beta \times 365 \times L \quad (3.14)$$

where β is the carbon emission factor per kWh.

3.5 Study Setup

This section presents the experimental set-ups used to carry out system design test both in the fluids laboratory and outdoors.

3.5.1 Wind Turbine Tunnel Test

Wind tunneling was carried out at the Fluids' laboratory in JKUAT to evaluate the performance of the designed WT rotor. The test setup was as presented in Plate 3.8. Through a 1.2 m square test section, the rotor was driven by a wind blower at varying wind speeds to a maximum of 10 m/s within the range of 0-10 m/s in a selected low wind speed regime.

An induction motor functioned as the load, where an inverter was utilized to control the frequency from high to low speed. The torque and rotational speed measured by the torque meter were utilized to compute the TSR and C_P using Equations (2.37) and (2.41).

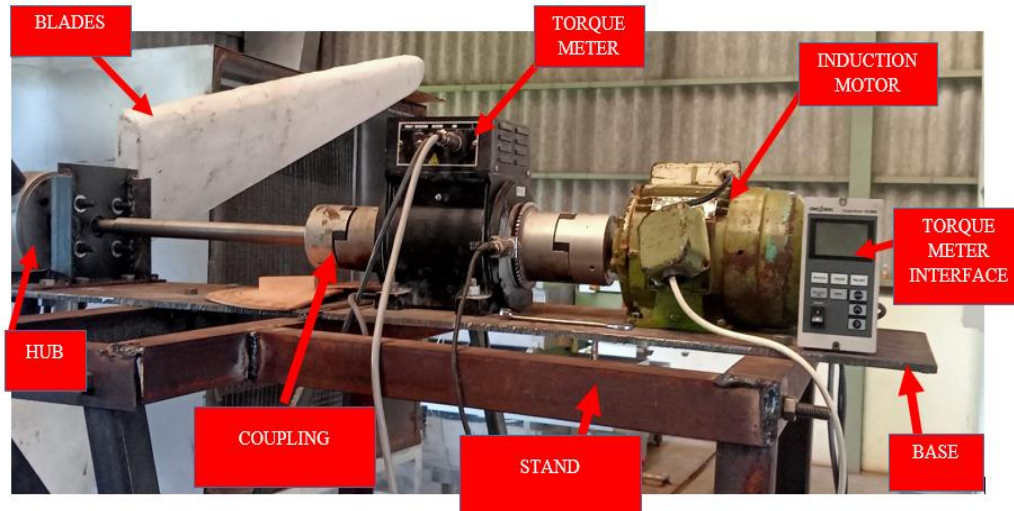


Plate 3.8: Wind Tunnel Test Experimental Set-Up

3.5.2 Field Test Setup

The PV module was mounted at the rooftop of the JICA workshop in JKUAT while the WT was installed at a hub height of 8 meters from the ground. Prevalent range of average wind speed between 3.0 m/s and 3.9 m/s around Juja which is a low wind regimes area as reported in a study by Saoke *et-al.*, 2012 and wind speed ranges of 2.78 m/s to 5.56 m/s in JKUAT as reported by Wekesa *et al.*, 2012 were found to be comparable to the average range of wind speeds of 2.5 m/s to 4.9 m/s in Machakos (Figure 4.2) classified also as a low wind speed regime area. Thus, out of convenience, the system was tested at IEEET in JKUAT where it was expected to give power performance characteristics applicable in other low wind speed regime areas like Machakos. The WT and solar systems were hybridized using a hybrid MPPT charge controller for solar and wind energy integration. All controller inputs and outputs were connected to a data logger for current and voltage data capturing at a frequency of 1 Hz. AcuRite sensor was mounted beside the turbine to capture wind speed and direction. The WT and speed sensor were as shown in Plate 3.9 while the installed solar system was as shown in Plate 3.10

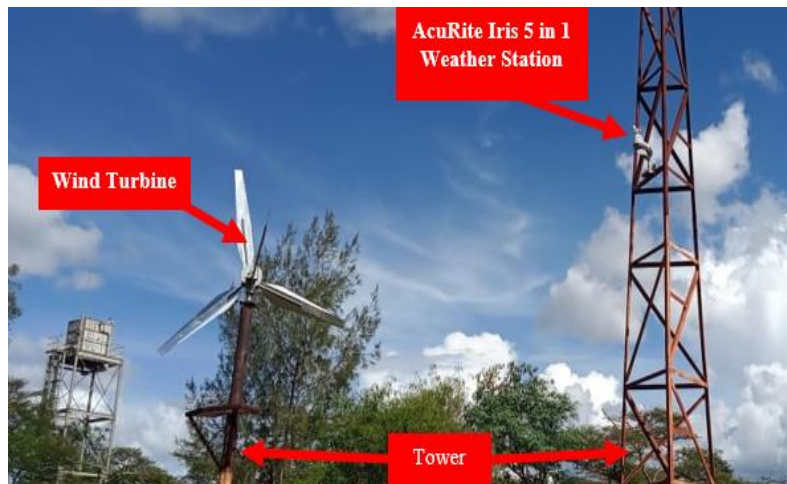


Plate 3.9: Wind Turbine and Acurite Iris 5 in 1 Sensor Installed at IEET, JKUAT in 2023



Plate 3.10: Solar PV System Installed at the JICA Workshop Rooftop, IEET in JKUAT

In addition to resource integration, the HCC shown in Plate 3.11 aided in protecting the battery from overcharge, over discharge and overload. Plate 3.12 shows AcuRite Iris, a 5 in 1 weather station data logger with a PC connected.

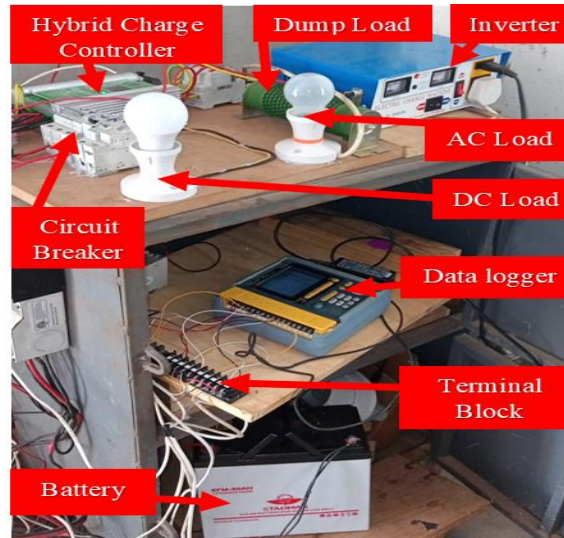


Plate 3.11: Setup of a Hybrid Charge Controller, Battery, Inverter and Loads Connected to a Data Logger

To charge the battery and power the loads, the WT and solar PV systems transformed wind mechanical energy and solar irradiance, respectively, to electrical energy. Even at low wind speeds, the MPPT hybrid charge controller ensured effective use of the available wind resource in charging the battery and supplying the loads. The wind speed at a tower height of 8 m was used in vertical shear analysis to estimate wind speeds at higher hub heights using Equation (2.9). The vertical distribution profile for wind speeds to a maximum of 50 m above the earth's surface was plotted. The shear analysis revealed the wind power potentials at higher altitudes, where the power densities were calculated using Equation (2.12). Actual energy generated was determined and extrapolated for the higher heights using Equation (2.11). Actual and expected output were correlated to determine the developed hybrid system's conversion efficiency. Plate 3.12 shows AcuRite Iris, a 5 in 1 weather station data logger with a PC connected for wind data capturing.



Plate 3.12: Acurite Iris 5 In 1 Data Logger with PC Connect

Battery charging voltage and load voltages were investigated and comparison done with the inputs from the sources to ascertain the system's power stability. Complementarity of wind and solar and its impact on battery charge and supply to the loads was investigated to determine the system's flexibility and reliability under changing weather conditions during daytime and nighttime. The designed hybrid system's effects on the environment and benefits for a 20-year lifespan were also examined.

3.6 Data Collection

In this research, inferences were drawn from primary data, which was collected through assessments presented in Figure 1.1. Energy demand data was collected using sample surveys, which employed the direct communication (interviews) with the energy consumers and questionnaire method in selected households of Machakos. Members provided the active appliances and responded to a set of questions which were used to calculate the daily average loads. Wind-solar resource data collection and systems tests were conducted using experimental techniques both in the field and laboratory environments.

3.7 Data Analysis

Data collected from the field assessments on energy demand, wind and solar distribution and energy potentials was analyzed using OriginPro8 software. Analysis

revealed the energy utilization levels in a rural household of Machakos. The average household load demand was determined to inform on the size of an apt wind-solar PV hybrid energy system for the region. Wind and solar distributions patterns and their energy potentials were analyzed to reveal complementarity pattern in terms of time, space and energy components. This was a significant characteristic of the two resources in the development of hybrid energy system. The characteristic reveals the viability of the two resources in overcoming the intermittence effects which results to fluctuations in power output.

Various profiles were plotted to present wind and solar characteristics on hourly, daily and monthly time scales. Graphical analysis was used to represent the daily and monthly minimum and maximum wind speeds and solar radiation levels, giving inference on their complementarity level. The distribution of wind speeds and direction in Machakos was represented by a wind rose, a profile of concentric circles showing the various percentage frequencies of time the wind blows from a certain direction. This would inform on system installation layout at site. Daily and monthly averages of wind speeds and solar insolation were calculated and presented. Wind turbine design test and optimization results were similarly analyzed and presented graphically. Quantitative analysis of the wind tunnel tests results was done in OriginPro8 and Microsoft Excel. Relationship profiles between wind speeds, RPMs, tip speed ratios and power coefficient variables at variable blade pitch angles were presented. This analysis provided the optimum operating conditions of the wind turbine for maximum wind energy conversion.

Based on the inference made from the field and wind tunnel results, a wind-solar PV hybrid energy system was developed. The systems power performance analysis was done to determine the system's level of flexibility under varying environmental conditions. Vertical wind shear analysis was done to determine the system's generation capacity at hub heights of 50 m and 100 m from the ground level. Lastly, system's economic viability was analyzed to determine its benefits and environmental impact upon implementation. These economic benefits were realized in terms of the avoided costs and CO₂ reduction level.

CHAPTER FOUR

RESULTS AND DISCUSSION

4.1 Introduction

This chapter presents research findings of solar and wind resource distribution, complementarity analysis and energy demand analysis. Further, wind tunnel test results, analysis of the developed hybrid system power performance as well as its economic viability are discussed.

4.2 Resource Distribution

4.2.1 Distribution of Wind Resource

Table 4.1 compares average monthly wind speeds at 20 m from January to December with the minimum, average, and maximum monthly temperatures in Machakos for the year 2019. The data in Table 4.1 was used to correlate average wind speeds and temperatures in the months of January to December. Figure 4.1 shows daily averages and peak wind speeds as an average of all wind speeds recorded in the year 2019. A Mean daily wind range of 3.0 m/s to 4.0 m/s was recorded. This range is closely correlated with wind speeds in a study by Ongaki *et al.* (2021) for Kisii region in Kenya, with a distribution that revealed average c and k values of 3.25 and 1.91 respectively, similar to the value obtained in this study. Wind speed clusters within this range were prevalent, with some days registering a peak of 9.0 m/s.

Table 4.1: Monthly Average Wind Speeds and Temperatures in Year 2019

Month of the year	Average wind speed (m/s)	Minimum temperature (°C)	Average temperature (°C)	Maximum temperature (°C)
Jan	2.7	10.0	19.5	25.0
Feb	2.9	10.0	20.3	26.0
Mar	3.7	12.0	20.7	27.0
Apr	3.9	13.0	20.0	25.0
May	4.1	12.0	19.0	23.0
June	4.9	10.0	17.4	22.0
July	4.5	9.0	16.5	22.0
Aug	3.9	9.0	17.0	22.0
Sep	3.4	9.0	18.5	25.0
Oct	3.1	11.0	20.1	25.0
Nov	2.6	12.0	19.4	24.0
Dec	2.6	11.0	19.2	24.0

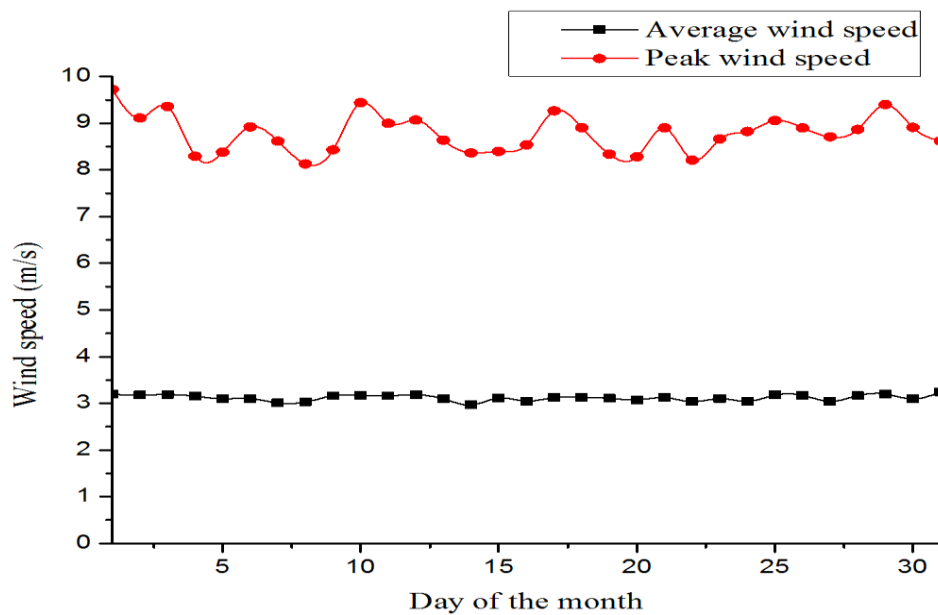


Figure 4.1: Daily Average and Peak Wind Speeds in 2019

Figure 4.2 shows the monthly average wind speeds and temperature extrapolated to show their monthly distribution. With the least possible temperature of 9 °C, June and July were the coolest months in comparison. Maximum mean wind speed was 4.9 m/s in June and 4.5 m/s in July. The hottest months were March and September, with maximum temperatures of 27 °C and 25 °C, respectively.

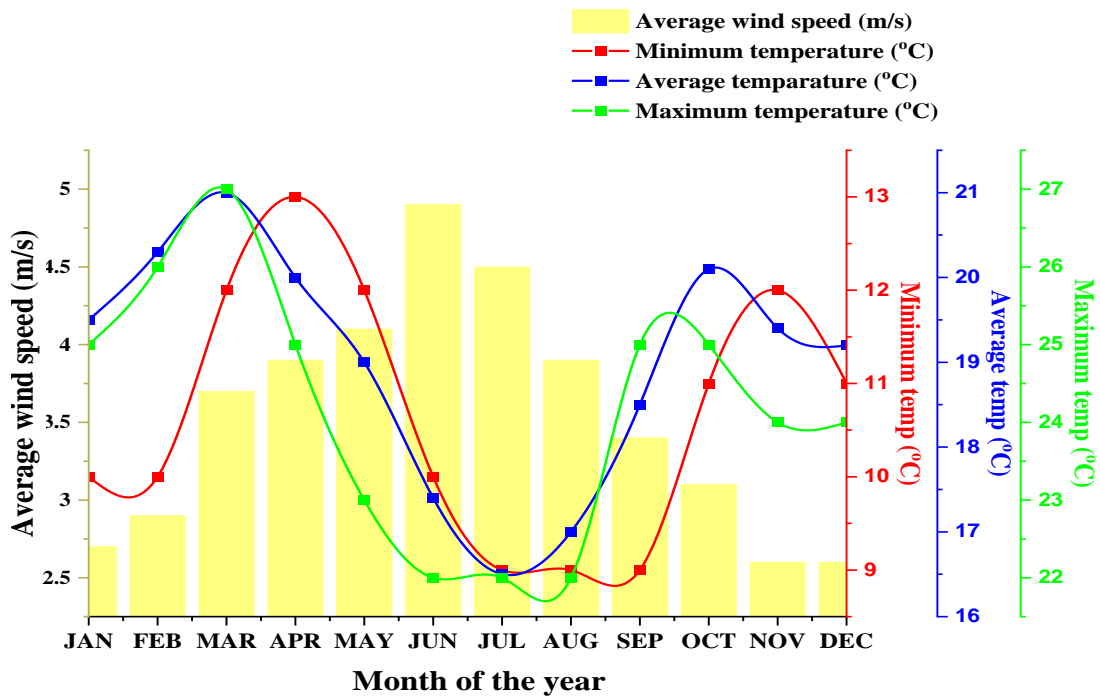


Figure 4.2: Average Monthly Wind Speed and Temperature in Year 2019

Monthly average wind velocities ranging from 2.5 m/s to 4.9 m/s at 20 m were observed at standard pressure and temperature. The wind speeds were compared to the wind speeds obtained in a study by Ongaki *et al.* (2021) whose distribution registered low wind speeds of 2.9 m/s on average at 10 m found to be unsuitable for large scale wind energy generation. However, increase in hub heights increased wind resource viability in driving small wind turbines for energy generation on small scale. This inference agrees with studies by Mukulo *et al.* 2014 for Mwingi-Kitui plateau, Kenya. As also suggested by Ongaki *et al.* (2021), exploitation of such low wind speed regimes similar to Machakos for energy generation calls for installation of higher efficiency and modern turbines with at higher heights to harness energy from higher wind speeds. Moreover, observe also that cold seasons give higher wind energy capacities than warm seasons, since wind energy is directly proportional to wind speeds and air density. This fact justifies the choice of wind energy in complementing solar energy during cold seasons.

4.2.1.1 Weibull's Analysis

Wind speed average (v), Weibull's c , and k variables are crucial in characterizing wind resource distribution and energy potential. These factors are revealed by the Weibull's distribution. Machakos Weibull's distribution of the wind resource profile is shown in Figure 4.3.

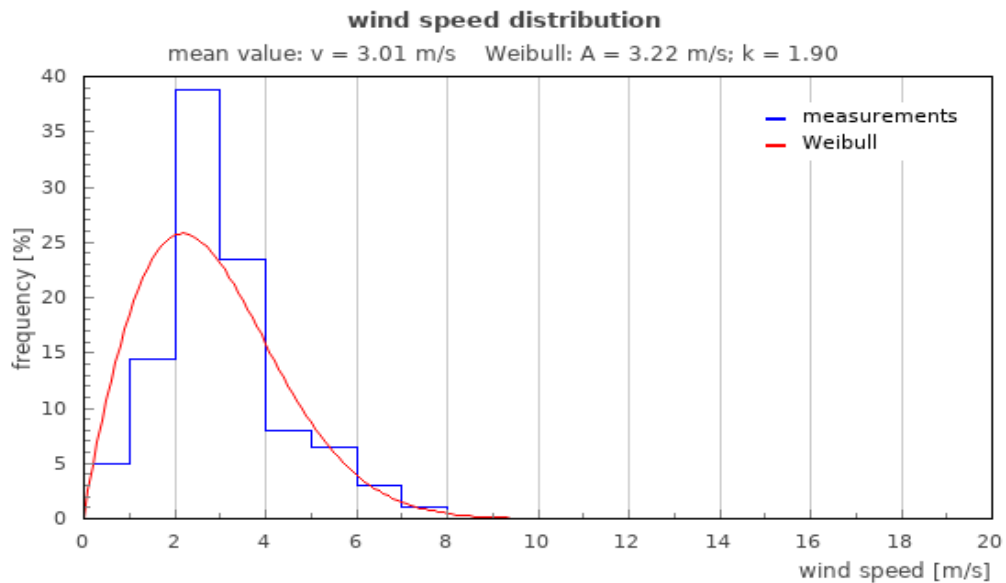


Figure 4.3: Weibull's Distribution for Wind Speeds Between 0-10.0 m/s

According to the analysis, wind speed range of 2.0 m/s to 4.0 m/s are prevalent, which could be considered low. Approximately 90% of the day, the site revealed a high probability of having wind speeds below 6.0 m/s whose energy returns could be low. This wind potential may not be appropriate for large-scale energy generation. Nevertheless, in order to exploit the available potential as a backup for solar systems, such wind regimes show the need for WT design optimization to achieve turbines that could operate in low wind speed regimes with a cut-in of 2.0 m/s. The skewed wind distribution as per the analysis, revealed low wind speeds, scale, and shape parameters. Thus, these findings imply that Machakos has low wind energy potential indicated by a c value of 3.22 m/s and a k value of 1.9 at an average wind speed of 3.01 m/s. Using findings of a study by Kamau *et al.* (2010), which reported a range of 2.5 to 3.05, the

k values were compared. Variations of k parameter have a significant impact on energy, since it shows the extent of resource variability (Li and Zhi, 2016).

The value of k has an inverse relationship with the wind speed variability. A high value of k gives a peaked distribution where wind speeds are close, implying less speed variation. The k value of 1.90 attained in this study suggests that the wind resource is highly variable, causing periodic changes in the power supply. The site under study was thus identified as a low wind area with the most probable wind speeds at 3.22 m/s as implied by the c value. These k and c values are comparable to the values obtained in a study by Ongaki *et al.* 2021 earlier presented in this section. This potential necessitated the use of an alternative source to satisfactorily meet the load demand. Further, the region could be classified in wind class of ≈ 1 by the values of c and k , making it unsuitable for producing wind energy on a large scale. However, with so much attention to advances in WT technology, wind power could be an option for electricity on small-scale. Such developments focus on WT aerodynamics and lightweight resources like composites for the blades (Nishizawa *et al.*, 2013). Moreover, large towers and lengthy blades make turbine installation in low-speed wind areas feasible (de Falani *et al.*, 2020).

Wind may be less reliable due to its erratic nature, but it could be useful through HES, which allow for multiple integration of energy resources. These results clearly show that energy demand for Machakos's even on a small-scale, cannot be fully satisfied by wind resources alone. By utilizing the complementarity phenomenon between energy resources, systems could be more flexible and reliable in meeting the load demand.

4.2.1.2 Wind Direction

The distribution of wind directions was presented in a wind rose diagram as a percentage of all outcomes during the data collection period as presented in Figure 4.4. It is evident that wind speeds originating from NE and SE directions have been found to have the highest prevalence over the year at frequencies of 28% and 35%, respectively. These directions could have been influenced by three hills surrounding the site. From the study findings, a HAWT with a yawing mechanism would be the most recommended turbine for installation in Machakos since it allows turning to align

with SE or NE directions for optimum power generation. As reported in literature, the choice of a HAWT in this study is justified since it permits yawing, which causes the rotor to turn towards directions in search of higher wind speeds, unlike VAWT (Elistratov & Kudryasheva, 2019; Wekesa *et al.*, 2015, Wekesa *et al.*, 2017; Wekesa, Wang, Wei & Kamau, 2014). This makes the lift driven turbines harvest maximum wind energy

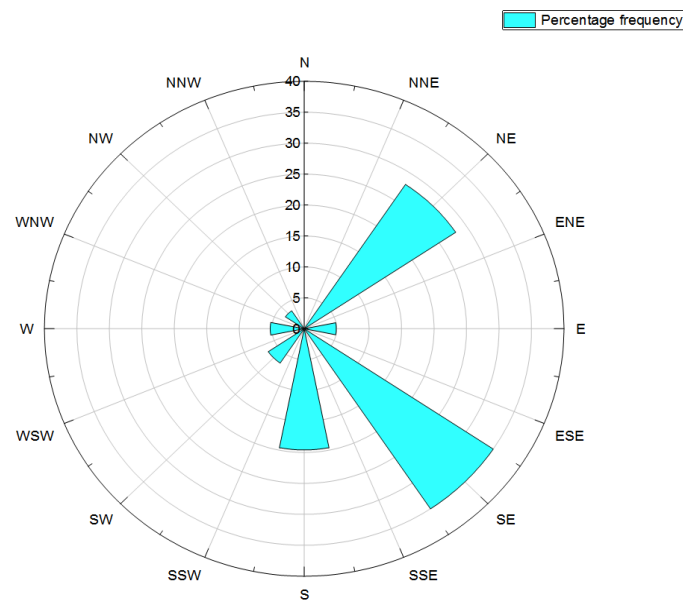


Figure 4.4: Distribution of Wind Flow Directions

4.2.2 Distribution of Solar Radiation

The PVGIS software was used to analyze and profile the findings of the solar PV assessment. Tables 4.2 display the GHI, DHI, and DNI distributions for real sky at fixed plane and while Table 4.3 presents the clear sky distributions under sun track option. This data was used to analyze the monthly solar resource potential in comparison to the measured values, as well as its complementary with wind resource. As also reported in a similar study by Kariuki and Sato (2018) CSI and GHI are higher and of low variability compared to DNI and DHI values, indicating that regions near the equator experience nearly constant insolation for most of the months.

Table 4.2: GHI, DHI, DNI, and CSI Monthly Peak Values at Fixed Plane

Month	DNI (W/m ²)	DHI (W/m ²)	GHI (W/m ²)	CSI (W/m ²)
Jan	682	215	898	1040
Feb	749	219	969	1100
Mar	719	244	965	1140
Apr	626	279	906	1130
May	434	306	741	1090
June	326	311	638	1070
July	310	308	619	1080
Aug	325	324	649	1120
Sep	596	256	853	1120
Oct	609	273	882	1080
Nov	549	267	817	1030
Dec	575	245	812	995

Due to the fact that solar radiation always falls normally on a PV module surface, tracking option had a higher solar irradiance in comparison to fixed plane option. Fixed angle mode was chosen since a sizable portion of the solar radiation falls uniformly on the surfaces in all regions close to the equator like Machakos.

Table 4.3: GHI, DHI, DNI, and CSI Monthly Peaks for Sun Track Option

Month	DNI (W/m ²)	DHI (W/m ²)	GHI (W/m ²)	CSI (W/m ²)
Jan	800	222	1030	1190
Feb	807	223	1030	1180
Mar	723	250	973	1150
Apr	631	274	908	1140
May	464	301	770	1120
June	347	307	660	1120
July	318	297	621	1120
Aug	326	321	650	1130
Sep	611	255	867	1130
Oct	628	285	915	1140
Nov	663	245	918	1160
Dec	681	258	946	1170

Figure 4.5 presents the hourly solar irradiance profile for the hottest month, while Figure 4.6 presents the coldest month of the year. Peak GHI was over 900 W/m² in March, while the lowest was 600 W/m² in July. Due to its proximity to the equator, Machakos experiences nearly similar solar irradiance values in the coldest and hottest months. PVGIS simulation data was validated using experimental solar irradiance data from ground measurements. Figure 4.7 presents the measured values of daily solar irradiance in March, June, and July. Similar to the outcomes of the simulation results presented in Figure 4.5 and 4.6, a maximum solar irradiance of 958 W/m² in March and minimum values of 502 W/m² and 618 W/m² in June and July were recorded, respectively. These monthly variations in solar resource potentials justify the need for another renewable complementing resource that would support the loads during the coldest months of the year, when solar insolation is at its worst. As previously

mentioned, wind energy is an excellent choice to complement solar energy when the solar irradiance is low.

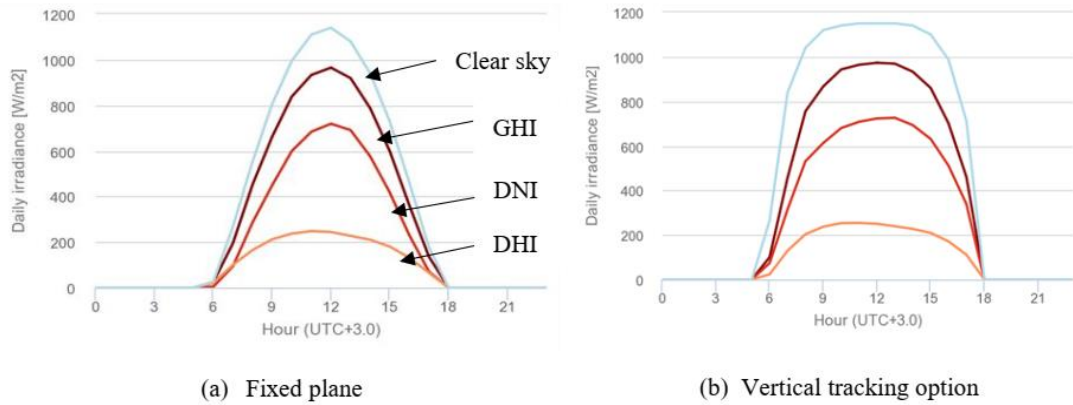


Figure 4.5: Daily Average Irradiance in March 2019 (a) at Fixed Plane and (b) at Vertical Tracking

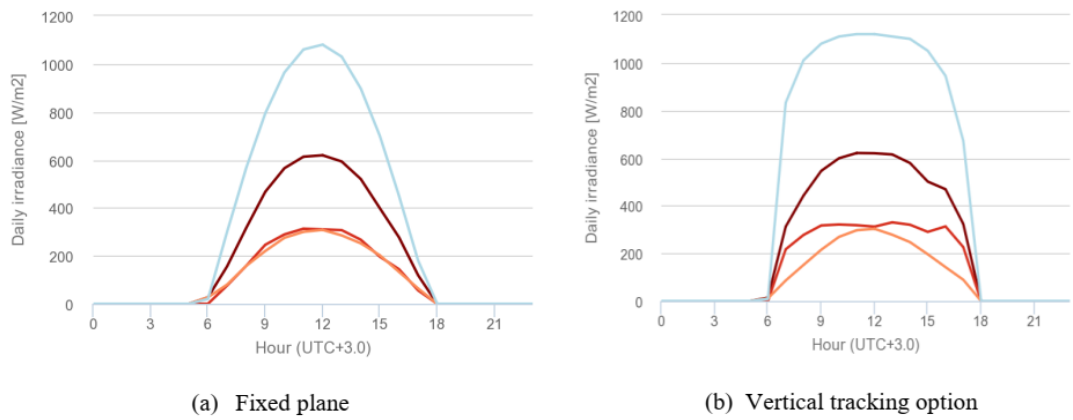


Figure 4.6: Daily Average Irradiance in July 2019, (a) at Fixed Plane and (b) at Vertical Tracking

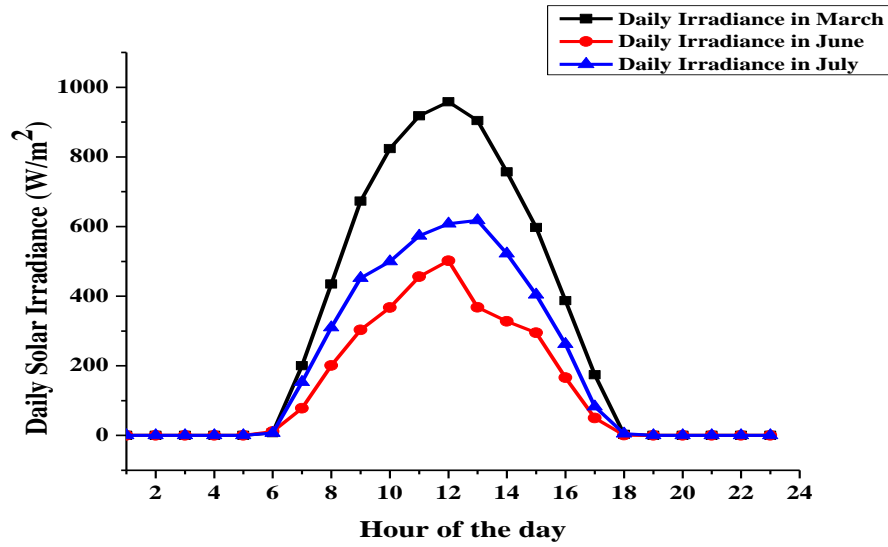


Figure 4.7: Daily Average Irradiance in March, June and July 2019

The simulation results of the measured monthly and daily average solar insolation, as well as the estimated average PV energy, are recorded in Table 4.4.

Table 4.4: Monthly and Daily Average Solar Insolation in the Year 2019

Month	Jan	Feb	Mar	Apr	May	Jun	Jul	Aug	Sep	Oct	Nov	Dec
Simulated Insolation (kWh/m ²)	195	189	213	192	169	146	145	151	182	193	173	179
Daily Average (kWh/m ²)	6.3	6.5	6.9	6.4	5.5	4.9	4.7	5.0	5.9	6.4	5.6	6.0
Measure Insolation (kWh/m ²)	186	180	212	184	157	141	139	148	174	184	165	171
Daily Average (kWh/m ²)	6.0	6.2	6.8	6.1	5.0	4.7	4.5	4.8	5.8	5.9	5.5	5.5
Simulated PV Energy (kWh)	157	148	170	157	141	123	122	127	149	157	140	146

An average daily insolation of 5.84 kWh/m² at a 1 kWp installed capacity is revealed, translating to a yearly solar insolation of 2130 kWh/m². According to the daily insolation, the area has 5.84 hours of peak sunlight per day under the usual test conditions of 1 kW/m² peak sunlight. The calculated daily insolation value of 5.84 kWh/m² closely compares to the value of 5.0 kWh/m² that was provided in a study by Oloo *et al.* (2015) and also lies within the daily insolation range of 5 – 7 kWh/m² reported in a study by Kariuki and Sato (2018).

In March and July, the insolation peak values were 213 kWh/m² and 145 kWh/m², respectively. These monthly potentials further translated to 6.9 kWh/m² and 4.7 kWh/m² daily in March and July, respectively. Note that, as recorded in Table 4.4, the ground measurements revealed average daily insolation of 6.8 kWh/m² and 4.5 kWh/m² in March and July, respectively. The simulation results strongly correlate to the ground measurement results, validating the PVGIS tool as also realized in a related study by Oloo *et al.* (2015). Further, these findings show that PVGIS is accurate and reliable in estimating solar resource energy potentials in inaccessible areas due to topology, insecurity, floods among other factors.

As reported in studies by Iakovleva *et al.* (2022), solar insolation varies with solar angles like latitude, declination, azimuth, hour angle which depend on the earth's position. Observe in Table 4.4 that these positions provided a daily insolation range of 4.7 kWh/m² to 6.9 kWh/m² implying that Machakos experiences between 4.7 to 6.9 hrs of peak sun. The close range in solar insolation not only show the adequate capacity but also the reliability of solar resource in creating access to electricity within the equatorial region, Oloo *et al.* (2015). Figure 4.8 presents a plot of the simulated monthly solar insolation.

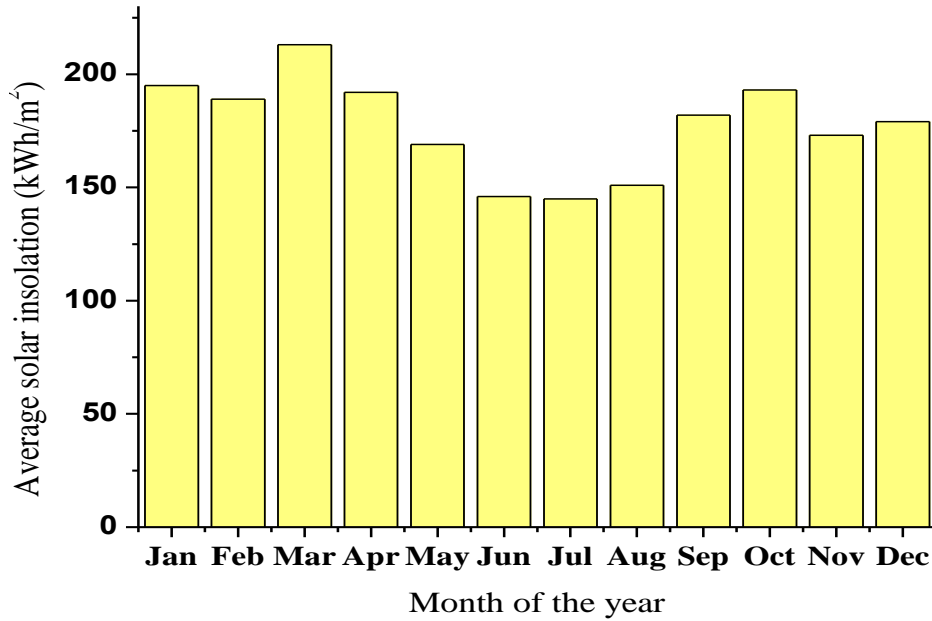


Figure 4.8: Simulated Solar Insolation

Annual PV energy was also simulated at a fixed solar panel tilt angle of 15°. Figure 4.9 presents the average monthly PV energy output profile. Results revealed an annual solar energy potential of 1740 kWh at 1 kWp installation capacity. In general, months with the sun's proximity to the equator have greater potential for energy than months when the sun is farther away. The maximum monthly average solar energy output is 170 kWh in March, while the lowest output was 122 kWh in July. The daily averages for March and July based on this potential are 5.5 kWh and 3.9 kWh, respectively. These results reveal that with a well sized energy system, Machakos being a stride from the equator has high solar irradiation enough to power rural households even in the worst month of solar radiation. This conclusion agrees with a Kenyan study by Akello, Saoke, Kamau and Ndeda (2022) who revealed the potential of regions a stride from the equator as potential areas for solar energy harvest.

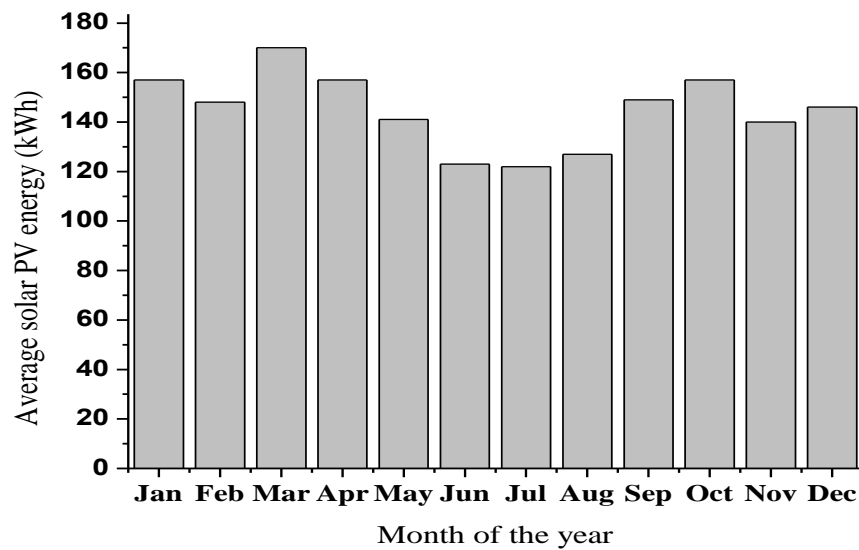


Figure 4.9: Simulated PV Energy Output

4.3 Wind and Solar Complementarity

Hourly, daily, and monthly interchange patterns were revealed by the wind and solar resources at the site. Depending on the time and weather, they were frequently found to be in and out of phase alternately. In Figure 4.10, the time series for solar and wind resources are presented on hourly timescale. Machakos receives 12 hours of sun radiation daily from 0600 hours to 1800 hours due to its proximity to the equator, as also reported in a study by Oloo *et al.* (2015). As a result, for a good percentage of the day, hybrid wind/PV systems are solely dependent on solar energy. With the absence of solar irradiance at night, solar PV systems alone are unable to power the loads. This condition increases the rate of battery discharge, depleting its backup power. The complementarity effect of wind resource with solar increase its techno-economic viability attracts its exploitation for integration through hybrid energy systems, as also suggested in the study by Johannsen *et al.* (2020). Thus, wind has been found to be a good energy source during periods of low solar energy.

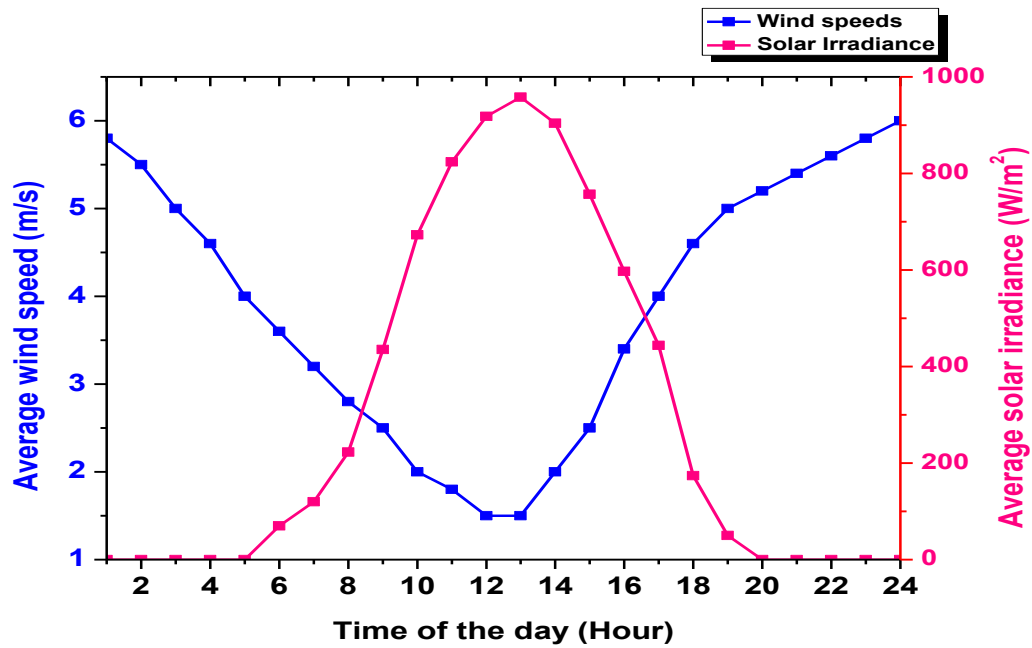


Figure 4.10: Hourly Time Series of Solar Irradiance and Wind Speed

It was observed that in the evening between 1700 and 0800 hours and during the day between 0800 and 1700 hours, wind and solar potentials were out of phase. This pattern points to intriguing possibilities for the complementarity in the production of wind-PV energy. Between 0800 hrs and 1700 hrs, solar radiation was sufficient and predominate. The trend changed for periods between 1700 hrs and 0800 hrs where wind resource dominated. This high level of complementarity could be attributed to the abrupt changes in weather brought on by rotation and revolution of the earth. Figure 4.10, in particular, reveals the appropriateness of wind and solar in driving HES and as also observed in a study by Jurasz *et al.* (2018) and Jurasz *et al.* (2020) considering complementarity metrics in sizing wind/solar hybrid systems have a positive impact on reliability and resource curtailment due to improper sizing. This effect could also reduce on large storage needs also observed in a study by Solomon *et al.* (2020)

Figure 4.11 illustrates the monthly switch over of wind and solar energies. The analysis revealed a negative correlation between the two resources, demonstrating strong complementarity during the different seasons of the year. Solar insolation was high in the first and last four months of the year, with peaks of 213 kWh/m² and 193 kWh/m²

in March and September, respectively. June and July recorded the lowest values of 146 kWh/m² and 145 kWh/m², respectively. Comparatively, the maximum average wind speeds were 4.9 m/s and 4.5 m/s in June and July, respectively. This change switched the potential from solar to wind. This trend ensured nonstop supply of power to households from January to December.

The erratic weather changes that occasionally result from shading effects and earth's movements lead to low energy capabilities of solar and wind resources. These changes partly result in power instability, a situation that could subject the energy storage facilities to high rates of discharge, prolonged low change states, and high operating temperatures as also highlighted in a study by Neto *et al.* (2020). In order to protect energy users from the detrimental effects of intermittent wind and solar resources, hybrid systems and substantial storage capacity are essential.

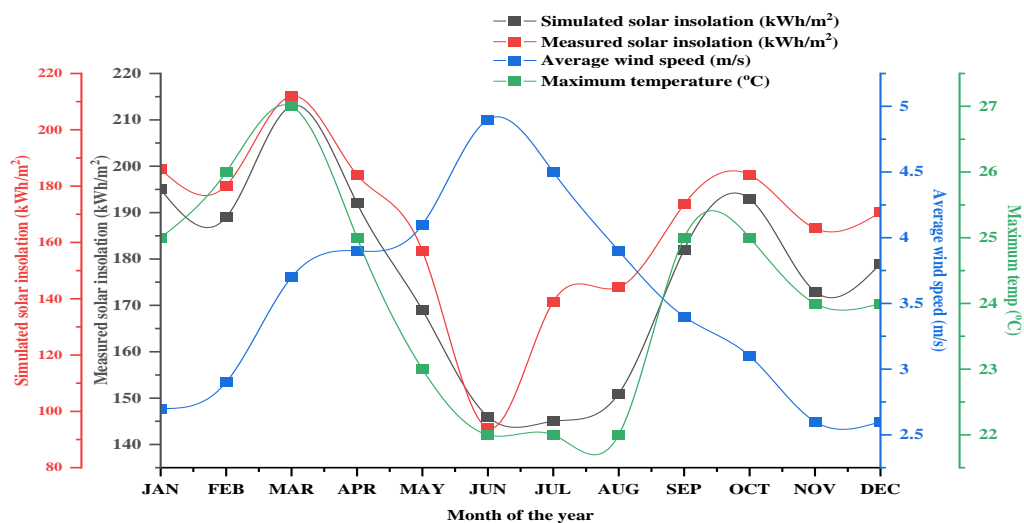


Figure 4.11: Solar and Wind Resource Monthly Complementarity

According to the complementarity analysis, hybrid systems have been found to be adaptable enough to provide consistent supply of energy in both promising and harsh weather circumstances. This study findings provide the knowledge needed on viability of complementarity in wind and solar systems' hybridization which was largely unrecognized in Kenya resulting in low spread rate of hybrid systems as suggested by Johannsen *et al.*, (2020). This development opens up on the potentials in small wind turbine technology in energy generation.

In this study, complementarity has been found to be fundamental in renewable energy systems since when one source's power output suddenly drops, the supply automatically switches to the other sources, increasing power stability and system's flexibility. As also suggested by Kumar *et al.* (2019) and observed from Figure 4.10 and 4.11, complementarity would reduce battery discharge time increasing its life span as well as battery capacity requirements decreasing the system's cost. With these strengths, therefore, complementarity effect could increase the penetration of small-scale wind/solar HES in remote areas. This view also agrees with inferences done in a study by Solomon *et al.*, (2020).

4.4 Energy Demand Analysis

In three selected zones of Machakos, data on energy consumption patterns was collected. Data analysis determined the household daily load and its load profile. Daily average energy loads in zones A, B and C are as shown in Tables 4.5 were a range of 0.97 kWh to 1.498 kWh across the three zones is reported. Table 4.6 presents the average daily loads below 1 kWh, a range where most of the rural household loads fall. Table 4.7 present the frequency distribution of households according to their daily energy consumption levels.

Table 4.5: Average Energy Loads per Cluster, Expressed in kWh

	Zone A	Zone B	Zone C
Cluster 1	0.97	1.008	1.375
Cluster 2	1.399	1.054	1.498
Cluster 3	0.943	0.954	1.356
Cluster 4	1.054	0.985	1.367
Average	1.09	0.99	1.4

Table 4.6: Cluster Average Energy Loads for Homes using less than 1 kWh daily

	Zone A (kWh)	Zone B (kWh)	Zone C (kWh)
Cluster 1	0.43	0.589	0.550
Cluster 2	0.64	0.578	0.579
Cluster 3	0.57	0.473	0.614
Cluster 4	0.50	0.645	0.643
Average	0.56	0.590	0.596

Table 4.7: Frequency Distribution of Household Loads

Load (kWh)	Zone A %	Zone B %	Zone C %	Total %
0-1	60	53	42	52
1-2	24	38	32	31
2-3	13	9	17	13
3-4	3	0	7	3
4-5	0	0	2	1
5-6	0	0	0	0

The frequency distribution of levels of energy utilization in three rural zones is presented in Figure 4.12 while Figure 4.13 presents the general energy demand distribution in all zones. 52% of consumers used below 1 kWh daily (Figure 4.13), with daily energy loads ranging from 0.052 kWh to 4.23 kWh. With an overall average of 1.161 kWh, the daily loads for the three sites were 1.092, 0.99, and 1.4 kWh. This indicates that the majority of rural families use less than 1.5 kWh of electricity each day. This low consumption could be a result of poor social-economic status attributed to low incomes, a situation that triggers the use of conventional sources of energy to meet the required energy demand. Further analysis on households consuming less than 1 kWh daily revealed an average daily consumption of 0.582 kWh where mean consumptions in zones A, B and C were 0.56 kWh, 0.59 kWh and 0.595 kWh, respectively. For an average household consuming less than 0.582 kWh a day, translated to 17.46 kWh per month and 213 kWh yearly. This demand is comparable to a monthly load of 15 kWh which translates to a daily average of 0.5 kWh reported in a study on energy preference and consumption intensity in Kenya by Mbaka,

Gikonyo and Kisaka (2019). Further, it was noted that demand is significantly influenced by people's habitat and way of life.

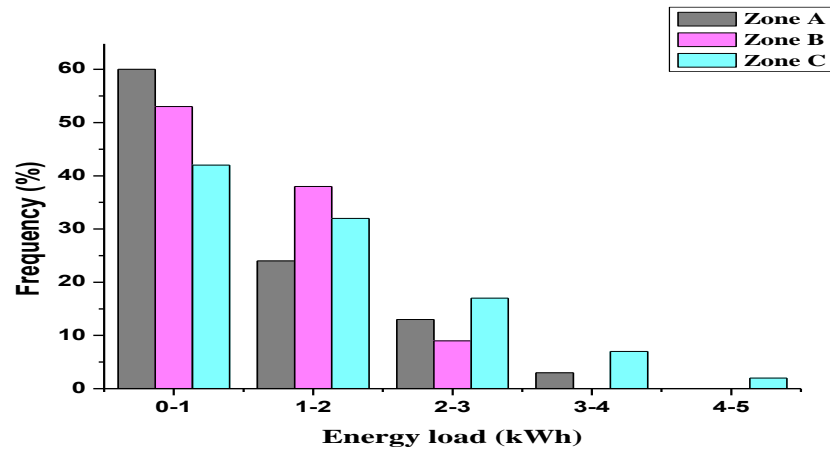


Figure 4.12: Levels of Energy Use in the Three Zones

In comparison to rural areas, people use more appliances in cities, hence the increase in energy consumption. The zones are part of the rural area of Machakos, where only a few homesteads have connection to the national grid. The few homes that are wired to the grid find it a challenge to meet the monthly bills due to the high cost of electricity.

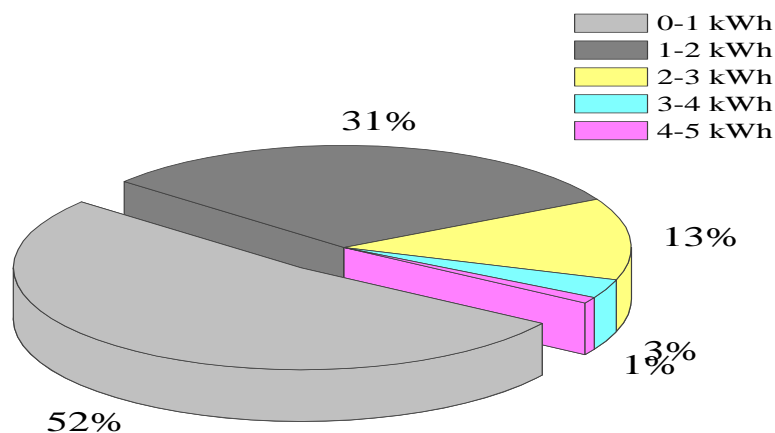


Figure 4.13: Patterns of Energy Consumption in Machakos

According to a study by Dominguez, Orehoung and Carmeliet 2021, much of the rural population in Kenya lacks access to electricity due to costs. Their poor economic status

only allows the connected few spend roughly 20 % of their little income on electricity with preference on lighting which takes about 60% of the bills (Ngare & Kioli, 2019). A similar scenario is revealed by the findings of this study. As also observed by Mbaka *et al.* (2019) economic status trigger the use of non-clean energy sources with the rural areas consuming larges proportions of the same. This study showed that a solution to overcome the energy access challenge and develop the best system design called for accurate estimation of the household consumption levels.

In spite of the challenges, a few of the economically stable households own small panels which hardly meet the necessary energy load demand. Notably, as a result of electricity cost, the majority of homes in remote areas do not use high power consuming appliances. Table 4.8 lists the devices that are commonly found in rural homes and have daily energy usage of below 1 kWh. In this study, hybrid system sizing took into account the household chosen from among the three zones.

Table 4.8: A Typical Rural Household's Load Demand in Machakos

Appliance	Rating (W)	Active hour in a day	Total units (Wh)
4 bulbs	11	5	220
2 Radios	50	3	300
3 Phones	8	2	48
1 Lamp	10	2	20
Total	178	12	588

Observe in Table 4.8 that low-wattage appliances in an average rural household have a limited time of use to avoid high electricity bills. Figure 4.14 presents the load profile for a typical rural household in Machakos. The profile reveals high energy loads in the evening.

In comparison, much electricity is utilized between 1700 hrs and 2200 hrs. After their day of activities, people return home during this time. At this time, the main energy-consuming devices are lighting, televisions, radios and phone chargers. When people sleep most appliances are put off minimizing electricity consumption significantly, except for a few bulbs, which use negligible energy. With absence of solar during the night, battery discharge is kept to a minimum. This study findings show that the need

to meet the nighttime energy load demand makes hybrid energy system that incorporates wind/solar renewable resources more viable since their complementarity daytime and nighttime meets the energy needs reliably.

Wind resource investigation have proven its feasibility as a supplement to solar energy due to its accessibility, particularly during times of low insolation. Thus, development of a site-specific wind PV hybrid energy system in this study is justified.

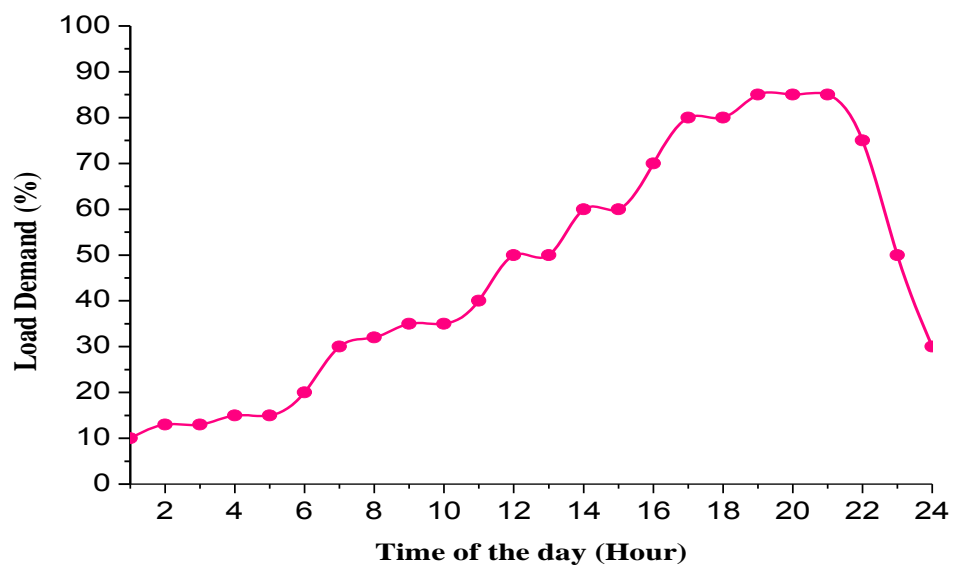


Figure 4.14: Load Demand Profile for a Typical Rural Household

4.5 Wind Tunnel Test Results

This section offers an examination of rotational speeds, TSR, and power coefficients for various wind speeds and blade pitch angles in addition to the optimization results. Figure 4.15 (a) and (b), respectively, shows a graph of RPMs vs wind speeds for rotors made of foam and aluminum. Compared to aluminum blades, Styrofoam blades reported speeds that were somewhat higher, between 60 and 102 rev/min. For the aluminum rotor blades, higher RPMs were achieved at pitch angles of 12°, 15°, and 18°, with a peak value at a pitch angle of 15°. The speed decreased for pitch angles greater than 18° due to increase in drag forces near the stalling point for large AOA. Rotor blades experienced a sharp decline in lift near the stalling point, which reduced lift to drag ratio, resulting in a low coefficient of power. Styrofoam blades showed

greater rotor speeds for pitch angles between 18° and 25° , and lower speeds at angles higher than 25° . The maximum rotor speed was reached at a pitch angle of 20° .

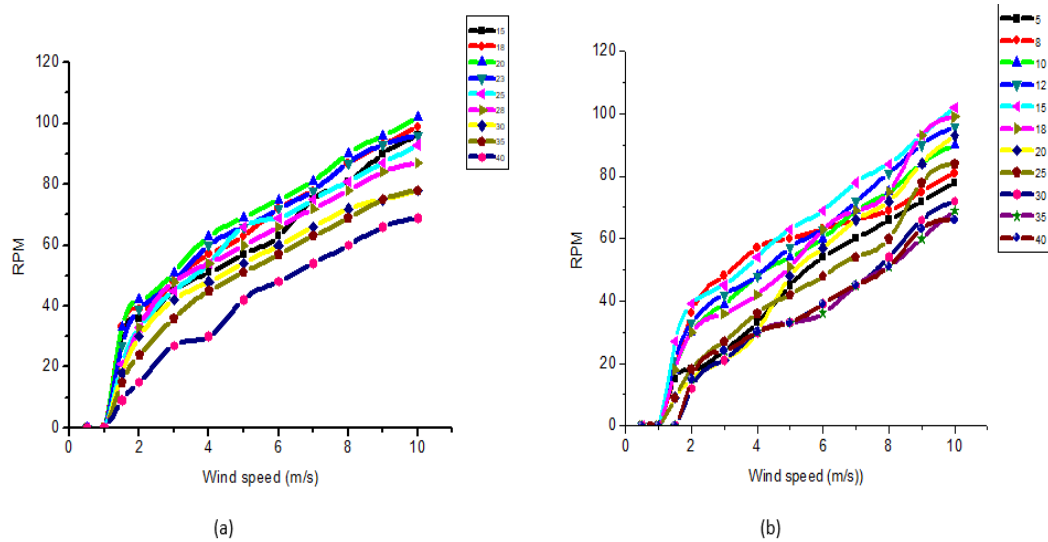


Figure 4.15: (a) RPM vs Wind Speeds for Styrofoam and (b) Aluminum Blades, respectively

According to Manwell *et al.* (2010), when rotor blades pitch at the critical angle, two thirds of the wind speed is transformed into kinetic energy, producing maximum possible power. As a result, the critical angles of the aluminum and foam blades were fixed at 15° and 20° , respectively. Below these angles, a lot of wind was obscured, increasing the drag impact. Pitch angles of 15° and 20° therefore provide the best operational conditions for the two types of rotor blades. Figure 4.16 (a) and (b) depict a graph of the TSR vs wind speeds for foam and aluminum rotors, respectively.

The TSR has a considerable effect on the C_P of the turbine. The analysis found that greater tip speed ratios had a tendency to lean toward low wind speeds, suggesting promising prospects for the turbine's energy conversion in low wind speed regimes. The aluminum blades' maximum TSR was 2.9 at a pitch angle of 15° , while the foam blades' maximum TSR was 3.1 at a pitch angle of 20° . Styrofoam blades recorded higher tip speed ratios in comparison to aluminum blades. Even though their performance characteristics were close, Styrofoam revealed to be a more efficient wind

energy converter than aluminum due to the slightly higher value of C_P it revealed. This good performance could be attributed to its low density of 0.96 g/cm^3 compared to aluminum at 2.7 g/cm^3 , the material is over 90% air making it light and easy to rotate faster than aluminum. Calculations and comparisons were made for both blade types' power coefficients and the corresponding TSRs.

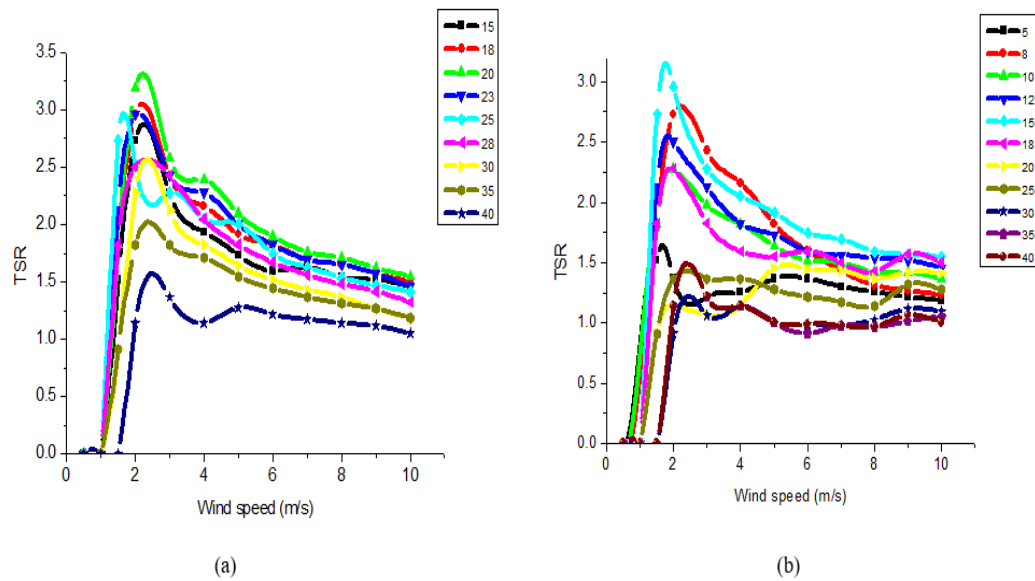


Figure 4.16: (a) TSR vs Wind Speeds for Styrofoam and (b) Aluminum Rotors, respectively

Utilizing the fabricated rotor blades, the extractable wind power was estimated using the coefficient. For aluminum and Styrofoam rotors respectively, Figures 4.17 (a) and (b) show graphs of the power coefficient against TSR whereas Figures 4.18 (a) and (b) present graphs of wind power estimates at optimal C_P verses wind speeds.

In accordance with a related study by Saoke *et al.* (2014), the optimal TSRs were observed to shift towards the right. This could be attributed to stall effects at low TSRs characterized by high AOA. Observe in Figure 4.17 (a) that, for the aluminum blades, a maximum C_P of 0.431 at a pitch angle of 15° was recorded. This coefficient corresponded to a TSR of 2.0. According to the graph of Figure 4.18 (a), a C_P of 0.431 corresponded to a power of 220 W. At a pitch angle of 20° , foam blades revealed a higher C_P of 0.465 in the graph of Figure 4.17 (b), corresponds to a TSR of 2.1. A

coefficient of 0.465 would result in a maximum wind power of 238 W according to Figure 4.18 (b). These C_p could strongly be attributed to the optimized blade design that enabled lift maximization even below the rated wind speed.

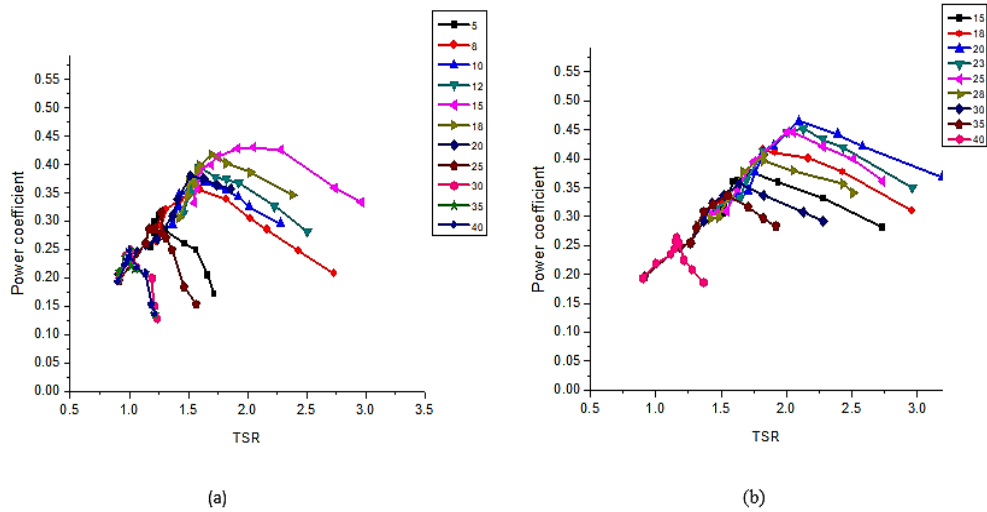


Figure 4.17: (a) C_P vs TSR for Aluminum Rotor and (b) Styrofoam Rotor, respectively

In line with literature, the power estimates were below the limit of 300 W calculated at the Betz limit C_P of 59.3%. Low C_P was realized below and after the optimum TSR, which could be attributed to increased drag forces which reduced lift force. The TSR results compared to those from Nishizawa study on tapered WT blades, which recorded a C_P of 0.39 at a TSR of 4.06 (Nishizawa, 2011). Additionally, Saoke, Nishizawa, Ushiyama, Kamau, (2015) reported a maximum power coefficient of 0.372 in a study on small tapered blades pitched at various angles. This C_P was found to be comparable to the findings in this study. It was noted that the rotor revolved at low speeds with wakes below the optimal TSR, implying that minimal wind was available for energy conversion as a large portion spilled past the blades. Above the optimal TSR, the rotor revolved quickly, acting like a wall and obfuscating wind. Thus, high wind speeds increased drag, which reduced lift force. Similar, higher pitch angles caused the rotor to stall, declining its power output. These findings strongly agree with findings by Wen *et al.* (2017) that, as TSR rises, C_P falls. By making sure that the WT systems operates at their optimum point, conditions which are detrimental to the WT hardware could be avoided.

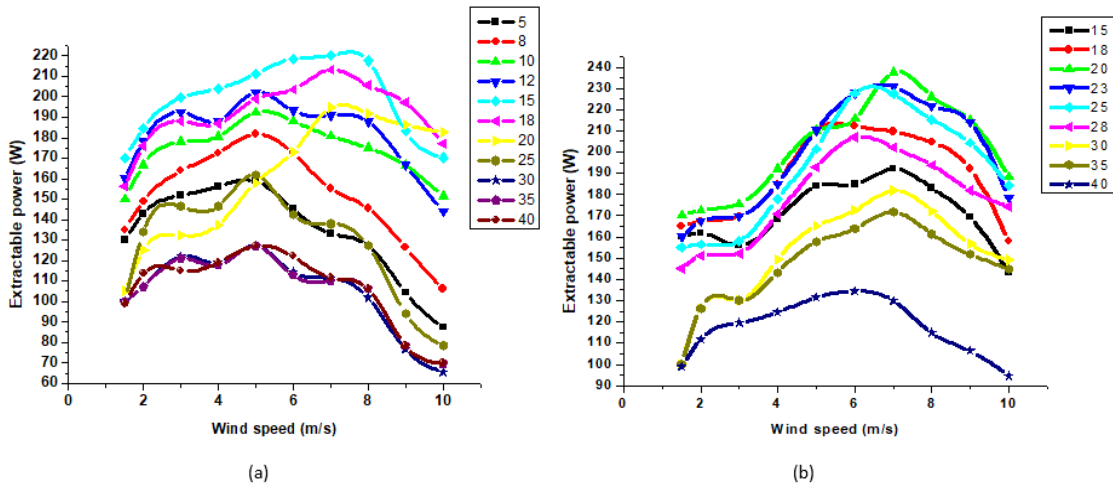


Figure 4.18: (a) Extractable Power vs Wind Speeds for Blades made of Aluminum and (b) Styrofoam, respectively

Expected power output at the best possible revealed C_P value of 0.465 was examined to characterize the power performance of the WT at the optimum TSR. Where power at a C_P of 0.465 and rated wind speed of 5 m/s was compared to the maximum expected power extractable at the Betz C_P value of 0.593. A graph of power at Betz limit verse WT output power is shown in Figure 4.19.

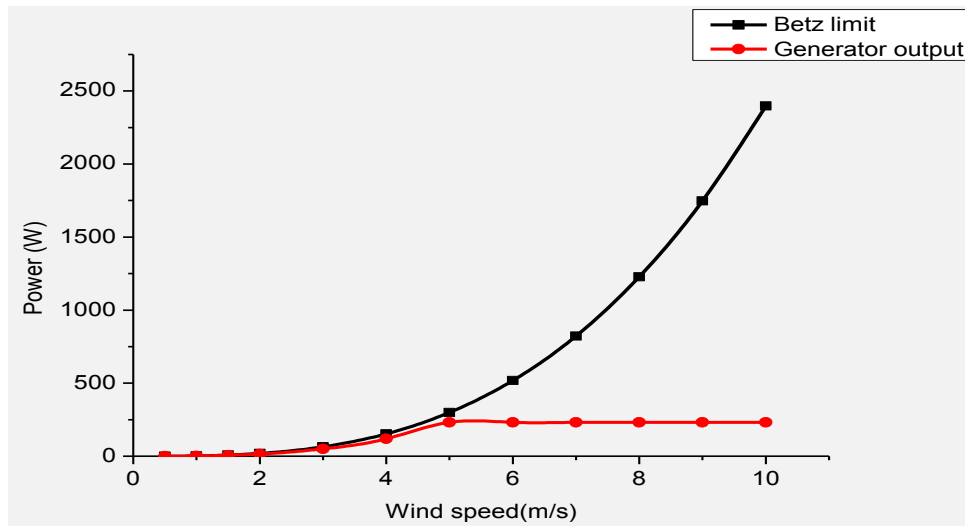


Figure 4.19: Expected WT Power Output

For a 200 W generator used in this study, the power reached its maximum at the rated wind speed of 5.0 m/s then remained constant for higher wind speeds. These findings reveal that, low wind speed regions like Machakos with average wind speeds of 3.0

m/s even though neglected, could be viable for small-scale power generation with wind turbines of cut in wind speed of 2.0 m/s, rated winds speed of 5.0 m/s and a cut-off wind speed of 15 m/s. At the optimal operating conditions revealed by the wind tunnel findings, the developed turbine could convert wind energy at a C_P of 46% and 43% for Styrofoam and aluminum blades, respectively. According to the configurations in Table 3.1, this power, closely reflects the anticipated WT power output of 235 W as per the design configuration. This amount of power would be adequate to support rural household loads and small-scale utilities.

4.6 Hybrid System Power Performance

A wind solar hybrid energy system was developed and a field test undertaken. This section presents analysis of vertical wind shear, voltage and current integration trend, battery charging, and load supply.

4.6.1 Wind Shear Analysis

Vertical wind distribution estimated applying the power law in Equation (2.9) and the energy potentials are reported. Figure 4.20 shows wind shear analysis and the corresponding WPDs to a hub height of 100 m above the ground. Observe from Figure 4.20 that, wind shear expands energy capacity, making a given site a suitable wind resource.

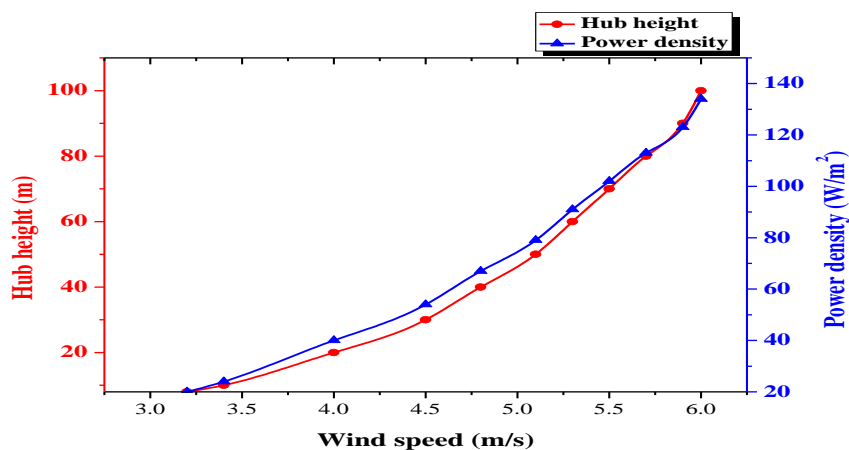


Figure 4.20: Vertical Wind Shear and Corresponding Power Densities

The shear analysis revealed power densities in a range of 20 W/m² to 140 W/m² from which a suitable turbine would extract significant energy from wind resource. At a shear coefficient of 0.25, wind energy was estimated using 3.2 m/s as the reference wind speed at a hub height of 8 m. For turbine hub heights between 10 and 100 meters above the ground, mean wind speeds of 3.4 m/s to 6.0 m/s were recorded. The vertical distribution profile agrees with the EPRA findings discussed earlier in the literature (EPRA, 2022). The developed WT, designed to operate optimally at a wind speed of 5 m/s, would generate maximum power at hub height of 50 m at an estimated wind speed of 5.1 m/s. A rotor of diameter 2.9 m and a C_P of 0.431, as previously reported in this study, which would produce 225 W from a WPD of 79 W/m².

These findings were compared to results in a study by Mwanzia *et al.* (2019), where empirical power densities ranging from 31.65 W/m² to 54 W/m² were reported. According to the study, the power densities corresponded to numerical densities ranging from 71.76 W/m² to 125.45 W/m² in a turbine hub height range of 40 m to 100 m, respectively. The revealed power densities in this study indicates the viability of wind resource especially in driving small wind turbines as also observed by Choge *et al.* (2013) in his study that reported a range of 40.67 W/m² to 80.379 W/m² at hub heights of 10 m and 20 m, respectively.

4.6.2 Power Performance Analysis

Figures 4.21 shows the input voltage integration, while Figure 4.22 shows the current integration from solar and WT systems through the MPPT controller to meet the loads and charge the battery. Wind was prevalent between 1800 hrs and 0600 hrs, while solar was most prevalent between 0600 hrs and 1800 hrs. At night, wind power supply predominated with an average voltage of 9.05 V and current of 4 A higher than solar power supply with an average of 2 V and 0.8 A. The trend interchanged between 0600 hrs and 1800 hrs where solar dominated maintaining the supply above an average voltage of 13.23 V and current of 5.4 A. The voltage and current values obtained translates to an average power of 71.4 W for a 100 W solar panel with a V_{max} of 18 V and I_{max} of 5.56 A at the standard test condition of 1000 W/m². This analysis revealed good complementarity between wind and solar energy supplies.

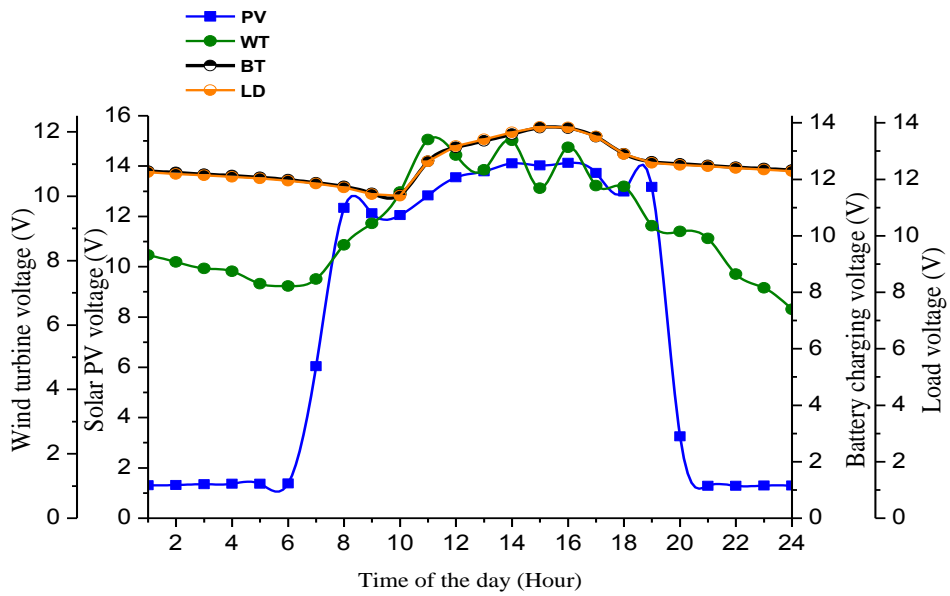


Figure 4.21: Voltage Outputs of the Hybrid Energy System

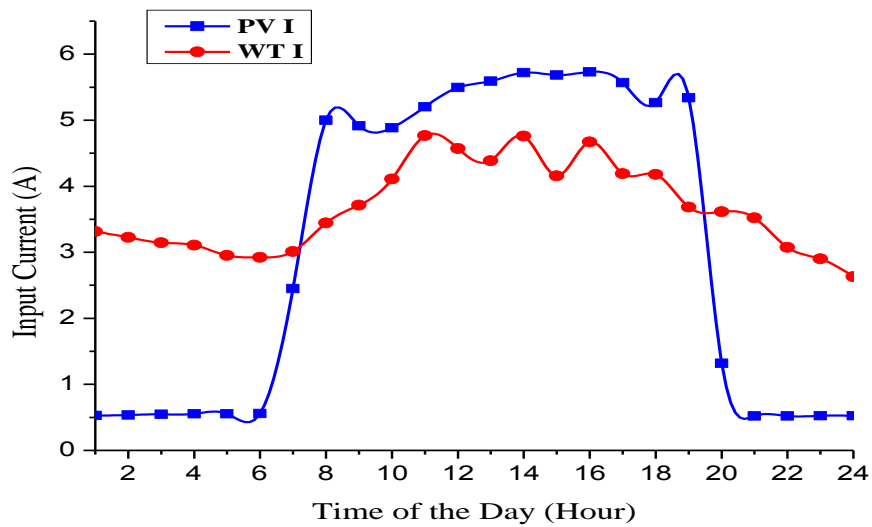


Figure 4.22: Output Currents of the Hybrid Energy System

The complementarity characteristic of wind and solar, earlier discussed in a previous section, is reflected and validated by the power performance findings. Wind voltage was found to be comparatively higher during the day than at night. This swapping in power potential can be attributed to increase in wind speeds caused by decrease in air

density when ambient temperatures rise. These results revealed good system flexibility in its operation, a characteristic that would overcome power outage due to sudden changes in weather, intermittency and cloud cover among other factors. This analysis justifies the suitability of the developed hybrid energy system in supplying stable power to rural households. Wind shear analysis to a turbine hub height of 50 m revealed more extractable energy capacity sufficient for rural electrification in Machakos. Figure 4.23 shows integration of solar power with wind power at varying turbine hub height.

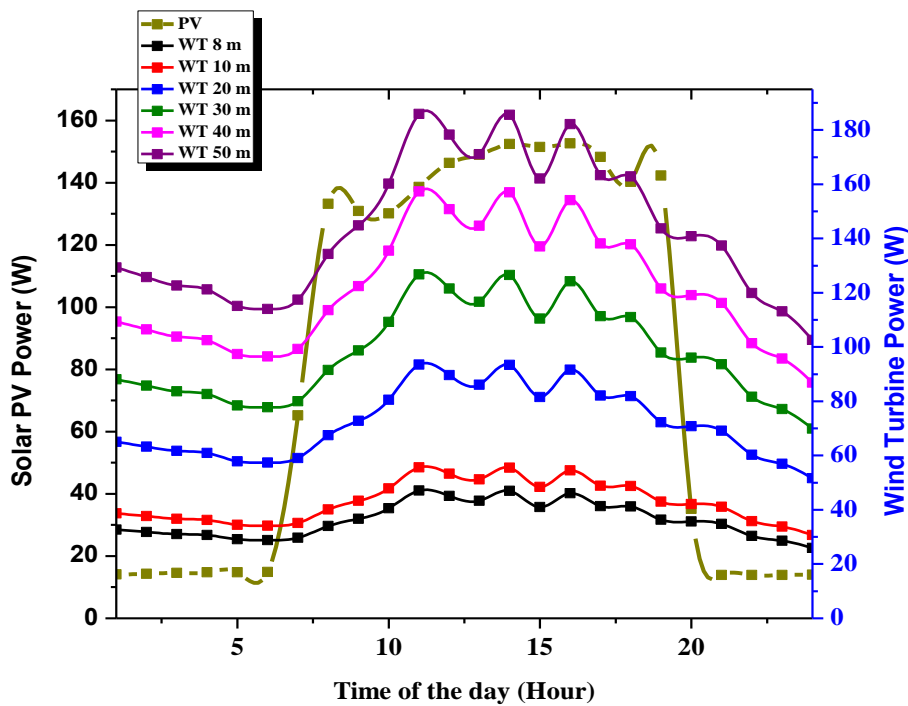


Figure 4.23: Wind Shear Analysis to a Hub Height of 50 m

Analysis revealed a huge energy potential in wind resource for heights above 10 m. In this study, hub heights of 8 m to 50 m were of much interest due to hub installation costs. Observe that, at WT hub heights of 8 m to 50 m, wind power increased from 36 W to 143 W, respectively. This increase translates to daily energy between 0.864 kWh and 3.432 kWh, respectively. Using the WPD range of 20 W/m² to 79 W/m² earlier presented in Figure 4.20, a rotor of diameter 2.9 m would generate 57 W to 225 W at a C_p of 0.431. This rate would translate to a daily energy of 1.368 kWh and 5.4 kWh, respectively. This daily potential was determined using Equations (2.17) and (2.18).

Table 4.9 shows the energy estimates of WT at higher hub height. WT power effectively complemented solar power, which revealed an average output of 143 W. This PV power translated to 0.835 kWh at 5.84 peak sun hours per day. This solar energy balanced with the wind turbine's energy of 0.864 kWh at 8 m hub height. Energy production capacity per year at 8 m hub height was 315 kWh. Despite the cost of turbine installation at higher height, more wind energy could be realized with a maximum of 1.3 MWh annually at hub height of 50 m above the ground. The findings in this study show that wind resource in low wind speed regimes could still be viable with increasing hub height enough to balance with solar energy from bigger PV systems. Despite the low wind resource potential higher heights turn out to be promising in energy generation using hybrid systems. Higher hub heights enable the creation of a balance in daily energy generation from two complementary technologies thus reducing the mismatch between generation and household energy demand. Moreover, more energy from higher hub heights improves on power stability by reducing power fluctuations. This development would minimize the need for higher storage capacities decreasing the systems investment cost.

Table 4.9: Annual Wind Turbine Energy Production at Increasing Hub Heights

Hub Height (M)	Expected Power (W)	Measured Power (W)	Daily Energy Production (kWh)	AEP (kWh)
8	57	36	0.864	315
10	67	43	1.032	377
20	113	72	1.728	631
30	154	98	2.352	858
40	191	121	2.904	1060
50	225	143	3.432	1253

4.6.3 Wind Solar PV Hybrid System Specifications

Table 4.10 show the appropriate HES suitable for a rural household in Machakos.

Table 4.10: Specifications of the Developed Wind-Solar Hybrid System

Component	Specification
Rotor diameter	2.9 m
Swept area	6.6 m ²
Number of blades	3
Power coefficient	0.431
Rotor power rating	220 W
Rated wind speed	5.0 m/s
Hub height	50 m
WT Generator rating	200 W
PV rating	165 W
HCC	15 A
Battery (Lead acid)-1 DOA	100 AH
Inverter	0.25 kW

Styrofoam blade performed slightly higher than aluminum however, Styrofoam is costly and cloud have adverse effects on health and environment. Thus, aluminum was chose which is cheap, readily available, non-toxic and easy to machine. Aluminum would generate power at a high C_p of 0.431 slightly below Styrofoam but sufficient to power small-scale energy loads. Based on these facts, aluminum was choses for application in low wind speed regimes. Table 4.9 shows that the developed hybrid system produced 63% of the projected power, taking into account power losses. Based on this performance, 200 W generator driven would be suitable for an average rural household electrification.

4.7 Economic Viability Analysis

Based on the economic analysis parameters discussed in section 3.4.8, the economic benefits of the developed HES were evaluated and tabulated in Table 4.11. The approximate investment cost of the wind-solar HES project was USD 631. Considering an average daily load demand of 0.588 kWh presented in Table 4.8, the approximate annual cash inflow (avoid cost) was USD 154 which factored grid electricity at Ksh 30 per unit and carbon direct air capture (DAC) annually. DAC plant capturing CO₂ at a rate of 4000 tCO₂ annually, costs at most USD 800 per ton (International Energy Agency, 2022; *Why Kenya Could Take the Lead in Carbon*

Removal, 2023). Using the economic models in section 3.4.8, analysis showed that installation of a HRES could be economically viable within the 20 years of the system life span. The analysis revealed a discounted payback period of 5.47 years, a net present value of USD 537 at a discount rate of 6 %. The present value of future cash inflows was estimated at USD 1168 which would give a profitability index of 1.85.

The net CO₂ emission reduction in life span of 20 years was 2.11 tons for a household, which translates to 633 tons for a whole village with similar household average loads. Considering carbon removal method from air using DAC plants, emission equivalent to 0.8% would be avoided. The obtained payback period of less than 6 years, the positive NPV value, and the profit index value which was greater than 1, revealed that the project is attractive and installation of a wind/solar hybrid energy system for small-scale energy generation in low wind speed regimes is economically viable.

Table 4.11: Hybrid Energy System’s Economic Viability

System Cost (USD)		Benefits	
Solar panel:	77	Energy load:	0.588 kWh
Battery:	77	Annual avoided costs:	USD 154
Inverter:	14	Economic life time:	20 years
Turbine:	231	Payback Period	5.47 years
Pole:	77	NPV:	USD 537
Controller:	116	PI:	1.85
Installation:	39	PV of future cash inflows:	USD 1168
Total cost	631		
CO ₂ reduction rate:		0.5 kg/kWh	
Net CO ₂ per Household:		2.11 Tons	
300 households:		633 Tons	

CHAPTER FIVE

CONCLUSIONS AND RECOMMENDATIONS

5.1 Conclusion

Despite the unpredictable nature of wind and solar resources in Machakos, their periodic complementarity has been found to be prevalent. Analysis revealed a negative correlation between the two resources on monthly, daily, and hourly time-scales. This relationship revealed a high degree of complementarity between wind and solar in Machakos, a characteristic that could make them more attractive increasing their exploitation for energy generation.

In this study, complementarity was found to be a feasible solution in overcoming the effects of resource intermittence and low wind speeds. The findings revealed a daily insolation of 5.84 kWh implying 5.84 PSH at a 1 kWp installation capacity. The highest average daily insolation, 6.9 kWh/m², occurred in March, and the lowest, 4.7 kWh/m², occurred in July. A skewed distribution of wind speeds was revealed, with Weibull's c and k values of 3.22 m/s and 1.9, respectively. This suggests that low wind speeds, which are highly variable are prevalent. Over 90% of the total wind speeds fell within a range of 1.0 m/s to 5.0 m/s at an average of 3.01 m/s and a WPD of 17 W/m² at a height of 20 m. This potential classifies Machakos in a wind class of ≈ 1 , a low wind speed regime. This fact makes such regions unsuitable for large-scale wind electricity production. However, wind complementarity with solar may make it economically viable in electricity generation. Therefore, Wind/solar resource energy potential and complementarity are viable for wind-solar PV hybrid energy systems installation in low wind speed regime areas.

Energy demand analysis showed that 52% of rural families consume below 1 kWh per day. The daily energy loads were between 0.052 and 4.23 kWh, where much of the household's consumption is below 1.5 kWh. For the majority of households that consume less than 1 kWh per day, an average rural household consumes 0.582 kWh per day. These levels of energy demand can satisfactorily be met using an optimized wind-solar PV hybrid energy system.

A solar panel was sized and a HAWT designed for the low-speed wind regime in Machakos. Two rotor blades, 2.9 m diameter were fabricated from aluminum and Styrofoam. Analysis showed a positively skewed TSR profile, indicating good performance at low wind speeds. At a pitch angle of 20° and a TSR of 2.1, the foam blades revealed a C_P of 0.465. Similar results were obtained with aluminum blades, which had a maximum C_P of 0.431 at 1.9 TSR and 15° pitch. With power coefficients of 0.431 and 0.465, the rotor blades yielded 220 W and 238 W, respectively, for aluminum and Styrofoam rotors. The findings showed that Styrofoam blades outperformed aluminum blades in wind energy conversion. The low density of Styrofoam, which makes it a superior material for wind turbine rotor blades, can be attributed to its good performance. However, this study considered aluminum due to the harmful effects on health and environment that might arise over time from the use of Styrofoam. A 235 W aluminum bladed rotor design of cut in wind speed of 2.0 m/s, rated wind speed of 5.0 m/s and a cut-off wind speed of 15.0 m/s would be suitable for wind energy harnessing in low-speed regimes.

The optimized WT generated 36 W from a low wind speed of 3.2 m/s at a hub height of 8 m. This translated to a daily energy output of 0.864 kWh which balanced with the daily PV energy output of 0.835 kWh at 5.84 PSH. Wind shear projection attained a wind speed of 5.1 m/s, at a hub height of 50 m. The power density at 50 m hub height was 79 W/m^2 which was sufficient for the wind turbine to generate at its maximum PowerPoint at its rated wind speed of 5.0 m/s. Further exploration of the vertical shear revealed more wind energy capacities at higher hub height, where hub heights of 50 m would generate between 143 W, translating to 3.432 kWh per day. In view of this analysis, a maximum hub height of 50 m would be optimal for a turbine rated at 5 m/s. Increase in hub height in low wind speed areas revealed increased power production creating a balance of energy generation from the two technologies. This balanced reduced mismatch between demand and energy generation by wind and solar resources. Power performance analysis revealed good wind-solar power integration and improved system power flexibility which could impact positively on system costs by minimizing the need for large storage capacities.

The hybrid system economic analysis revealed a NPV of USD 537, a discounted payback period of 5.47 years and a profit index of 1.85. A single household would reduce 2.11 tons of CO₂ within the 20 years of system economic life span. Further, the developed wind-solar hybrid energy system has been found to be a promising solution to the energy crisis, global warming and climate change mitigation. This development supports the increase in share of renewables in energy generation agenda of the COP28, as well as the achievement of the SDGs. With a profit index greater than 1, a positive NPV value, the wind/solar hybrid energy system project has been found economically viable for installation in low wind speed areas. The findings of this study could be shared to renewable energy research communities and stakeholders for consideration.

5.2 Recommendations

With the promising results generated by aforementioned findings emerging from the study, the following were observed:

1. Wind-solar hybrid energy systems are viable solutions in overcoming resource intermittence and make complementary regimes more viable for small-scale energy generation.
2. Wind turbines with large sweep area, variable pitching and yawing mechanism are recommended for energy harnessing in low wind speed regime areas to optimize energy and capture maximum wind speeds from SE and NE direction which are prevalent.
3. Further studies need to focus on other low-density materials to enhance WT power coefficients in other low wind speed areas.
4. Further studies need to focus on efficient gear system designs that would increase the WT generator speed in low wind speed areas. However, mechanical knowledge is required.

REFERENCES

- Aboagye, B., Gyamfi, S., Ofori, E. A., & Djordjevic, S. (2021). Status of renewable energy resources for electricity supply in Ghana. *Scientific African*, *11*, e00660. <https://doi.org/10.1016/j.sciaf.2020.e00660>
- Adebayo, J. K., Layeni, A. T., Nwaokocha, C. N., Oyedepo, S. O., & Folarin, S. O. (2019). Design and fabrication of a vertical axis wind turbine with introduction of plastic gear. *Journal of Physics: Conference Series*, *1378*(4). <https://doi.org/10.1088/1742-6596/1378/4/042098>
- Adeyeye, K. A., Ijumba, N., & Colton, J. S. (2021). A Technol-Economic Model for Wind Energy Cost Analysis for *Low Wind Speed Areas*. *Processes*, *9*(8), 1463. <https://doi.org/10.3390/pr9081463>
- Adzic, E., Ivanovic, Z., Adzic, M., & Katie, V. (2009). Maximum power search in wind turbine based on fuzzy logic control. *Acta Polytechnica Hungarica*, *6*(1), 131–149.
- African Union commission. (2015). African Union, Agenda 2063. *Popular Version*, *03*, 1–24. Retrieved from agenda2063@africa-union.org www.agenda2063.au.int.
- Aghenta, L. O., & Tariq Iqbal, M. (2019). Design and dynamic modelling of a hybrid power system for a house in Nigeria. *International Journal of Photoenergy*, 2019. <https://doi.org/10.1155/2019/6501785>
- Ahmed, N. A., Miyatake, M., & Al-Othman, A. K. (2008). Power fluctuations suppression of stand-alone hybrid generation combining solar photovoltaic/wind turbine and fuel cell systems. *Energy Conversion and Management*, *49*(10), 2711–2719. <https://doi.org/10.1016/j.enconman.2008.04.005>
- Aho, J., Buckspan, A., Laks, J., Fleming, P., Jeong, Y., Dunne, F., Churchfield, M., Pao, L., & Johnson, K. (2012). A tutorial of wind turbine control for supporting grid frequency through active power control. *Proceedings of the American Control Conference*, 3120–3131. <https://doi.org/10.1109/ACC.2012.6315180>

- Akello, P. O. O., Saoke, C. O., Kamau, J. N., & Ndeda, J. O. H. (2022). Assessment of measured and satellite-derived DNI databases for concentrated solar industrial thermal application in Kericho, Kenya. *Proceedings of the 2022 Sustainable Research and Innovation Conference*, 105–112.
- Akikur, R. K., Saidur, R., Ping, H. W., & Ullah, K. R. (2013). Comparative study of stand-alone and hybrid solar energy systems suitable for off-grid rural electrification: A review. *Renewable and Sustainable Energy Reviews*, *27*, 738–752. <https://doi.org/10.1016/j.rser.2013.06.043>
- Al-shamani, A. N., Yusof, M., Othman, H., Mat, S., Ruslan, M. H., Abed, A. M., & Sopian, K. (2013). Design & Sizing of Stand-alone Solar Power Systems A house Iraq. *Recent Advances in Renewable Energy Sources*, 145–150. <https://pdfs.semanticscholar.org/ac10/c05f8a9e233407132e0e86161f47c4840e98.pdf>
- Ali, W., Farooq, H., Rehman, A. U., Awais, Q., Jamil, M., & Noman, A. (2019). Design considerations of stand-alone solar photovoltaic systems. *2018 International Conference on Computing, Electronic and Electrical Engineering, ICE Cube 2018*, 1–6. <https://doi.org/10.1109/ICECUBE.2018.8610970>
- Almi, M. F. (2014). Energy Management of Wind/Pv and Battery Hybrid System. *International Journal of New Computer Architectures and Their Applications*, *4*(4), 30–38. <https://doi.org/10.17781/p003>
- Andrew, W. (2017). *Angle of Attack | AeroToolbox*. Retrieved August 25, 2022, from <https://aerotoolbox.com/angle-of-attack/>
- Anjum, L. (2014). *Wind Resource Estimation Techniques-An Overview*. *3*(2), 26–38.
- Apunda, M. O., & Nyangoye, B. O. (2017). Challenges and opportunities of wind energy technology. *International Journal of Development Research*, *9*(06), 14174–14177. <https://doi.org/10.13140/RG.2.2.15229.82403>
- Ardany, M. D., Pandiangan, P., & Hasan, M. (2021). Lift Force of Airfoil (NACA 0012, NACA 4612, NACA 6612) With Variation of Angle of Attack and Camber:

- Computational Fluid Dynamics Study. *Computational And Experimental Research In Materials And Renewable Energy*, **4**(2), 80. <https://doi.org/10.19184/cerimre.v4i2.28372>
- Arikan, Y., Arslan, Ö. P., & Çam, E. (2015). The analysis of wind data with Reyleigh distribution and optimum turbine and cost analysis in Elmadag, Turkey. *Istanbul Univeristy-Journal Electrical and Electronics Engineering (IU-JEEE)*, **15**(1),1907-1912.
- Ariyo, F. K., Famutimi, B. D., Olowu, T. O., Akintade, S. A., & Abbas, A. (2016). *Web-Based Application for the Sizing of a Photovoltaic (PV) Solar Power System American Journal Of Engineering Research (AJER)*. **7**, 219–222.
- Asim, T., Islam, S. Z., Hemmati, A., & Khalid, M. S. U. (2022). A Review of Recent Advancements in Offshore Wind Turbine Technology. In *Energies*, **15**(2). MDPI. <https://doi.org/10.3390/en15020579>
- Aslam Bhutta, M. M., Hayat, N., Farooq, A. U., Ali, Z., Jamil, S. R., & Hussain, Z. (2012). Vertical axis wind turbine - A review of various configurations and design techniques. *Renewable and Sustainable Energy Reviews*, **16**(4), 1926–1939. <https://doi.org/10.1016/j.rser.2011.12.004>
- Badwawi, R. Al, Abusara, M., & Mallick, T. (2015). A Review of Hybrid Solar PV and Wind Energy System. *Smart Science*, **3**(3), 127–138. <https://doi.org/10.1080/23080477.2015.11665647>
- Bardal, L. M., & Sætran, L. R. (2017). Influence of turbulence intensity on wind turbine power curves. *Energy Procedia*, **137**, 553–558. <https://doi.org/10.1016/j.egypro.2017.10.384>
- Beckman, W. A., Blair, N., & Duffie, J. A. (2020). *Solar Engineering of Thermal Processes, Photovoltaics and Wind*. Fifth Edition. John Wiley & Sons, Inc. Hoboken, New Jersey. <https://doi.org/10.1002/9781119540328>.
- Bekele, G. (2009). *Study into the Potential and Feasibility of a Standalone Solar-wind Hybrid Electric Energy Supply System (KTH/REFR/09/64-SE)*[Doctoral Thesis ,

Royal Institute of Technology).

- Bekele, G., & Tadesse, G. (2012). Feasibility study of small Hydro/PV/Wind hybrid system for off-grid rural electrification in Ethiopia. *Applied Energy*, **97**, 5–15. <https://doi.org/10.1016/j.apenergy.2011.11.059>
- Bekirsky, N., Hoicka, C. E., Brisbois, M. C., & Camargo, R. L. (2022). Many actors amongst multiple renewables: A systematic review of actor involvement in complementarity of renewable energy sources. *Renewable and Sustainable Energy Reviews*, **161**, 112368. <https://doi.org/10.1016/j.rser.2022.112368>
- Benghanem, M., Haddad, S., Alzahrani, A., Mellit, A., Almohamadi, H., Khushaim, M., & Aida, M. S. (2023). Evaluation of the Performance of Polycrystalline and Monocrystalline PV Technologies in a Hot and Arid Region: An Experimental Analysis. *Sustainability*, **15**(20), 14831. <https://www.mdpi.com/2071-1050/15/20/14831>
- Bernal-Agustín, J. L., & Dufo-López, R. (2009). Simulation and optimization of stand-alone hybrid renewable energy systems. *Renewable and Sustainable Energy Reviews*, **13**(8), 2111–2118. <https://doi.org/10.1016/j.rser.2009.01.010>
- Bhandari, B., Lee, K. T., Lee, G. Y., Cho, Y. M., & Ahn, S. H. (2015). Optimization of hybrid renewable energy power systems: A review. *International Journal of Precision Engineering and Manufacturing - Green Technology*, **2**(1), 99–112. <https://doi.org/10.1007/s40684-015-0013-z>
- Bhawan, S., & Puram, R. K. (2011). CO2 Baseline Database for the Indian Power Sector User Guide Government of India Ministry of Power Central Electricity Authority. *Ministry of Power, March*, 32. https://cea.nic.in/wp-content/uploads/baseline/2020/07/user_guide_ver14.pdf
- Bianchi, F. D., De Battista, H., & Mantz, R. J. (2006). *Wind turbine control systems: Principles, modelling and gain scheduling design*. Springer-Verlag London Ltd.
- Blaabjerg, F., & Ma, K. (2017). Wind Energy Systems. *Proceedings of the IEEE*, **105**(11), 2116–2131. <https://doi.org/10.1109/JPROC.2017.2695485>

- Bogno, B., Sawicki, J. P., Petit, P., Aillerie, M., Charles, J. P., Hamandjoda, O., & Beda, T. (2018). 230 VDC elementary block in off-grid PV systems. *Sustainable Energy Technologies and Assessments*, **29**, 1–11. <https://doi.org/10.1016/j.seta.2018.06.013>
- Burnett, B. N. (2023). *Technology and innovation, inclusion, frontline communities, and finance*.
- Burton, T., Jenkins, N., Sharpe, D., & Bossanyi, E. (2011). *Conceptual Design of Horizontal Axis Wind Turbines*. Second Edition. John Wiley and Sons, Ltd. <https://doi.org/10.1002/9781119992714.ch6>
- Castelli, M. R., & Benini, E. (2010). Effect of blade inclination angle on a darrieus wind turbine. *Proceedings of the ASME Turbo Expo*, **5**, 857–869. <https://doi.org/10.1115/GT2010-23332>
- CBK. (2024). *Monetary Policy Committee* [Press Release]. https://www.centralbank.go.ke/uploads/mpc_press_release/1332335136_MPC%20Press%20Release%20-%20Meeting%20of%20February%206%202024.pdf
- Cengiz, Mehmet, & Mamis, M. (2015). A research on determining the panel inclination angle in terms of the place and seasons. *Journal of Multidisciplinary Engineering Science and Technology (JMEST)*, **2**, 2172–2177.
- Choge, D. K., Rotich, S. K., Tonui, J. K., & Maritim, J. K. (2013). Wind energy probability distributions for Eldoret. *International Journal of Advanced Research*, **1**(6). <http://www.journalijar.com>
- Consul, C. A., Willden, R. H. J., Ferrer, E., & McCulloch, M. D. (2009). Influence of Solidity on the Performance of a Cross-Flow Turbine. *Proceedings of the 8th European Wave and Tidal Energy Conference, Uppsala, Sweden, 2016*, 484–493.
- Couto, A., & Estanqueiro, A. (2020). Exploring wind and solar PV generation complementarity to meet electricity demand. *Energies*, **13**(6). <https://doi.org/10.3390/en13164132>

- Cozzi, L., & Gould, T. (2021). *World Energy Outlook 2021*. International Energy Agency. 1–386. www.iea.org/weo
- Cvrlje, D., & Ćorić, T. (2010). Macro & micro aspects of standard of living and quality of life in a small transition economy: The case of Croatia. *EFZG Working Paper Series*, **385**(02), 1–12.
- Danao, L. A., Edwards, J., Eboibi, O., & Howell, R. (2014). A numerical investigation into the influence of unsteady wind on the performance and aerodynamics of a vertical axis wind turbine. *Applied Energy*, **116**, 111–124. <https://doi.org/10.1016/j.apenergy.2013.11.045>
- Daut, I., Irwanto, M., Suwarno, Irwan, Y. M., Gomesh, N., & Ahmad, N. S. (2011). Potential of wind speed for wind power generation in Perlis, Northern Malaysia. *Telkomnika*, **9**(3), 575–582. <https://doi.org/10.12928/telkomnika.v9i3.750>
- de Falani, S. Y. A., González, M. O. A., Barreto, F. M., de Toledo, J. C., & Torkomian, A. L. V. (2020). Trends in the technological development of wind energy generation. *International Journal of Technology Management and Sustainable Development*, **19**(1), 43–68. https://doi.org/10.1386/tmsd_00015_1
- de Oliveira Costa Souza Rosa, C., da Silva Christo, E., Costa, K. A., & Santos, L. dos. (2020). Assessing complementarity and optimising the combination of intermittent renewable energy sources using ground measurements. *Journal of Cleaner Production*, **258**, 120946. <https://doi.org/10.1016/j.jclepro.2020.120946>
- Delbeke, J., Runge-Metzger, A., Slingenberg, Y., & Werksman, J. (2019). *The Paris agreement. towards a climate-neutral europe: curbing the trend*, 24–45. <https://doi.org/10.4324/9789276082569-2>
- DeMarrais, Gerard, A. (1958). Wind-Speed Profiles At Brookhaven National Laboratory. In *Journal of Meteorology*, **16**, 181–190.
- Diemuodeke, E. O., Addo, A., Dabipi-Kalio, I., Oko, C. O. C., & Mulugetta, Y. (2017). Domestic energy demand assessment of coastline rural communities with solar electrification. *Energy and Policy Research*, **4**(1), 1–9.

<https://doi.org/10.1080/23815639.2017.1280431>

- Dihrab, S. S., & Sopian, K. (2010). Electricity generation of hybrid PV/wind systems in Iraq. *Renewable Energy*, **35**(6), 1303–1307. <https://doi.org/10.1016/j.renene.2009.12.010>
- Dinkelman, T. (2011). The effects of rural electrification on employment: New evidence from South Africa. *American Economic Review*, **101**(7), 3078–3108. <https://doi.org/10.1257/aer.101.7.3078>
- Dixit, V., & Bhatia, J. (2013). Analysis and Design of a Domestic Solar-Wind Hybrid Energy System for Low Wind Speeds. *International Journal of Computer Applications*, **72**(22), 40–44.
- Dominguez, C., Orehounig, K., & Carmeliet, J. (2021). Estimating hourly lighting load profiles of rural households in East Africa applying a data-driven characterization of occupant behavior and lighting devices ownership. *Development Engineering*, **6**, 100073. <https://doi.org/10.1016/j.deveg.2021.100073>
- Dondariya, C., Porwal, D., Awasthi, A., Shukla, A. K., Sudhakar, K., Murali, M. M., & Bhimte, A. (2018). Performance simulation of grid-connected rooftop solar PV system for small households: A case study of Ujjain, India. *Energy Reports*, **4**, 546–553. <https://doi.org/10.1016/j.egy.2018.08.002>
- Eboibi, O. (2013). *The influence of Blade Chord on the Aerodynamics and Performance of Vertical Axis Wind Turbines*. [Doctoral Thesis, The University of Sheffield] http://etheses.whiterose.ac.uk/4730/1/Eboibi_Thesis_Oct_2013.pdf
- Edwards, J. M., Angelo Danao, L., & Howell, R. J. (2012). Novel experimental power curve determination and computational methods for the performance analysis of vertical axis wind turbines. *Journal of Solar Energy Engineering, Transactions of the ASME*, **134**(3), 1–11. <https://doi.org/10.1115/1.4006196>.
- Elistratov, V., & Kudryasheva, I. (2019). Regimes, management and economics of energy complexes on the basis of renewable energy sources for autonomous power supply. In *E3S Web of Conferences*, 124, 0-4. EDP Sciences.

<https://doi.org/10.1051/e3sconf/201912404023>.

- Elprocus, F. (2020). Horizontal Axis Wind Turbine: Construction, Types & Its Applications. Retrieved from <https://www.elprocus.com/horizontal-axis-wind-turbine/>.
- Elsayed, S., Sherif, A., Hassaan, M., Adel, B., Samhay, A. E., Ayman, C., & Haggag, E. (2022). Performance Study of Monocrystalline, Polycrystalline, and Thin-film Solar PV Modules in the Egyptian Environment. *ACSE*. Retrieved from <https://www.researchgate.net/publication/362332068>.
- Emejamara, F. C., Tomlin, A. S., & Millward-Hopkins, J. T. (2015). Urban wind: Characterisation of useful gust and energy capture. *Renewable Energy*, *81*(2015), 162–172. <https://doi.org/10.1016/j.renene.2015.03.028>.
- EPRA. (2022). *Energy & Petroleum Statistics Report*. *14*(3). <https://doi.org/10.1021/ie50147a014>.
- Erbach, G., & Roniger, J. (2023). COP28 climate change conference: Outcomes. *At a Glance - Towards Climate Neutrality*. EPRS | European Parliamentary Research Service. Retrieved from [https://www.europarl.europa.eu/thinktank/en/document/EPRS_ATA_\(2023\)757574](https://www.europarl.europa.eu/thinktank/en/document/EPRS_ATA_(2023)757574).
- Evans, A., Strezov, V., & Evans, T. J. (2009). Assessment of sustainability indicators for renewable energy technologies. *Renewable and Sustainable Energy Reviews*, *13*(5), 1082–1088. <https://doi.org/10.1016/j.rser.2008.03.008>.
- Fesli, U., Bayir, R., & Özer, M. (2009). Design and implementation of a domestic solar-wind hybrid energy system. *ELECO 2009 - 6th International Conference on Electrical and Electronics Engineering*, 29–33.
- Fu, P., & Rich, P. M. (1999). Design and Implementation of the Solar Analyst: an ArcView Extension for Modeling Solar Radiation at Landscape Scales. *19th Annual ESRI User Conference, February*, 1–24.
- Global COP28 The United Nations Climate Change Conference, Dubai, United Arab Emirates (UAE). *November*, 1–21.

- Gomez, U. E. Y., Lopez, J. A. Z., Jimenez, A. R., Lopez, G. V., and Villalon, J. J. L, (2014). Design and manufacturing of wind turbine blades of low capacity using cad/cam techniques and composite materials. *Energy Procedia*, 57, 682–690. <https://doi.org/10.1016/j.egypro.2014.10.223>.
- Gooding, J., Crook, R., & Tomlin, A. S. (2015). Modelling of roof geometries from low-resolution LiDAR data for city-scale solar energy applications using a neighbouring buildings method. *Applied Energy*, 148, 93–104. <https://doi.org/10.1016/j.apenergy.2015.03.013>.
- Gooding, J, Smith, CJ, Crook, R *et al.* (1 more author) (2015) *Solar Resource Estimation Using a Radiative Transfer with Shading (RTS) Model*. In: EU PVSEC 2015 Conference Proceedings. European PV Solar Energy Conference and Exhibition 2015, 14-18 Sep 2015, Hamburg, Germany. ,2800 - 2805. ISBN 3-936338-39-6.
- Goswami, D. Y. (2015). *Principles of Solar Engineering*. CRC press, Taylor& Francis Group. <https://doi.org/10.1201/b18119>.
- Hansen, M. O. L. (2015). *Aerodynamics of wind turbines*. Routledge, Taylor& Francis Group, NewYork. <https://www.routledge.com/Aerodynamics-of-Wind-Turbines/Hansen/p/book/9781138775077>.
- Helman, C. (2021). How green is wind power, really? A new report tallies up the carbon cost of renewables. *Forbes*, 1–5. Retrieved from <https://www.forbes.com/sites/christopherhelman/2021/04/28/how-green-is-wind-power-really-a-new-report-tallies-up-the-carbon-cost-of-renewables/?sh=19cebdde73cd>
- Hemeida, A. M., El-Ahmar, M. H., El-Sayed, A. M., Hasanien, H. M., Alkhalaf, S., Esmail, M. F. C., & Senjyu, T. (2020). Optimum design of hybrid wind/PV energy system for remote area. *Ain Shams Engineering Journal*, 11(1), 11–23. <https://doi.org/10.1016/j.asej.2019.08.005>.

- Hofierka, J., & Suri, M. (2002). The solar radiation model for Open source GIS: implementation and applications. International GRASS users conference in Trento, Italy, September 2002. *Proceedings of the Open Source Gis - Grass Users Conference, September, 11–13*. <http://citeseerx.ist.psu.edu/viewdoc/summary?doi=10.1.1.19.9831>.
- Honsberg, C., & Bowden, S. (2019). Average Solar Radiation | PVEducation. *Www.Pveducation.Org*. Retrieved from <https://www.pveducation.org/pvcdrom/properties-of-sunlight/average-solarradiation#%0Ahttps://www.pveducation.org/pvcdrom/properties-of-sunlight/average-solar-radiation>
- Iakovleva, E., Guerra, D., Tcvetkov, P., & Shklyarskiy, Y. (2022). Technical and Economic Analysis of Modernization of Solar Power Plant: A Case Study from the Republic of Cuba. *Sustainability (Switzerland)*, **14**(2). <https://doi.org/10.3390/su14020822>.
- IISD. (2016). UN Sustainable Development Goals; 2030 Agenda for Sustainable Development. *Journal for International Institute for Sustainable Development*, **1**(1), 1–35. Retrieved from <https://www.iisd.org/system/files/publications/sustainable-development-goals-iisd-perspectives.pdf>
- Indhumathy D, & Sukkiramathi K. (2007). Estimation of Weibull Parameters for Wind speed calculation at Kanyakumari in India. *International Journal of Innovative Research in Science, Engineering and Technology (An ISO, 3297(1), 2319–8753*. www.ijirset.com
- Ingram, G. (2011). Wind turbine blade analysis using the blade element momentum method. Version 1.1. *Durham University Journal*, 1–21.
- International Energy Agency. (2022). Direct Air Capture: A key technology for net zero. *International Encyclopedia of Geography*, 1–76. https://iea.blob.core.windows.net/assets/78633715-15c0-44e1-81df-41123c556d57/DirectAirCapture_Akeytechnologyfornetzero.pdf.
- International Renewable Energy Agency (IRENA). (2022). World energy transitions outlook 2022: 1.5° C pathway -Executive Summary. *World Energy Transitions*,

1–54. Retrieved from [https://irena.org/Digital-Report/World-Energy-Transitions-Outlook-2022%0Ahttps://irena.org/publications/2021/March/World - Energy- Transitions-Outlook](https://irena.org/Digital-Report/World-Energy-Transitions-Outlook-2022%0Ahttps://irena.org/publications/2021/March/World-Energy-Transitions-Outlook).

Jacques, D. A., Gooding, J., Giesekam, J. J., Tomlin, A. S., & Crook, R. (2014). Methodology for the assessment of PV capacity over a city region using low-resolution LiDAR data and application to the City of Leeds (UK). *Applied Energy*, **124**, 28–34. <https://doi.org/10.1016/j.apenergy.2014.02.076>.

Jayapriya, J., Muruganandam, D., Raguraman, D., Senthilkumar, B., & Dhinakaran, V. (2019). Design and fabrication of multi-rotor horizontal axis wind turbine. *International Journal of Engineering and Advanced Technology*, **8**(6), 3500–3504. <https://doi.org/10.35940/ijeat.F9528.088619>.

Jha A. R. (2011). *Wind Turbine Technology*. In CRC Press.

Jha, N., Prashar, D., Rashid, M., Khanam, Z., Nagpal, A., AlGhamdi, A. S., & Alshamrani, S. S. (2022). Energy-Efficient Hybrid Power System Model Based on Solar and Wind Energy for Integrated Grids. *Mathematical Problems in Engineering*, **2022**. <https://doi.org/10.1155/2022/4877422>.

Jochem, A., Höfle, B., Rutzinger, M., & Pfeifer, N. (2009). Automatic roof plane detection and analysis in airborne lidar point clouds for solar potential assessment. *Sensors*, **9**(7), 5241–5262. <https://doi.org/10.3390/s90705241>.

Johannsen, R. M., Østergaard, P. A., & Hanlin, R. (2020). Hybrid photovoltaic and wind mini-grids in Kenya: Techno-economic assessment and barriers to diffusion. *Energy for Sustainable Development*, **54**(2020), 111–126. <https://doi.org/10.1016/j.esd.2019.11.002>.

Johnson, C. (2012). Mathematical Physics of BlackBody Radiation. <https://www.csc.kth.se/~cgjoh/ambblack.pdf>.

Jossen, A., Garche, J., & Sauer, D. U. (2004). Operation conditions of batteries in PV applications. *Solar Energy*, **76**(6), 759–769. <https://doi.org/10.1016/J.SOLENER.2003.12.013>.

- Jurasz, J., Beluco, A., & Canales, F. A. (2018). The impact of complementarity on power supply reliability of small scale hybrid energy systems. *Energy*, **161**, 737–743. <https://doi.org/10.1016/j.energy.2018.07.182>.
- Jurasz, J., Canales, F. A., Kies, A., Guezgouz, M., & Beluco, A. (2020). A review on the complementarity of renewable energy sources: Concept, metrics, application and future research directions. *Solar Energy*, **195**, 703–724. <https://doi.org/10.1016/j.solener.2019.11.087>.
- Kabaka, K. T., & Gwang'ombe, F. (2007). Challenges in small hydropower development in Tanzania: rural electrification perspective. *International Conference on Small Hydropower–Hydro. Sri Lanka, (October), 22–24*.
- Kahlen, L., Kirdziel, M.-J., Day, T., & Schiefer, T. (2019). *The role of geothermal and coal in Kenya's electricity sector and implications for sustainable development. (November), 1–55*.
- Kaluwa, C., Oduma, J., Abdirahman, F. A., Kitoga, B. K., Opondoh, A. A., Muchibi, J., Bagnol, B., Rosenbaum, M., Onchaga, S., Stanley, M., & Amuguni, J. H. (2022). *Using the Women Empowerment in Livestock Index (WELI) to Examine Linkages between Women Smallholder Livestock Farmers' Empowerment and Access to Livestock Vaccines in Machakos County of Kenya: Insights and Critiques*.
- Kamau, J. N., Kinyua, R., & Gathua, J. K. (2010). 6 years of wind data for Marsabit, Kenya average over 14 m/s at 100 m hub height; An analysis of the wind energy potential. *Renewable Energy*, **35**(6), 1298–1302. <https://doi.org/10.1016/j.renene.2009.10.008>.
- Karafil, A., Ozbay, H., Kesler, M., & Parmaksiz, H. (2016). Calculation of optimum fixed tilt angle of PV panels depending on solar angles and comparison of the results with experimental study conducted in summer in Bilecik, Turkey. *ELECO 2015 - 9th International Conference on Electrical and Electronics Engineering*, 971–976. <https://doi.org/10.1109/ELECO.2015.7394517>.

- Kariuki, B. W., & Sato, T. (2018). Interannual and spatial variability of solar radiation energy potential in Kenya using Meteosat satellite. *Renewable Energy*, **116**, 88–96. <https://doi.org/10.1016/j.renene.2017.09.069>.
- Kartite, J., & Cherkaoui, M. (2019). Study of the different structures of hybrid systems in renewable energies: A review. *Energy Procedia*, **157**(2018), 323–330. <https://doi.org/10.1016/j.egypro.2018.11.197>.
- Kassem, Y., Çamur, H., & Aateg, R. A. F. (2020). Exploring solar and wind energy as a power generation source for solving the electricity crisis in Libya. *Energies*, **13**(14). <https://doi.org/10.3390/en13143708>.
- Kassenga, G. R. (2008). The status and constraints of solar photovoltaic energy development in Tanzania. *Energy Sources, Part B: Economics, Planning and Policy*, **3**(4), 420–432. <https://doi.org/10.1080/15567240701421807>.
- Kaushika, N. D., Mishra, A., & Rai, A. K. (2018). *Solar photovoltaics: Technology, system design, reliability and viability*. *Solar Photovoltaics: Technology, System Design, Reliability and Viability* (pp. 1–167). Springer International Publishing. <https://doi.org/10.1007/978-3-319-72404-1>
- Kausika, B. B., & van Sark, W. G. J. H. M. (2021). Calibration and validation of ArcGIS solar radiation tool for photovoltaic potential determination in the Netherlands. *Energies*, **14**(7). <https://doi.org/10.3390/en14071865>
- Kaygusuz, K. (2001). Renewable energy: Power for a sustainable future. In *Energy Exploration and Exploitation* , **19**(6), pp. 603–626). <https://doi.org/10.1260/0144598011492723>
- Keshavan, B. K., Ramu, T. S., & Sankar, V. (2016). Probabilistic modeling and forecasting of wind power. In *International Journal of Performability Engineering*. **12**(04).
- Kezerashvili, R. Y. (2009). Light and electromagnetic waves teaching in engineering education. *International Journal of Electrical Engineering and Education*, **46**(4), 343–353. <https://doi.org/10.7227/IJEEE.46.4.4>.

- Khandker, S. R., Samad, H. A., Ali, R., & Barnes, D. F. (2014). Who benefits most from rural electrification? Evidence in India. *Energy Journal*, *35*(2), 75–96. <https://doi.org/10.5547/01956574.35.2.4>.
- Kiplagat, J. K., Wang, R. Z., & Li, T. X. (2011). Renewable energy in Kenya: Resource potential and status of exploitation. *Renewable and Sustainable Energy Reviews*, *15*(6), 2960–2973. <https://doi.org/10.1016/J.RSER.2011.03.023>.
- Kitchens, C. P. F. (2013). Flip the Switch: The Impact of the Rural Electrification Administration. *The Journal of Economic History*, *75*, 1935–1940.
- Koester, R. J. (2014). Solar Energy. *International Encyclopedia of Environmental Politics*, 426–427. Taylor and Francis. https://doi.org/10.1007/978-94-007-4189-8_3.
- Komor, P. (2009). Wind and Solar Electricity: Challenges and Opportunities. *The Pew Center on Global Climate Change*, June.
- Konstantinidis, E. I., & Botsaris, P. N. (2016). Wind turbines: Current status, obstacles, trends and technologies. *IOP Conference Series: Materials Science and Engineering*, *161*(1). <https://doi.org/10.1088/1757-899X/161/1/012079>.
- Kothari, C. R. (2015). Research methodology: Methods and technics. *Syria Studies*, *7*(1). https://www.researchgate.net/publication/269107473_What_is_governance/link/548173090cf22525dcb61443/download%0Ahttp://www.econ.pf.edu/~reynal/Civilwars_12December2010.pdf%0Ahttps://think-asia.org/handle/11540/8282%0Ahttps://www.jstor.org/stable/41857625.
- Kothari, S., Kaushik, S. C., & Panwar, N. L. (2009). Approach to calculate solar radiation inside a semi- cylindrical greenhouse. *Journal of Engineering and Technology Research*, *1*(2), 14–18. <http://www.academicjournals.org/JETR>.
- Kumar, C. R. J., Kumar, V. D., & Majid, M. A. (2019). Wind energy programme in India: Emerging energy alternatives for sustainable growth. *Energy and Environment*, *30*(7), 1135–1189. <https://doi.org/10.1177/0958305X19841297>

- Lasnier, F., & Gan Ang, T. (2017). *Photovoltaic engineering handbook (ebook)*. Routledge. <https://www.routledge.com/Photovoltaic-Engineering-Handbook/Lasnier/p/book/9780852743119>.
- Lazarov, V. D., Zarkov, Z., & Bochev, I. (2005). *Hybrid Power Systems with Renewable Energy Sources-Types, Structures, Trends for Research and Development Machine Learning for Irradiance Prediction View project COST Project H2020 View project*. May 2014. <https://www.researchgate.net/publication/236012467>.
- Letcher, T. M. (2017). *Wind Energy Engineering: A Handbook for Onshore and Offshore Wind Turbines*. Elsevier, Academic Press.
- Li, G., & Zhi, J. (2016). Analysis of Wind Power Characteristics. *Large-Scale Wind Power Grid Integration*, 19–51. China Electric Power Press. Published by Elsevier Inc. All rights reserved. <https://doi.org/10.1016/b978-0-12-849895-8.00002-6>.
- Lin, B. Q. (2003). Electricity demand in the People's Republic of China: Investment requirement and environmental impact. *ERD Working Paper Series*, **37**, 1–25.
- Lukač, N., Žlaus, D., Seme, S., Žalik, B., & Štumberger, G. (2013). Rating of roofs' surfaces regarding their solar potential and suitability for PV systems, based on LiDAR data. *Applied Energy*, **102**, 803–812. <https://doi.org/10.1016/j.apenergy.2012.08.042>.
- Lund, H. (2005). Large-scale integration of wind power into different energy systems. *Energy*, **30**(13), 2402–2412. <https://doi.org/10.1016/j.energy.2004.11.001>.
- Maalawi, K. Y., & Badr, M. A. (2003). A practical approach for selecting optimum wind rotors. *Renewable Energy*, **28**(5), 803–822. [https://doi.org/10.1016/S0960-1481\(02\)00028-9](https://doi.org/10.1016/S0960-1481(02)00028-9).
- Magambo, B., & Kiremu, C. (2010). *A Study of Household Electricity Demand and Consumption Patterns in Nairobi*. [Masters thesis, University of Nairobi] http://erepository.uonbi.ac.ke/bitstream/handle/11295/4184/Magambo_A_Study

of Household Electricity Demand and Consumption Patterns in Nairobi.pdf?sequence=1&isAllowed=y

- Malik, M. Z., Zehra, K., Ali, I., Ubedullah, Ismail, M., Hussain, A., Kumar, V., Abid, M., & Baloch, M. H. (2020). Solar-Wind Hybrid Energy Generation System. *Proceedings - 2020 23rd IEEE International Multi-Topic Conference, INMIC 2020*. <https://doi.org/10.1109/INMIC50486.2020.9318083>
- Manwell, J. F., McGowan, J. G., & Rogers, A. L. (2010). *Wind Energy Explained: Theory, Design and Application*. John Wiley & Sons. <https://doi.org/10.1002/9781119994367>
- Marr, J. M., & Wilkin, F. P. (2012). A better presentation of Planck's radiation law. *American Journal of Physics*, *80*(5), 399–405. <https://doi.org/10.1119/1.3696974>.
- Masters, G. M. (2004). *Wind Power Systems. Renewable and Efficient Electric Power Systems*. John Wiley & Sons. <https://doi.org/10.1002/0471668826.ch6>.
- Mbaka, C. K., Gikonyo, J., & Kisaka, O. M. (2019). Households' energy preference and consumption intensity in Kenya. *Energy, Sustainability and Society*, *9*(1). <https://doi.org/10.1186/s13705-019-0201-8>.
- Misak, S., & Prokop, L. (2010). Off-grid power systems. *2010 9th Conference on Environment and Electrical Engineering, EEEIC 2010*, 14–17. <https://doi.org/10.1109/EEEIC.2010.5490003>.
- Modi, V., McDade, S., Lallement, D., & Saghir, J. (2005). *Energy Services for the Millennium Development Goals*. The International Bank for Reconstruction and Development/The World Bank and the United Nations Development Programme http://www.unmillenniumproject.org/documents/MP_Energy_Low_Res.pdf.
- Mohammed, A., Rekioua, D., & Mezzai, N. (2013). Experimental study of a PV water pumping system. *Journal of Electrical Systems*, *9*(2), 212–222.
- Mousa, H. H. H., Youssef, A. R., & Mohamed, E. E. M. (2019). Modified P&O MPPT algorithm for optimal power extraction of five-phase PMSG based wind

- generation system. *SN Applied Sciences*, **1**(8), 1–16.
<https://doi.org/10.1007/s42452-019-0878-5>
- Mousa, K., AlZu'bi, H., & Diabat, A. (2010). Design of a hybrid solar-wind power plant using optimization. *2010 2nd International Conference on Engineering System Management and Applications, ICESMA 2010, May 2014*.
- Msyani, C. M. (2013). Current Status of Energy Sector in Tanzania. *Executive Exchange on Developing an Ancillary Service Market*, 1–21. [https://www.usea.org/sites/default/files/event-/Tanzania Power Sector.pdf](https://www.usea.org/sites/default/files/event-/Tanzania%20Power%20Sector.pdf)
- Mukulo, B. M., Ngaruiya, J. M., & Kamau, J. N. (2014). Determination of wind energy potential in the Mwingi-Kitui plateau of Kenya. *Renewable Energy*, **63**, 18–22.
<https://doi.org/10.1016/j.renene.2013.08.042>.
- Mulaudzi, S. K. (2018). *An assessment of the potential of Solar Photovoltaic (PV) and hybrid renewable energy application in South Africa*. [Doctoral Thesis, Newcastle University, Newcastle upon Tyne, NE1 7RU, United Kingdom].
<http://www.ieee-pes.org/meetings-and-conferences/conference-calendar/monthly>.
- Mwakitalima, I. J. J., King'ondy, C. K. K., & King, C. K. (2015). Electricity Demand Evaluation for Rural Electrification A Case Study of Kikwe Village in Tanzania. *International Journal of Engineering Research & Technology (IJERT)*, **4**(06), 1025–1028.
- Mwanzia, J. N., Wekesa, D. W., & Kamau, J. N. (2019). Analysis of Wind Resource Potential for Small-Scale Wind Turbine Performance in Kiseveni, Kenya. *International Journal of High Energy Physics*, **6**(1), 17.
<https://doi.org/10.11648/j.ijhep.20190601.13>
- Nelson, V. (2013). *Wind energy: Renewable energy and the environment*. second edition. CRC Press. <https://doi.org/10.1201/b15566>.
- Nema, P., & Nema, R. (2010). PV-solar / wind hybrid energy system for GSM/CDMA type mobile telephony base station. *International Journal of Energy and*

Environment, **1**(2), 359-366.

- Neto, P. B. L., Saavedra, O. R., & Oliveira, D. Q. (2020). The effect of complementarity between solar, wind and tidal energy in isolated hybrid microgrids. *Renewable Energy*, **147**, 339–355. <https://doi.org/10.1016/J.RENENE.2019.08.134>
- Ngare, I. & Kioli, J. (2019). A review of energy access in kenya. *Researchjournali Journal of Electrical Engineering*, **3**(1), 1-6.
- Nguyen, H. T., & Pearce, J. M. (2012). Incorporating shading losses in solar photovoltaic potential assessment at the municipal scale. *Solar Energy*, **86**(5), 1245–1260. <https://doi.org/10.1016/j.solener.2012.01.017>
- Nijssen, R., & Povl, B. (2013). *Advances in wind turbine blade design and materials*. Woodhead publishing limited, Sawton, Cambridge.
- Nishizawa, Y. (2011). An Experimental Study of the Shapes of Rotor for Horizontal-Axis Small Wind Turbines. *Wind Turbines*. In Tech. <https://doi.org/10.5772/15057>
- Nishizawa, Y., Shengning, C., Elson, R., & Ushiyama, I. (2013). An experimental study on performance of curved-plate bladed rotor. *Renewable Energy*, **49**, 6–9. <https://doi.org/10.1016/J.RENENE.2012.01.077>
- Njiru, C. W., & Letema, S. C. (2018). Energy Poverty and Its Implication on Standard of Living in Kirinyaga, Kenya. *Journal of Energy*, **2018**, 1–12. <https://doi.org/10.1155/2018/3196567>
- Oğuz, Y., & Özsoy, M. F. (2015). Sizing, design, and installation of an isolated wind-photovoltaic hybrid power system with battery storage for laboratory general illumination in Afyonkarahisar, Turkey. *Journal of Energy in Southern Africa*, **26**(4), 70–80. <https://doi.org/10.17159/2413-3051/2016/v26i4a2113>
- Okinda, V., Odero, N. A., Okinda, V. O., & Odero, N. A. (2016). Modelling, Simulation and Optimal Sizing of a Hybrid Wind, Solar PV Power System in Northern Kenya multi objective dynamic economic dispatch with renewable

- energy cost functions View project Renewable Energy View project Modelling, Simulation and Optimal. *International Journal of Renewable Energy Research*, **6**(4). <https://www.researchgate.net/publication/319165281>
- Oloo, F., Olang, L., & Strobl, J. (2015). Spatial modelling of solar energy potential in Kenya. *International Journal of Sustainable Energy Planning and Management*, **6**(2016), 17–30. <https://doi.org/10.5278/ijsepm.2015.6.3>
- Ondraczek, J. (2013). The sun rises in the east (of Africa): A comparison of the development and status of solar energy markets in Kenya and Tanzania. *Energy Policy*, **56**, 407–417. <https://doi.org/10.1016/j.enpol.2013.01.007>
- Ongaki, N. L., Maghanga, C. M., & Kerongo, J. (2021). Evaluation of the Technical Wind Energy Potential of Kisii Region Based on the Weibull and Rayleigh Distribution Models. *Journal of Energy*, **2021**, 1–17. <https://doi.org/10.1155/2021/6627509>
- Ould Bilal, B., Sambou, V., Ndiaye, P. A., Kébé, C. M. F., & Ndongo, M. (2010). Optimal design of a hybrid solar-wind-battery system using the minimization of the annualized cost system and the minimization of the loss of power supply probability (LPSP). *Renewable Energy*, **35**(10), 2388–2390. <https://doi.org/10.1016/J.RENENE.2010.03.004>
- Page, B. Turan, G., & Zapantis, A. (2020). Global Status of CCS 2020. *Global status report* <https://www.globalccsinstitute.com/resources/global-status-report/>
- Pagnini, L. C., Burlando, M., & Repetto, M. P. (2015). Experimental power curve of small-size wind turbines in turbulent urban environment. *Applied Energy*, **154**, 112–121. <https://doi.org/10.1016/j.apenergy.2015.04.117>
- Paidipati, J., Frantzis, L., Sawyer, H., & Kurrasch, A. (2009). *Rooftop photovoltaics market penetration scenarios*. (NREL/SR-581-42306), 1–26.
- Panahandeh, B., Bard, J., Outzourhit, A., & Zejli, D. (2011). Simulation of PV-wind-hybrid systems combined with hydrogen storage for rural electrification. *International Journal of Hydrogen Energy*, **36**(6), 4185–4197.

<https://doi.org/10.1016/j.ijhydene.2010.07.151>

- Pande, J., Nasikkar, P., Kotecha, K., & Varadarajan, V. (2021). A review of maximum power point tracking algorithms for wind energy conversion systems. *Journal of Marine Science and Engineering*, *9*(11), 1–30. <https://doi.org/10.3390/jmse9111187>
- Radha C. C., Laxmi, D. A. J., & Sangeetha, P. (2017). Optimized energy efficient solution with stand alone PV system. *MATTER: International Journal of Science and Technology*, *3*(1), 16–27. <https://doi.org/10.20319/MIJST.2017.31.1627>
- Rahrah, K., Rekioua, D., Rekioua, T., & Bacha, S. (2015). Photovoltaic pumping system in Bejaia climate with battery storage. *International Journal of Hydrogen Energy*, *40*(39), 13665–13675. <https://doi.org/10.1016/j.ijhydene.2015.04.048>
- Raja, D. (2019.). *Understating Solar Radiation Measurement Methods using Pyrheliometer and Pyranometer*. Retrieved May 2, 2024, from <https://circuitdigest.com/tutorial/solar-radiation-measurement-methods-using-pyrheliometer-and-pyranometer>
- Rathod, A. P. S., Mittal, P., & Kumar, B. (2017). Analysis of factors affecting the solar radiation received by any region. *2016 International Conference on Emerging Trends in Communication Technologies, ETCT 2016*, 1–4. <https://doi.org/10.1109/ETCT.2016.7882980>
- Rawat, R. (2013). *Feasibility and Sensitivity Analysis of Hybrid Energy Systems for Uninterrupted Power Supply*. [Masters dissertation, Centre for Energy & Environment National Institute of Technology Hamirpur-177005, H.P, India]. <https://doi.org/10.13140/RG.2.1.1082.9845>
- Ray, M. L., Rogers, A. L., & McGowan, J. G. (2006). Analysis of Wind Shear Models and Trends in Different Terrains. *AWEA Wind Power 2005 Conference*, (June 2006), 4–7. Retrieved from https://www.researchgate.net/publication/251965566_Analysis_of_wind_shear_models_and_trends_in_different_terrain

- Reinhard, H. (2006). *Demand side value of PV - Report of the IEE project PV Upscale-Urban Scale Photovoltaic Systems*. Vienna University of Technology, Institute of Power Systems and Energy Economics, Energy Economics Group (EEG)
- Rezzouk, H., & Mellit, A. (2015). Feasibility study and sensitivity analysis of a stand-alone photovoltaic-diesel-battery hybrid energy system in the north of Algeria. *Renewable and Sustainable Energy Reviews*, **43**, 1134–1150. <https://doi.org/10.1016/j.rser.2014.11.103>
- Risso, A., Beluco, A., & Rita de, R. de C. (2019). Qualitative evaluation of spatial complementarity between renewable energy resources with complementarity roses. *MethodsX*, **6**, 800–804. <https://doi.org/10.1016/J.MEX.2019.04.005>
- Sanajaoba, S. (2019). Optimal sizing of off-grid hybrid energy system based on minimum cost of energy and reliability criteria using firefly algorithm. *Solar Energy*, **188**(2019), 655–666. <https://doi.org/10.1016/j.solener.2019.06.049>
- Santos, T., Gomes, N., Brito, M. C., Freire, S., Fonseca, A., & Tenedório, J. A. (2011). Solar potential analysis in Lisbon using LiDAR data. *Proceedings of the 31st EARSeL Symposium*, 13–19. [http://www.earsel.org/symposia/2011-symposium-Prague/Proceedings/PDF/Coastal Zones/3 ok25-a2393-Santos_et_al.pdf](http://www.earsel.org/symposia/2011-symposium-Prague/Proceedings/PDF/Coastal%20Zones/3%20ok25-a2393-Santos_et_al.pdf)
- Saoke, C., Kamau, J. N. and Kinyua, R. (2012). *Determination of the Shape k Scale c parameters and the wind power density for a selected site in Juja*. **4**(May), 41–46.
- Saoke, C. O., Kamau, J. N., Kinyua, R., Nishizawa, Y., & Ushiyama, I. (2015). Power Performance of an Inversely Tapered Wind Rotor and its Air Flow Visualization Analysis Using Particle Image Velocimetry (PIV). *American Journal of Physics and Applications*, **3**(1), 6. <https://doi.org/10.11648/j.ajpa.20150301.12>
- Saoke, C. O. Kamau, J. N., Nishizawa, Y., Kinyua, R., Ushiyama, I. & Nakajo, Y. (2014). Design and fabrication and testing of a low speed wind turbine generator using tapered type rotor blade made from fibre reinforced plastic. *International Journal of Renewable and Sustainable Energy*, **3**(1), 20. <https://doi.org/10.11648/J.IJRSE.20140301.14>

- Saoke, C., Nishizawa, Y., Ushiyama, I. Kamau, J. N., Nakajo, Y., & Kinyua, R. (2015). Development of a Small Wind Turbine Adopting Folded-Plate Blades- Performance of Blades with One and Two straight Folding Lines. *The 2015 JKUAT Scientific Conference*.
- Sayed, M. A., Kandil, H. A., & Shaltot, A. (2012). Aerodynamic analysis of different wind-turbine-blade profiles using finite-volume method. *Energy Conversion and Management*, **64**, 541–550. <https://doi.org/10.1016/j.enconman.2012.05.030>
- Scheurich, F., & Brown, R. E. (2013). Modelling the aerodynamics of vertical-axis wind turbines in unsteady wind conditions. *Wind Energy*, **16**(1), 91–107. <https://doi.org/10.1002/WE.532>
- Schubel, P. J., & Crossley, R. J. (2012). Wind Turbine Blade Design. *Energies*, **5**(9), 3425–3449. <https://doi.org/10.3390/EN5093425>
- Senthil Kumar, R., Puja Priyadharshini, N., & Natarajan, E. (2015). Experimental and numerical analysis of photovoltaic solar panel using thermoelectric cooling. *Indian Journal of Science and Technology*, **8**(36). <https://doi.org/10.17485/ijst/2015/v8i36/87646>
- Senthil, R., Araavind, S., & Ghosh, N. (2018). Optimization techniques for solar photovoltaic-wind turbine hybrid energy systems. *International Journal of Mechanical Engineering and Technology*, **9**(1), 646–654.
- Seppälä, A. (1996). Load research and load estimation in electricity distribution. [Doctoral dissertation, Helsinki University of Technology (Espoo, Finland)].
- Shabbir, R., & Taneez, M. (2013). Rural and Urban Household Demand Analysis for Electricity in Pakistan. *International Journal of Emerging Trends in Engineering and Development*, April, **6**(3), 185-191.
- Shankar, R. N., Kumar, L. R., & Ramana, M. V. (2019). Design and fabrication of multi-rotor horizontal axis wind turbine. *International Journal of Engineering and Advanced Technology*, **8**(6), 3500–3504. <https://doi.org/10.35940/ijeat.F9528.088619>

- Sharma, P., Bojja, H., & Yemula, P. (2016). Techno-economic analysis of off-grid rooftop solar PV system. *2016 IEEE 6th International Conference on Power Systems, ICPS 2016, ii*. <https://doi.org/10.1109/ICPES.2016.7584208>
- Shubham Nandurkar, Tirthraj Lonare, Vaishnavi Fulzele, & Pranay Bagde. (2017). Design and Fabrication of Vertical Axis Wind Turbine with Magnetic Repulsion. *International Journal of Engineering Research And*, **6**(05). <https://doi.org/10.17577/ijertv6is050462>
- Singh, A., & Sharma, R. (2024). Review paper on CFD analysis of different NACA airfoil series. *11*(3), 345–364.
- Singh, B., & Sharma, S. (2018). PMBLDCG based stand-alone wind energy conversion system for small scale applications. *International Journal of Engineering, Science and Technology*, **4**(1), 65–73. <https://doi.org/10.4314/ijest.v4i1.8s>
- Singh, P., Vinay, T .R., Balyan, A. Gangadhara & Prabhu, S. M. (2021). P-V and I-V Characteristics of Solar Cell. *Design Engineering*, **6**, 520–528.
- Singh, R. K., Ahmed, M. R., Zullah, M. A., & Lee, Y. H. (2012). Design of a low Reynolds number airfoil for small horizontal axis wind turbines. *Renewable Energy*, **42**, 66–76. <https://doi.org/10.1016/J.RENENE.2011.09.014>
- Skretas, S. B., & Papadopoulos, D. P. (2009). Efficient design and simulation of an expandable hybrid (wind-photovoltaic) power system with MPPT and inverter input voltage regulation features in compliance with electric grid requirements. *Electric Power Systems Research* **79**(9), 1271–1285). <https://doi.org/10.1016/j.epsr.2009.03.010>
- Soetedjo, A., Lomi, A., & Widodo Puji Mulayanto. (2011). Modeling of wind energy system with MPPT control. *Proceedings of the 2011 International Conference on Electrical Engineering and Informatics, ICEEI 2011, May*. <https://doi.org/10.1109/ICEEI.2011.6021836>

- Solomon, A. A., Child, M., Caldera, U., & Breyer, C. (2020). Exploiting wind-solar resource complementarity to reduce energy storage need. *AIMS Energy*, *8*(5), 749–770. <https://doi.org/10.3934/ENERGY.2020.5.749>
- Solomon, A. A., Kammen, D. M., & Callaway, D. (2016). Investigating the impact of wind-solar complementarities on energy storage requirement and the corresponding supply reliability criteria. *Applied Energy*, *168*, 130–145. <https://doi.org/10.1016/J.APENERGY.2016.01.070>
- Srikanth, M., Vijay Muni, T., VishnuVardhan, M., & Somesh, D. (2018). Design and simulation of PV-wind hybrid energy system. *Journal of Advanced Research in Dynamical and Control Systems*, *10*(4), 999–1005.
- Ssenyimba, S., Kiggundu, N., & Banadda, N. (2020). Designing a solar and wind hybrid system for small-scale irrigation: A case study for Kalangala district in Uganda. *Energy, Sustainability and Society*, *10*(1), 1–18. <https://doi.org/10.1186/s13705-020-0240-1>
- Sterl, S. (2021). A Grid for all Seasons: Enhancing the Integration of Variable Solar and Wind Power in Electricity Systems Across Africa. *Current Sustainable/Renewable Energy Reports*, *8*(4), 274–281. <https://doi.org/10.1007/s40518-021-00192-6>
- Stoffel, T., Renné, D., Myers, D., Wilcox, S., Sengupta, M., George, R., & Turchi, C. (2012). Concentrating solar power: best practices handbook for the collection and use of solar resource data. In *Concentrating Solar Power: Data and Directions for an Emerging Solar Technology* (1–148). Nova Science Publishers, Inc.
- Sun, W., & Harrison, G. P. (2019). Wind-solar complementarity and effective use of distribution network capacity. *Applied Energy*, *247*, 89–101. <https://doi.org/10.1016/J.APENERGY.2019.04.042>
- Šúri, M., Huld, T. A., Dunlop, E. D., & Ossenbrink, H. A. (2007). Potential of solar electricity generation in the European Union member states and candidate countries. *Solar Energy*, *81*(10), 1295–1305. <https://doi.org/10.1016/j.solener.2006.12.007>

- Szabó, S., Bódis, K., Huld, T., & Moner-Girona, M. (2011). Energy solutions in rural Africa: Mapping electrification costs of distributed solar and diesel generation versus grid extension. *Environmental Research Letters*, *6*(3). <https://doi.org/10.1088/1748-9326/6/3/034002>
- Takada, A., Ijuin, H., Matsui, M., & Yamada, T. (2024). Seasonal Analysis and Capacity Planning of Solar Energy Demand-to-Supply Management: Case Study of a Logistics Distribution Center. *Energies*, *17*(1). <https://doi.org/10.3390/en17010191>
- The World Bank. (2017). *State of Electricity Access. State of Electricity Access Report 2017*, 32. Retrieved from www.worldbank.org.
- Thomaidis, N. S., Santos-Alamillos, F. J., Pozo-Vázquez, D., & Usaola-García, J. (2016). Optimal management of wind and solar energy resources. *Computers and Operations Research*, *66*, 284–291. <https://doi.org/10.1016/j.cor.2015.02.016>
- Tigabu, A. (2016). *A desk assessment on the overviews of current solar and wind energy projects in Kenya (IREK Report No. 1). Innovation and Renewable Electrification in Kenya (IREK), African Centre for Technology Studies (Vol. X, pp. 1–24). Retrieved from http://irekproject.net/files/2015/11/Solar_and_wind_energy_projects_Kenya-IREK.pdf*
- Timilsina, G. R., Kurdgelashvili, L., & Narbel, P. A. (2012). Solar energy: Markets, economics and policies. *Renewable and Sustainable Energy Reviews*, *16*(1), 449–465. <https://doi.org/10.1016/j.rser.2011.08.009>
- Tovey, M. (1992). Books Reviews: Green issues in design. Design Council. Burall, P. *Green Issues in Design*, *13*(1), 98–99.
- Trade, E. (2014). World Energy Council World Energy Council. *World Energy Council*.
- Twidell, J. and Weir, T. (2015). *Renewable Energy Resources*. Routledge.
- Udoakah, Y., & Ikafia, U. (2017). Determination of Weibull Parameters and Analysis of Wind Power Potential in Coastal and Non-Coastal Sites in Akwa Ibom State.

Nigerian Journal of Technology, **36**(3), 923–929.
<https://doi.org/10.4314/njt.v36i3.36>

- Ulgen, K., & Hepbasli, A. (2002). Determination of Weibull parameters for wind energy analysis of Izmir, Turkey. *International Journal of Energy Research*, **26**(6), 495–506. <https://doi.org/10.1002/er.798>
- Ullah, K. R., Saidur, R., Ping, H. W., Akikur, R. K., & Shuvo, N. H. (2013). A review of solar thermal refrigeration and cooling methods. *Renewable and Sustainable Energy Reviews*, **24**, 499–513. <https://doi.org/10.1016/j.rser.2013.03.024>
- UNESA. (2015). THE 17 GOALS | Sustainable Development. *Department of Economic and Social Affairs | Sustainable Development*. Retrieved from <https://sdgs.un.org/goals>
- US EIA. (2013). International Energy Outlook 2013 - DOE/EIA-0484(2013). *Outlook 2013*, 312.
- Voss, K., & Reise, C. (2012). Photovoltaic systems. *Sustainable Solar Housing: Volume 2 - Exemplary Buildings and Technologies*, **9781849772808**, 23–227. <https://doi.org/10.4324/9781849772808>
- Wekesa, D. W., Mutuku, J. N., & Kamau, J. N. (2012). Microcontroller-based data logging instrumentation system for wind speed and direction measurements. *Journal of Agriculture, Science and Technology (JAGST)*, **14**(1), 177–190.
- Wekesa, D. W., Saoke, C. O., & Kamau, J. N. (2020). An experimental investigation into performance characteristics of H-shaped and Savonius-type VAWT rotors. *Scientific African*, **10**, e00603. <https://doi.org/10.1016/j.sciaf.2020.e00603>
- Wekesa, D. W., Wang, C., & Wei, Y. (2016). Empirical and numerical analysis of small wind turbine aerodynamic performance at a plateau terrain in Kenya. *Renewable Energy*, **90**, 377–385. <https://doi.org/10.1016/j.renene.2016.01.004>
- Wekesa, D. W., Wang, C., Wei, Y., & Danao, L. A. M. (2014). Influence of operating conditions on unsteady wind performance of vertical axis wind turbines operating within a fluctuating free-stream: A numerical study. *Journal of Wind Engineering*

- and Industrial Aerodynamics*, **135**, 76–89. <https://doi.org/10.1016/J.JWEIA.2014.10.016>
- Wekesa, D. W., Wang, C., Wei, Y., & Danao, L. A. M. (2017). Analytical and numerical investigation of unsteady wind for enhanced energy capture in a fluctuating free-stream. *Energy*, **121**, 854–864. <https://doi.org/10.1016/j.energy.2017.01.041>
- Wekesa, D. W., Wang, C., Wei, Y., & Kamau, J. N. (2014). Wind resource assessment and numerical simulation for wind turbine airfoils. *2014 15th International Workshop on Research and Education in Mechatronics, REM 2014*. <https://doi.org/10.1109/REM.2014.6920224>
- Wekesa, D. W., Wang, C., Wei, Y., Kamau, J. N., & Danao, L. A. M. (2015). A numerical analysis of unsteady inflow wind for site specific vertical axis wind turbine: A case study for Marsabit and Garissa in Kenya. *Renewable Energy*, **76**, 648–661. <https://doi.org/10.1016/j.renene.2014.11.074>
- Wekesa, D. W., Wang, C., Wei, Y., & Zhu, W. (2016). Experimental and numerical study of turbulence effect on aerodynamic performance of a small-scale vertical axis wind turbine. *Journal of Wind Engineering and Industrial Aerodynamics*, **157**, 1–14. <https://doi.org/10.1016/j.jweia.2016.07.018>
- Wen, B., Tian, X., Dong, X., Peng, Z., & Zhang, W. (2017). Influences of surge motion on the power and thrust characteristics of an offshore floating wind turbine. *Energy*, **141**, 2054–2068. <https://doi.org/10.1016/J.ENERGY.2017.11.090>
- White, S. (2018). *Solar Photovoltaic Basics: A Study Guide for the NABCEP Associate Exam: Second Edition*. *Solar Photovoltaic Basics: A Study Guide for the NABCEP Associate Exam: Second Edition* (1–188). Taylor and Francis. <https://doi.org/10.4324/9781315103396>
- Why Kenya could take the lead in carbon removal. (2023). Retrieved from <https://www.economist.com/middle-east-and-africa/2023/06/15/why-kenya-could-take-the-lead-in-carbon-removal>

- Wiatros-Motyka, M., Jones, D., Broadbent, H., Fulghum, N., Dizon, R., & Macdonald, P. (2022). *Lead authors Analysis contributors*. <https://ember-climate.org/insights/research/global-electricity-mid-year-insights-2022/>
- Wiginton, L. K., Nguyen, H. T., & Pearce, J. M. (2010). "Quantifying Solar Photovoltaic Potential on a Large Scale for Renewable Energy Regional Policy" & "Quantifying Rooftop Solar Photovoltaic Potential for Regional Renewable Energy Policy. *Computers, Environment and Urban Systems*, **34**, 345–357.
<http://ssrn.com/abstract=2006710><http://dx.doi.org/10.1016/j.compenvurbsys.2010.01.001>
- Wigness, S. (2023). What is the Carbon Footprint of Solar Panels? Retrieved from <https://www.solar.com/learn/what-is-the-carbon-footprint-of-solar-panels/#:~:text=Residential%20solar%20panels%20emit%20around,first%20three%20years%20of%20operation>.
- Wind And Solar Power System, Wind Solar Hybrid System, Solar Wind Turbine*. (n.d.). Retrieved May 2, 2024, from <https://www.solarpowermanufacturer.com/solar-products/wind-and-solar-power-system.html>
- Wind Energy Variability and Intermittency in the UK: New Reports | Claverton Group*. (2009). Retrieved March 13, 2022, from <https://claverton-energy.com/wind-energy-variability-new-reports.html>
- Wolfram, C., Shelef, O., & Gertler, P. (2012). How Will Energy Demand Develop in the Developing World? *Journal of Economic Perspectives*, **26**(1), 119–138. <https://doi.org/10.1257/JEP.26.1.119>
- Xu, L., Ruan, X., Mao, C., Zhang, B., & Luo, Y. (2013). An improved optimal sizing method for wind-solar-battery hybrid power system. *IEEE Transactions on Sustainable Energy*, **4**(3), 774–785. <https://doi.org/10.1109/TSTE.2012.2228509>
- Yamane, T. (1967). *Statistics: An Introductory Analysis* (2nd ed.). Harper and Row.


- Yang, H., Wei, Z., & Chengzhi, L. (2009). Optimal design and techno-economic analysis of a hybrid solar-wind power generation system. *Applied Energy*, **86**(2), 163–169. <https://doi.org/10.1016/j.apenergy.2008.03.008>
- Zaekhan, Z., & Nachrowi, N. D. (2015). The Impact of Renewable Energy and GDP per Capita on Carbon Dioxide Emission in the G-20 Countries. *Economics and Finance in Indonesia*, **60**(2), 145. <https://doi.org/10.7454/efi.v60i2.71>
- Zeraatpisheh, M., Arababadi, R., & Pour, M. S. (2018). Economic analysis for residential solar PV systems based on different demand charge tariffs. *Energies*, **11**(12). <https://doi.org/10.3390/en11123271>
- Zhang, J., Chowdhury, S., Messac, A., & Hodge, B. M. (2013). Assessing long-term wind conditions by combining different measure-correlate-predict algorithms. *Proceedings of the ASME Design Engineering Technical Conference*, **3 A**(iii), 1–12. <https://doi.org/10.1115/DETC2013-12695>

APPENDICES

Appendix I: Contributions of the Thesis

a) Muchiri, K., Kamau, J. N., Wekesa, D. W., Saoko, C. O., Mutuku, J. N., & Gathua, J. K. (2023). Wind and solar resource complementarity and its viability in wind / PV hybrid energy systems in Machakos, Kenya. *Scientific African*, 20, e01599. <https://doi.org/10.1016/j.sciaf.2023.e01599>


Scientific African 20 (2023) e01599




Contents lists available at ScienceDirect

Scientific African

journal homepage: www.elsevier.com/locate/sciaf



Wind and solar resource complementarity and its viability in wind/PV hybrid energy systems in Machakos, Kenya



Kennedy Muchiri^{a,*}, Joseph Ngugi Kamau^a, David Wafula Wekesa^b,
Churchill Otieno Saoko^a, Joseph Ndisya Mutuku^a, Joseph Kimiri Gathua^c

^a Institute of Energy and Environmental Technology, Jomo Kenyatta University of Agriculture and Technology P.O. Box 62000-00200, Nairobi, Kenya

^b Department of Physics, Multimedia University of Kenya, P.O. Box 15653- 00503, Nairobi, Kenya

^c Department of Physics, Kenyatta University, P.O. Box 43844-00100, Nairobi, Kenya

ARTICLE INFO

Article history:
Received 30 November 2020
Revised 11 February 2023
Accepted 17 February 2023

Editor: D.E. Gyampoh

Keywords:
Wind resource
Solar resource
Weibull distribution
Wind-solar complementarity

ABSTRACT

Integration of intermittent renewable energy resources provides the potential to mitigate the impact of the variability of independent sources. The intermittent nature creates stability, reliability and power quality problems in power grids. Wind and solar energies are the most viable resources whose complementarity could be deployed in the development of hybrid renewable energy systems to enhance their performance. In this study, wind-solar resource complementarity is investigated to establish its viability in hybrid energy systems in Machakos, a rural-urban town whose geographical location is 1°31'S, 39°16'E in the Eastern region of Kenya. The study findings could be fundamental in energy planning and developments in the area to provide more flexible and dependable hybrid energy systems which would supply energy services under constantly changing conditions. Ground measurements included PVGIS simulation and experimental tools installed at a height of 20 m. Weibull's distribution model and energy potential of wind resource are investigated to characterize wind resource for energy generation. The Wind distribution revealed a positively skewed profile with scale (c) and shape (k) parameter values of 2.68 m/s (\approx 3.0 m/s) and 1.9 at a mean wind speed of 2.47 m/s, respectively. The findings revealed a wind power density of 17 W/m² at an average wind speed of 3.0 m/s. Further, an annual solar insolation of 5.8 kWh/m² with monthly average of 178 kWh/m² translating to daily insolation of 2130 kWh/m² at an installation capacity of 1 kWp is reported. The months with minimum and maximum solar insolation were July and March which recorded monthly averages of 145 kWh/m² and 213 kWh/m² translating to a daily average of 4.7 kWh/m² and 6.9 kWh/m², respectively. The understanding gained from this study could be useful to the renewable energy research community and can be extended to stakeholders in PV and wind energy systems for micro grids and utility applications.

© 2023 The Author(s). Published by Elsevier B.V. on behalf of African Institute of Mathematical Sciences / Next Einstein Initiative.
This is an open access article under the CC BY-NC-ND license (<http://creativecommons.org/licenses/by-nc-nd/4.0/>)

b) Muchiri, K., Kamau, J. N., Wekesa, D. W., Saoke, C. O., Mutuku, J. N., & Gathua, J. K. (2022). Design and Optimization of a Wind Turbine for Rural Household Electrification in Machakos, Kenya. *Journal of Renewable Energy*, 2022, 1–9. <https://doi.org/10.1155/2022/8297972>

Hindawi
Journal of Renewable Energy
Volume 2022, Article ID 8297972, 9 pages
<https://doi.org/10.1155/2022/8297972>



Research Article

Design and Optimization of a Wind Turbine for Rural Household Electrification in Machakos, Kenya

Kennedy Muchiri¹, Joseph Ngugi Kamau¹, David Wafula Wekesa²,
Churchill Otieno Saoke¹, Joseph Ndisya Mutuku¹ and Joseph Kimiri Gathua³

¹Institute of Energy and Environmental Technology, Jomo Kenyatta University of Agriculture and Technology, Nairobi, Kenya

²Department of Physics, Multimedia University of Kenya, Nairobi, Kenya

³Department of Physics, Kenyatta University, Nairobi, Kenya

Correspondence should be addressed to Kennedy Muchiri; muchirikennedy1985@gmail.com

Received 17 March 2022; Revised 3 August 2022; Accepted 18 August 2022; Published 15 September 2022

Academic Editor: Jing Shi

Copyright © 2022 Kennedy Muchiri et al. This is an open access article distributed under the Creative Commons Attribution License, which permits unrestricted use, distribution, and reproduction in any medium, provided the original work is properly cited.

Machakos is an area characterized by low wind speeds in the range of 0.5 m/s to 5 m/s with an annual average wind speed of 3.5 m/s. Maximum power generation from wind requires the appropriate design of the conversion system. In this study, two HAWT rotor blades were fabricated using Styrofoam and aluminium with a pitching mechanism to maximize power. The system was tested in a wind tunnel environment at a wind speed range of 0 m/s–20 m/s. RPMs and torque were measured and then used to calculate the TSR and power coefficients at different pitching angles. Energy optimization was performed by varying the pitch angles from 0 to 40 degree and rotational speeds, blade shape, and also a variation of blade materials. The analysis of tip speed ratios showed positive skewness implying high potential for significant energy generation at low wind speeds. At the rated wind speed of 5 m/s, Styrofoam blades performed optimally at a pitch angle of 20 degree with a tip speed ratio (TSR) of 2.1 corresponding to a C_p of 0.465. This translates to 238 W of power. Aluminium type performed optimally at a pitch angle of 15 degree with a TSR of 1.9 corresponding to a C_p of 0.431, a power estimate of 220 W. These findings showed that Styrofoam blades were more effective and thus suitable for application in wind systems. The understanding gained from this study could be useful to the HAWT research community and can be extended to the turbine designs for small-scale microgrids and utility applications.

c) Muchiri, K., Kamau, J. N., Wekesa, D. W., Saoke, C. O., Mutuku, J. N., & Gathua, J. K. (2021). Energy Demand and Its Implication on Wind/PV System Sizing in Machakos, Kenya. *International Journal of Sustainable and Green Energy*, 10 (3), 92. <https://doi.org/10.11648/j.ijrse.20211003.12>

International Journal of Sustainable and Green Energy

2021: 10(3): 92-98

<http://www.sciencepublishinggroup.com/ijrse>

doi: 10.11648/j.ijrse.20211003.12

ISSN: 2575-2189 (Print); ISSN: 2575-1549 (Online)



Energy Demand and Its Implication on Wind/PV System Sizing in Machakos, Kenya

Kennedy Muchiri^{1,*}, Joseph Ngugi Kamau¹, David Wafula Wekesa², Churchill Otieno Saoke¹, Joseph Ndisya Mutuku¹, Joseph Kimiri Gathua³

¹Institute of Energy and Environmental Technology, Jomo Kenyatta University of Agriculture and Technology, Nairobi, Kenya

²Department of Physics, Multimedia University of Kenya, Nairobi, Kenya

³Department of Physics, Kenyatta University, Nairobi, Kenya

Email address:

Muchirikennedy1985@gmail.com (K. Muchiri)

*Corresponding author

To cite this article:

Kennedy Muchiri, Joseph Ngugi Kamau, David Wafula Wekesa, Churchill Otieno Saoke, Joseph Ndisya Mutuku, Joseph Kimiri Gathua.

Energy Demand and Its Implication on Wind/PV System Sizing in Machakos, Kenya. *International Journal of Sustainable and Green Energy*, Vol. 10, No. 3, 2021, pp. 92-98. doi: 10.11648/j.ijrse.20211003.12

Received: August 4, 2021; Accepted: August 17, 2021; Published: August 24, 2021

Abstract: Energy is an essential factor underpinning all elements of economy in the society. Its utilization greatly depends on the individual's lifestyle and habitation. In rural areas, people use less electronic appliances compared to urban areas. However, the rapid development in technology and variety of applications have triggered the desire for more power in both rural and urban regions. To meet the energy demand, the world's generation capacity has to keep growing. Renewable energy sources offer a better solution in quenching this demand. This paper presents the findings on energy utilization and a suitable sized wind/PV system model for an average rural household in Machakos. Energy demand assessment was done using probability sampling which involved clustering and random selection of households. The range of daily energy load in Machakos was found to be 0.052 to 4.23 kWh with most of the households consuming less than 1.5 kWh in a day. The daily average energy consumption for the three selected zones namely: Katheka-kai, Kiandani and Kathiani were 1.092, 0.99 and 1.4 kWh respectively, with an average load of 1.161 kWh. Over 50% of the households consume less than 1 kWh per day where the average loads were 0.56, 0.59 and 0.595 kWh respectively, with a daily average of 0.582 kWh. A wind/PV systems was sized for a sample household with a load of 0.588 kWh. Based on the minimum month solar insolation of 4.677 kWh/m² and the available wind speed range of 1.0-10.0 m/s in the sites, a stand-alone wind/PV hybrid system was sized with component sizes as: 12 V, 165 W Panel, 12 V, 250 AH battery, 12 V, 225 W inverter and a wind turbine with a cut in, rated and cut-off wind speeds of 1.0, 5.0 and 15.0 m/s.

Keywords: Energy Demand, Load Profile, Rural Electrification, PV Sizing, Wind Turbine Sizing

Appendix II: Questionnaire used to Collect Energy Demand Data

The questionnaire contents entailed household size, source of electricity in the household, number of electrical appliances available, their power rating as well as their active hours in a day, household's monthly income and average monthly power bill as per KPLC. The data was used to determine the daily load profile and the daily average energy demand.

PhD Research Work

Research Title: Development of a Wind-Solar PV Hybrid System for Small-Scale Power Generation in Machakos, Kenya

Institution: Jomo Kenyatta University of Agriculture and Technology

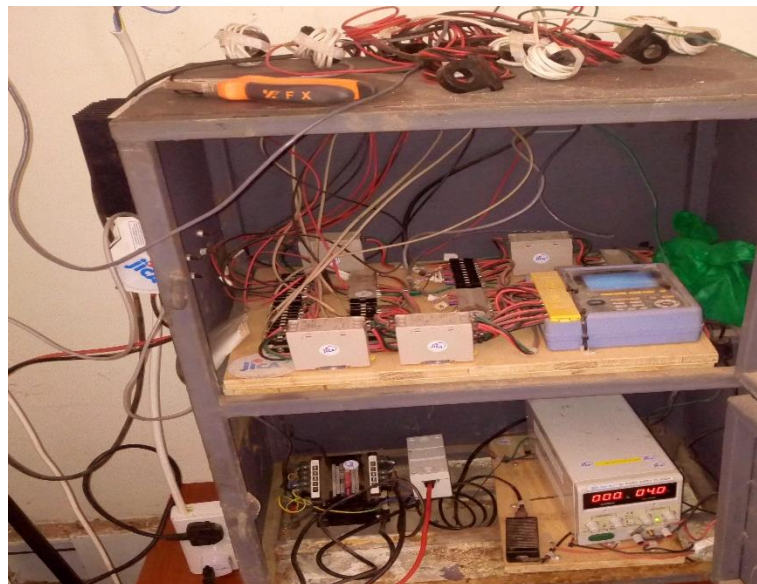
Field Study Objective: To perform energy utilization analysis for the determination of the appropriate hybrid system size for a rural household in Machakos.

S/no	Content		Feedback	
1	Household number			
2	Household size			
3	Monthly income			
4	Source of electrical energy			
5	Average monthly electrical bill			
6	Total number of appliances in the household, power rating and number of hours they are in use per day			
	Appliance	Quantity	Power rating	Active hours
7	Sessions of the day the appliances are active			
	Session of the day	Active appliances	Time in hours	
	<ul style="list-style-type: none"> • Morning: • Mid-morning: • Afternoon: • Evening: • At night: 			

Appendix III: Installation of Experimental Set-Ups in Machakos



Appendix IV: Data Logging System used in Capturing Wind and Solar Resource Assessment Data



Appendix V: Styrofoam Material used in Rotor Blade Fabrication



Appendix VI: Styrofoam Blade Fabrication at the IEET Workshop, JKUAT



Appendix VII: Co-ordinates of NACA 4418 Airfoil

1	0	30	0	100		0	0	0	0	0
0.95	0.0189	28.5	0.0189	95		0.0189	-0.0211	-0.0055	0.0244	0.04
0.9	0.0346	27	0.0346	90		0.0346	-0.0299	-0.0093	0.0439	0.0645
0.8	0.0622	24	0.0622	80		0.0622	-0.0406	-0.0167	0.0789	0.1028
0.7	0.0855	21	0.0855	70		0.0855	-0.0467	-0.0245	0.11	0.1322
0.6	0.1044	18	0.1044	60		0.1044	-0.0467	-0.0324	0.1368	0.1511
0.5	0.1185	15	0.1185	50		0.1185	-0.0549	-0.0402	0.1587	0.1734
0.4	0.127	12	0.127	40		0.127	-0.0556	-0.047	0.174	0.1826
0.3	0.1276	9	0.1276	30		0.1276	-0.0549	-0.0526	0.1802	0.1825
0.25	0.124	7.5	0.124	25		0.124	-0.0526	-0.0549	0.1789	0.1766
0.2	0.1172	6	0.1172	20		0.1172	-0.047	-0.0556	0.1728	0.1642
0.15	0.1066	4.5	0.1066	15		0.1066	-0.0402	-0.0549	0.1615	0.1468
0.1	0.0911	3	0.0911	10		0.0911	-0.0324	-0.0467	0.1378	0.1235
0.075	0.0806	2.25	0.0806	7.5		0.0806	-0.0245	-0.0467	0.1273	0.1051
0.05	0.0675	1.5	0.0675	5		0.0675	-0.0167	-0.0406	0.1081	0.0842
0.025	0.05	0.75	0.05	2.5		0.05	-0.0093	-0.0299	0.0799	0.0593
0.0125	0.0376	0.375	0.0376	1.25		0.0376	-0.0055	-0.0211	0.0587	0.0431
0	0	0	0	0		0	0	0	0	0
0.0125	-0.0211	0.375	-0.0211	1.25						0
0.025	-0.0299	0.75	-0.0299	2.5						
0.05	-0.0406	1.5	-0.0406	5						
0.075	-0.0467	2.25	-0.0467	7.5						
0.1	-0.0506	3	-0.0506	10						
0.15	-0.0549	4.5	-0.0549	15						
0.2	-0.0556	6	-0.0556	20						
0.25	-0.0549	7.5	-0.0549	25						
0.3	-0.0526	9	-0.0526	30						
0.4	-0.047	12	-0.047	40						
0.5	-0.0402	15	-0.0402	50						
0.6	-0.0324	18	-0.0324	60						
0.7	-0.0245	21	-0.0245	70						
0.8	-0.0167	24	-0.0167	80						
0.9	-0.0093	27	-0.0093	90						
0.95	-0.0055	28.5	-0.0055	95						
1	0	30	0	100						

Appendix VIII: Lift to Drag Ratios of NACA 4418 and the Other Similar

Airfoils

pitch angl	naca4418	clark ym	1ah93w	17	goe 290	goe 646	e856	fx66a175	fx6617a2	fx66182	goe679	s804
-13.25	-4.09853											
-13	-12.8915											
-12.75	14.787											
-12.5	-16.2799		-6.14663				-3.88916			-3.242		
-12.25	-17.5335		-9.76976				-5.38997		-2.79144	-3.69348		
-12	-18.2703		-11.9151				-7.16387		-5.32738	-4.36034		
-11.75	-19.3054		-13.4547				-8.3635		-6.12274	-6.02343		
-11.5	-19.79		-13.6349				-9.62015		-6.85782	-6.8523		
-11.25	-19.816		-14.0279			-2.56359	-10.2483	-2.30132	-7.72108	-7.66937		-7.05623
-11	-20.0561		-14.5606			-2.46215	-11.1399	-2.53656	-9.09462	-9.30052		-8.18211
-10.75	-20.5786		-15.1011			-14.1546	-11.9086	-3.74862	-9.60726	-10.0442		-9.17065
-10.5	-20.3696		-15.6355			-7.59264	-12.4919	-6.54264	-9.92491	-10.7452		-10.3202
-10.25	-20.2031		-16.1664			-10.5645	-13.9341	-7.2055	-10.2675	-11.3614		-11.4823
-10	-20.4338		-16.4026			-15.2355	-13.9263	-7.76778	-10.7266	-11.6875		-11.7417
-9.75	-20.0779	-10.2613	-16.3334			-16.8273	-14.4499	-8.28761	-11.1597	-11.6895		-12.0916
-9.5	-19.704	-11.4123	-16.3389			-18.0694	-15.0622	-8.54602	-11.5508	-11.7469		-12.5369
-9.25	-19.6698	-12.6317	-16.377			-17.5734	-14.8542	-8.62942	-11.8557	-11.823		-12.9006
-9	-19.1694	-13.9305	-16.3664	-2.92311	-18.0145	-15.0302	-8.73028	-11.9702	-11.8204	-3.34941	-13.1259	
-8.75	-18.6139	-15.1841	-16.077	-9.18646	-17.8591	-15.0931	-8.82353	-11.8171	-11.7088	-6.78151	-12.5879	
-8.5	-18.3373	-15.7119	-15.8079	-9.89945	-17.5857	-15.0821	-8.86109	-11.63	-11.4134	-8.71272	-12.5571	
-8.25	-17.7103	-15.4309	-15.5255	-11.0802	-17.4357	-14.9901	-8.79015	-11.3798	-11.0725	-11.3218	-12.1592	
-8	-16.9817	-15.7965	-15.1596	-11.6245	-16.9528	-14.8549	-8.56439	-11.0717	-10.6308	-12.9866	-11.5453	
-7.75	-16.4717	-16.1765	-14.6677	-11.8669	-16.5517	-14.4457	-8.21343	-10.7275	-10.2911	-14.201	-10.7202	
-7.5	-15.7666	-16.4288	-14.1589	-11.9401	-15.961	-14.0715	-7.85405	-10.2948	-9.82136	-15.1093	-9.9495	
-7.25	-14.8848	-16.1333	-13.6367	-11.8214	-15.3368	-13.5402	-7.41826	-9.7803	-9.33542	-14.6791	-9.12287	
-7	-14.2048	-15.713	-12.38	-11.6484	-14.6488	-13.005	-7.13884	-9.3059	-8.7833	-14.3429	-8.30248	
-6.75	-13.4185	-15.7115	-12.3061	-11.283	-13.9752	-11.9557	-6.23647	-8.7446	-8.23783	-14.6026	-7.45881	
-6.5	-12.359	-15.1248	-11.5682	-10.7913	-13.0363	-11.1778	-5.62656	-8.38314	-7.6692	-13.7681	-5.66202	
-6.25	-11.5314	-14.4207	-10.7669	-10.2177	-12.4748	-10.176	-4.83356	-7.72708	-7.00736	-13.8453	-4.68247	
-6	-10.6152	-14.1074	-9.93377	-9.65371	-11.4531	-9.21891	-4.16298	-7.1224	-6.37578	-12.9433	-3.63553	
-5.75	-9.37473	-13.3856	-9.02428	-8.97047	-10.9009	-8.29865	-3.35484	-6.4562	-5.70707	-12.5784	-2.52961	
-5.5	-8.47749	-12.5258	-8.08676	-8.1442	-9.8825	-7.1927	-2.6624	-5.83486	-5.1377	-11.6849	-1.35452	
-5.25	-7.34382	-12.0429	-7.12628	-7.3237	-8.66875	-5.67717	-2.01039	-5.25513	-4.08013	-11.3	-0.03029	
-5	-5.95578	-11.0276	-6.0886	-6.39616	-8.30942	-4.17588	-6.01019	-4.83123	-2.82687	-10.261	1.364449	
-4.75	-4.98834	-10.2169	-4.93044	-5.46109	-7.13884	-2.50827	0.656595	-4.29399	-1.4965	-9.63161	2.93224	
-4.5	-3.65193	-9.56891	-3.83907	-4.42032	-5.81034	-0.85479	1.867004	-3.17477	-0.2276	-8.54299	4.71908	
-4.25	-2.12239	-8.40743	-2.70987	-3.37287	-5.61502	0.621253	3.065863	-1.89638	0.999529	-7.9384	6.159052	
-4	-1.05779	-7.75483	-1.54496	-2.29492	-4.46869	2.249322	4.226519	-0.6472	2.13581	-6.82184	7.649358	
-3.75	0.053616	-6.88956	-0.26096	-1.14885	-3.910525	3.910525	4.444483	0.578022	3.22314	-5.40506	9.165265	
-3.5	1.801711	-5.64593	0.937819	0.009877	-3.14797	5.155579	6.668201	1.779026	4.342285	-5.01116	10.57377	
-3.25	3.335033	-5.13504	2.250903	1.259804	-1.95355	6.513859	7.923573	2.955072	5.530269	-3.54881	11.96544	
-3	4.9484	-3.94409	3.560718	2.507289	-0.5071	7.950703	9.206276	4.054554	6.721163	-2.98797	13.19829	
-2.75	6.28125	-2.20662	4.813452	3.733075	-0.76851	9.307245	10.42013	5.19761	7.957331	-1.34404	14.5277	
-2.5	8.124006	-1.77361	6.08971	5.026557	0.364155	10.81438	11.63284	6.334096	9.0839	0.539054	15.83159	
-2.25	9.38732	0.165414	7.395668	6.308951	1.772889	12.15116	12.87229	7.50114	10.181	1.225014	17.07988	
-2	11.15613	0.73391	8.702532	7.479675	1.399626	13.69312	14.14938	8.71188	11.29454	3.500779	18.37749	
-1.75	12.59662	2.358197	10.01576	8.706444	2.516556	15.02116	15.447	9.809264	12.46285	6.603618	19.66735	
-1.5	14.2865	4.154901	11.23373	9.966635	3.910525	16.44632	16.54128	10.83635	13.68421	7.278036	20.87907	
-1.25	15.90884	4.404952	12.26619	11.0586	3.442118	17.88695	17.65297	11.90905	14.90566	10.76586	22.28629	
-1	17.47899	5.978662	13.35366	12.12277	4.381395	19.22427	18.78581	13.02065	15.89732	11.58429	23.46076	
-0.75	19.28127	7.969012	14.43159	13.32084	5.813291	20.64244	19.95016	14.18011	16.79947	14.63941	24.68234	
-0.5	20.69886	8.843009	15.61115	14.62694	7.613451	21.96429	21.13821	15.46949	17.89066	15.79805	26.01294	
-0.25	22.58749	12.03235	16.66578	15.61918	6.541423	23.25825	22.32223	16.3984	18.84952	17.35002	27.25248	
0	23.86912	16.12245	17.7598	16.447	8.469191	24.64472	23.14337	17.20387	19.90422	20.01954	28.38662	
0.5	26.9311	19.2389	18.4036	17.80577	10.9292	26.88564	24.03617	18.12063	21.0282	21.62928	29.565	
0.75	28.36982	23.38631	19.1457	20.94564	13.64308	27.07557	24.96938	19.08775	22.06555	22.77848	30.80622	
1	30.12069	27.51024	19.95775	24.07258	11.42296	28.35567	25.96265	20.09071	22.54769	23.2206	31.90935	
1.25	31.73121	30.47708	21.0008	25.59796	13.69419	29.65057	26.93236	21.13821	23.1658	24.19029	33.0029	
1.5	34.01811	31.20544	21.83418	25.52457	16.34086	30.611	27.98114	22.26981	23.97016	25.02033	33.93925	
1.75	35.98324	33.23572	22.85583	25.50237	13.82784	31.75101	28.54307	22.67143	24.83765	26.17353	35.02354	
2	38.41463	33.72305	23.37262	26.15023	16.28831	32.96129	29.01953	23.18408	25.81053	27.31667	36.01213	
2.25	39.8893	34.95408	23.7656	27.23477	19.24899	33.9202	29.6392	23.88885	26.86992	30.81911	36.81587	
2.5	40.63078	36.86178	24.45523	27.16121	16.51689	34.79486	30.35714	24.66098	26.84252	30.61087	37.5969	
2.75	41.56503	37.46071	25.33742	27.56823	19.12389	35.79774	31.16747	25.54795	26.9577	30.50286	38.42271	
3	41.84711	38.3235	26.20084	28.36899	22.007	36.90058	31.98493	26.52956	27.7968	31.0288	39.21017	
3.25	42.56194	39.46252	27.4772	28.77228	19.93596	37.68822	32.64196	26.78867	28.88764	32.21498	40.00442	
3.5	43.17188	40.95687	28.11966	28.41823	23.22052	38.32618	32.34686	26.56202	28.82791	31.43183	40.75011	
3.75	43.53878	41.90212	28.34859	29.05339	27.95121	39.13089	32.34954	26.82331	28.80961	32.2827	41.19467	
4	44.33147	41.5792	29.25501	30.05656	29.2051	40.09845	32.59273	27.38759	28.43021	31.73298	41.66949	
4.25	44.64697	42.01442	30.43285	29.40152	31.6055	40.92386	33.04821	28.19491	28.7813	32.04536	42.15359	
4.5	45.05185	43.00526	32.7429	29.84263	35.57143	41.2533	33.63702	29.11862	29.44142	32.10388	42.64827	
4.75	45.83973	42.71663	31.44113	30.97351	33.26153	41.77456	34.22995	28.16996	30.18945	31.75704	43.16132	
5	46.30033	42.90516	30.99043	30.42531	36.92338	42.48542	34.15539	27.40653	26.91629	32.66694	43.70489	
5.25	46.6978	43.10236	31.24	30.99037	35.96567	43.3776	32.13372	27.67403	27.24729	31.6133	43.95661	
5.5	46.74322	43.02573	32.0065	32.39903	38.74946	43.74009	31.96313	28.33942	27.93351	32.01519	43.95745	
6	47.1153	43.12554	32.99533	31.55637	37.52542	43.88768	32.12308	29.16033	28.68994	31.69797	44.06008	
6.25	47.16005	43.22085	29.91251	32.67023	41.11111	44.51404	32.59304	24.95333	16.05051	31.29416	44.10381	
6.5	47.36793	42.78692	30.48984	33.23858	39.6381	45.39386	27.98015	25.52304	15.13781	32.16585	44.25955	
6.75	47.51948	43.37993	31.33255	33.14406	41.78939	46.09026	27.14138	26.3476	13.91453	40.88257	44.50199	
7	47.33844	42.62295	32.43668	34.78461	41.26966	45.7084	27.19329	27.35592	14.12295	41.02947	44.83018	
7.25	47.70361	42.54702	27.42624	33.89701	42.1791	45.31778	27.69483	21.4025	14.4892	40.96322	45.17655	
7.5	47.19984	43.08909	28.64072	35.45747	42.3901	45.30991	13.98755	18.52473	14.97106	40.07317	44.9535	
7.75	47.11858	42.06213	30.15728	34.90122	42.56476	45.64372	14.24608	16.57825	14.03414	40.70617	43.969	
8	46.92766</											

**Appendix IX: WT Testing in a Wind Tunnel Facility in the Fluids Laboratory,
JKUAT**



Appendix X: Rotational Speeds of Styrofoam and Aluminum Blades at different Wind Speeds

M/S	STYROFOAM									m/s	ALUMINIUM											
	15	18	20	23	25	28	30	35	40		5	8	10	12	15	18	20	25	30	35	40	
0.5	0	0	0	0	0	0	0	0	0	0.5	0	0	0	0	0	0	0	0	0	0	0	0
1	0	0	0	0	0	0	0	0	0	1	0	0	0	0	0	0	0	0	0	0	0	0
1.5	30	33	33	27	21	18	18	15	9	1.5	15	18	18	21	27	18	9	9	0	0	0	0
2	36	39	42	39	33	33	30	24	15	2	18	36	30	33	39	30	15	18	12	15	15	15
3	45	48	51	48	45	48	42	36	27	3	24	48	39	42	45	36	21	27	21	24	24	24
4	51	57	63	60	54	54	48	45	30	4	33	57	48	48	54	42	30	36	30	30	30	30
5	57	63	69	66	66	60	54	51	42	5	45	60	54	57	63	51	48	42	33	33	33	33
6	63	72	75	72	69	66	60	57	48	6	54	63	60	63	69	63	57	48	39	36	39	39
7	75	78	81	78	75	72	66	63	54	7	60	66	69	72	78	69	66	54	45	45	45	45
8	81	87	90	87	81	78	72	69	60	8	66	69	75	81	84	75	72	60	54	51	51	51
9	90	93	96	93	87	84	75	75	66	9	72	75	84	90	93	93	84	78	66	60	63	63
10	96	99	102	96	93	87	78	78	69	10	78	81	90	96	102	99	93	84	72	69	66	66

Appendix XI: Power Coefficient and different TSRs for the Styrofoam Blade

Cp VRS TSR STYROFOAM																	
15	15	18	18	20	20	23	23	25	25	28	28	30	30	35	35	40	40
1.4577	0.31335	1.50325	0.32314	1.5488	0.33293	1.4577	0.31335	1.41214	0.30356	1.32104	0.28397	0.91106	0.19584	0.91106	0.19584	0.90061	0.1936
1.51844	0.31694	1.56905	0.3275	1.61966	0.33807	1.56905	0.3275	1.46782	0.30637	1.41721	0.29581	1.18438	0.24721	1.18438	0.24721	1	0.21869
1.51844	0.30557	1.6513	0.3323	1.70824	0.34376	1.6513	0.3323	1.53742	0.30938	1.48047	0.29793	1.26536	0.25464	1.26536	0.25464	1.11352	0.23408
1.53742	0.32902	1.69197	0.3621	1.75705	0.37603	1.69197	0.3621	1.62689	0.34817	1.56182	0.33424	1.36659	0.29246	1.30965	0.28028	1.13883	0.24372
1.59436	0.36007	1.82212	0.41151	1.82212	0.41151	1.82212	0.41151	1.7462	0.39436	1.67028	0.37722	1.43167	0.32333	1.36659	0.30863	1.14883	0.25719
1.62689	0.36176	1.82212	0.41517	1.89804	0.42205	2.00433	0.44569	2.00433	0.44569	1.82212	0.40517	1.51844	0.33764	1.44251	0.32076	1.15883	0.26323
1.73102	0.37586	1.91323	0.41042	2.09544	0.46499	2.12581	0.45158	2.04989	0.4451	1.82212	0.39564	1.63991	0.35608	1.5488	0.3363	1.17136	0.25434
1.936	0.35825	2.16377	0.40039	2.39154	0.44254	2.27765	0.43347	2.27765	0.42147	2.04989	0.37932	1.82212	0.33717	1.70824	0.3161	1.21475	0.22478
2.27765	0.33147	2.4295	0.37623	2.58134	0.421	2.4295	0.41923	2.50542	0.4	2.4295	0.35623	2.12581	0.3067	1.82212	0.29717	1.27549	0.20802
2.73318	0.28038	2.96095	0.30958	3.18871	0.36877	2.96095	0.34958	2.73318	0.36038	2.50542	0.34118	2.27765	0.29198	1.92212	0.28359	1.36659	0.18519

Appendix XII: Rotor Power at different TSRs of the Styrofoam Blade

15	15	18	18	20	20	23	23	25	25	28	28	30	30	35	35	40	40
1.4577	160.091	1.50325	165.092	1.5488	170.094	1.4577	160.091	1.41214	155.089	1.32104	145.08	0.91106	100.055	0.91106	100.055	0.90061	98.9102
1.51844	161.925	1.56905	167.32	1.61966	172.72	1.56905	167.32	1.46782	156.524	1.41721	151.129	1.18438	126.3	1.18438	126.3	1	111.729
1.51844	156.116	1.6513	169.772	1.70824	175.627	1.6513	169.772	1.53742	158.062	1.48047	152.212	1.26536	130.096	1.26536	130.096	1.11352	119.591
1.53742	168.096	1.69197	184.997	1.75705	192.114	1.69197	184.997	1.62689	177.88	1.56182	170.763	1.36659	149.418	1.30965	143.195	1.13883	124.517
1.59436	183.96	1.82212	210.24	1.82212	210.24	1.82212	210.24	1.7462	201.479	1.67028	192.722	1.43167	165.189	1.36659	157.679	1.14883	131.398
1.62689	184.823	1.82212	212.11	1.89804	215.625	2.00433	227.703	2.00433	227.703	1.82212	207.001	1.51844	172.5	1.44251	163.876	1.15883	134.484
1.73102	192.027	1.91323	209.684	2.09544	237.563	2.12581	230.712	2.04989	227.402	1.82212	202.132	1.63991	181.921	1.5488	171.816	1.17136	129.942
1.936	183.03	2.16377	204.559	2.39154	226.094	2.27765	221.46	2.27765	215.329	2.04989	193.795	1.82212	172.26	1.70824	161.495	1.21475	114.84
2.27765	169.348	2.4295	192.216	2.58134	215.089	2.4295	214.185	2.50542	204.36	2.4295	181.998	2.12581	156.693	1.82212	151.824	1.27549	106.277
2.73318	143.246	2.96095	158.164	3.18871	188.405	2.96095	178.6	2.73318	184.118	2.50542	174.309	2.27765	149.173	1.92212	144.886	1.36659	94.6136

Appendix XIII: Power Coefficient at different TSRs for the Aluminum Blade

Cp VRS TSR ALUMINIUM																					
5	5	8	8	10	10	12	12	15	15	18	18	20	20	25	25	30	30	35	35	40	40
1.18438	0.25459	1.22993	0.26439	1.36659	0.29376	1.4577	0.31335	1.5488	0.33293	1.42353	0.306	0.91106	0.20584	0.91106	0.19584	0.91061	0.19575	0.9103	0.19568	0.90106	0.19369
1.21475	0.27966	1.26536	0.29131	1.41721	0.32627	1.51844	0.34958	1.56905	0.36123	1.49674	0.34458	1.0629	0.2447	1.13883	0.26218	0.92106	0.20975	0.91106	0.20975	0.968	0.22285
1.21475	0.29742	1.30965	0.32065	1.42353	0.34854	1.53742	0.37642	1.59436	0.39036	1.50325	0.36805	1.13883	0.25883	1.17136	0.28679	0.97614	0.239	0.968	0.237	0.97614	0.225
1.25271	0.3056	1.43167	0.33783	1.49674	0.35318	1.56182	0.36854	1.69197	0.39925	1.5488	0.36547	1.23883	0.26873	1.21475	0.28664	0.98698	0.2329	0.97614	0.23034	0.98698	0.2329
1.25271	0.31082	1.59436	0.35559	1.51844	0.37675	1.59436	0.39559	1.7462	0.41326	1.56905	0.38931	1.36659	0.30908	1.27549	0.31647	1.01217	0.24866	1.00217	0.24866	1.00217	0.24866
1.30152	0.2843	1.82212	0.33802	1.63991	0.36822	1.73102	0.37812	1.91323	0.42792	1.59436	0.39827	1.41214	0.33846	1.27549	0.27861	1.02494	0.22388	1.01229	0.22112	1.00217	0.23891
1.4659	0.26048	2.02212	0.30398	1.82212	0.35398	1.82212	0.37398	2.04989	0.43073	1.69436	0.41723	1.51721	0.38087	1.31598	0.2701	1.0629	0.21815	1.04772	0.21504	1.0629	0.21815
1.5659	0.24946	2.16377	0.28498	1.92212	0.34261	1.92581	0.36805	2.27765	0.42576	1.82212	0.40261	1.63167	0.37534	1.36659	0.24946	1.19327	0.19957	1.13883	0.20788	1.13883	0.20788
1.6659	0.2042	2.4295	0.24747	2.01397	0.32607	2.22581	0.32654	2.73318	0.35841	2.02212	0.3856	1.74251	0.36444	1.46659	0.1842	1.21352	0.15009	1.18883	0.1535	1.18883	0.1535
1.71844	0.17098	2.73318	0.20776	2.27765	0.29647	2.50542	0.28211	2.96095	0.33341	2.37765	0.34647	1.8577	0.35714	1.56659	0.15388	1.23883	0.12823	1.21475	0.13678	1.21475	0.13678

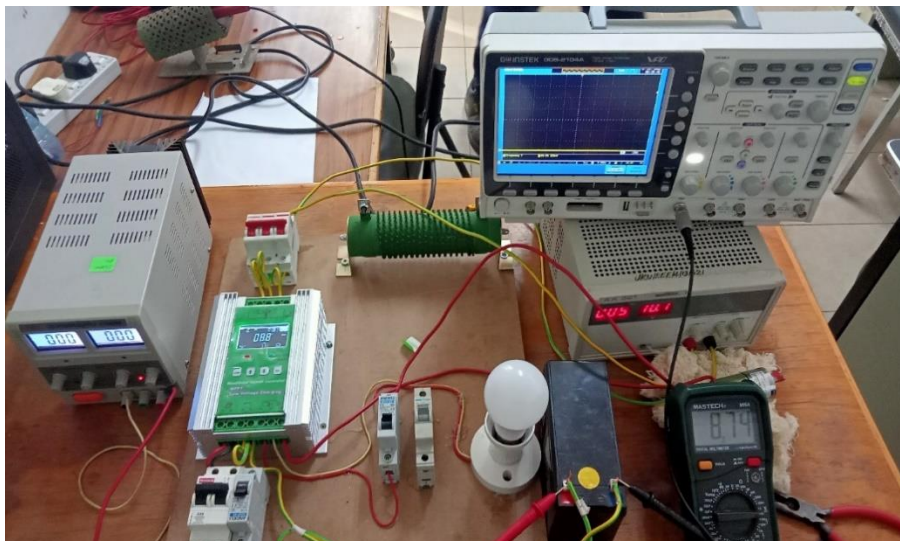
Appendix XIV: Rotor Power at different TSRs of the Aluminum Blade

POWER VSR TSR																					
5	5	8	8	10	10	12	12	15	15	18	18	20	20	25	25	30	30	35	35	40	40
1.18438	130.07	1.22993	135.077	1.36659	150.082	1.4577	160.091	1.5488	170.094	1.42353	156.335	0.91106	105.164	0.91106	100.055	0.91061	100.009	0.9103	99.9729	0.90106	98.9562
1.21475	142.878	1.26536	148.83	1.41721	166.691	1.51844	178.6	1.56905	184.552	1.49674	176.046	1.0629	125.017	1.13883	133.948	0.92106	107.161	0.91106	107.161	0.968	113.854
1.21475	151.952	1.30965	163.82	1.42353	178.069	1.53742	192.313	1.59436	199.435	1.50325	188.037	1.13883	132.236	1.17136	146.521	0.97614	122.105	0.968	121.083	0.97614	114.953
1.25271	156.131	1.43167	172.597	1.49674	180.44	1.56182	188.287	1.69197	203.977	1.5488	186.719	1.23883	137.294	1.21475	146.444	0.98698	118.989	0.97614	117.681	0.98698	118.989
1.25271	158.798	1.59436	181.671	1.51844	192.482	1.59436	202.107	1.7462	211.135	1.56905	198.898	1.36659	157.909	1.27549	161.685	1.01217	127.04	1.00217	127.04	1.00217	127.04
1.30152	145.249	1.82212	172.694	1.63991	188.124	1.73102	193.182	1.91323	218.624	1.59436	203.476	1.41214	172.919	1.27549	142.342	1.02494	114.38	1.01229	112.97	1.00217	122.059
1.4659	133.079	2.02212	155.303	1.82212	180.848	1.82212	191.066	2.04989	220.06	1.69436	213.163	1.51721	194.586	1.31598	137.994	1.0629	111.453	1.04772	109.864	1.0629	111.453
1.5659	127.449	2.16377	145.596	1.92212	175.039	1.92581	188.037	2.27765	217.521	1.82212	205.693	1.63167	191.761	1.36659	127.449	1.19327	101.96	1.13883	106.206	1.13883	106.206
1.6659	104.326	2.4295	126.432	2.01397	166.589	2.22581	166.829	2.73318	183.112	2.02212	197.003	1.74251	186.192	1.46659	94.1078	1.21352	76.681	1.18883	78.4232	1.18883	78.4232
1.71844	87.3537	2.73318	106.145	2.27765	151.467	2.50542	144.13	2.96095	170.339	2.37765	177.012	1.8577	182.463	1.56659	78.6173	1.23883	65.5127	1.21475	69.8809	1.21475	69.8809

Appendix XV: Fabricated and Assembled Wind Turbine at the Engineering Workshop, JKUAT



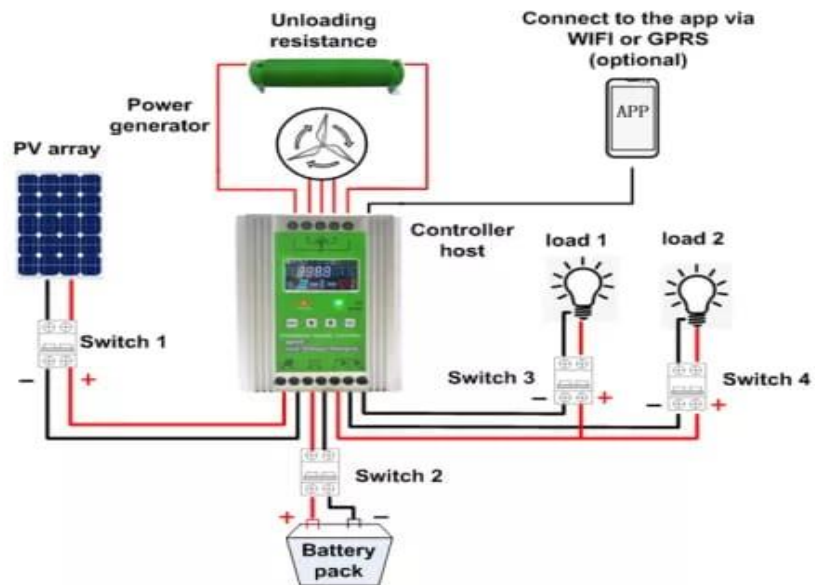
Appendix XVI: Wind-Solar Hybrid Interface Testing at Electrical Laboratory, JKUAT



Appendix XVII: Wind-Solar Hybrid Charge Controller used to Hybridize Wind and Solar Energies



Appendix XVIII: Hybrid Charge Controller Connections to the Sub-Systems



Appendix XIX: Wind Tunnel Facility in the Fluids Laboratory, JKUAT

The wind tunnel is 4.6 m long with a 1.2 m square test section running at an average Re of about 160000 (Wekesa *et al.*, 2020)

